Podocyte Injury Causes Chronic Kidney Disease in the Ercc1 Deficient Mouse Model of Accelerated Aging

by

Kathryn E. Wack

B.S., Biological Sciences, Carnegie Mellon University, 2000

M.S., Toxicology/Biological Engineering, Massachusetts Institute of Technology, 2004

Submitted to the Graduate Faculty of

University of Pittsburgh, School of Medicine in partial fulfillment

of the requirements for the degree of

Doctor of Philosophy in Cell Biology

University of Pittsburgh

2014

UNIVERSITY OF PITTSBURGH

School of Medicine
Cell Biology

This dissertation was presented

by

Kathryn E. Wack, PhD

It was defended on

July 23, 2014

and approved by

Thomas Kleyman, MD, Cell Biology

Laura Niedernhofer, MD, PhD, Scripps Florida, Dept. of Metabolism & Aging

Youhua Liu, PhD, Pathology

Jeffrey Isenberg, PhD, MPH, Dept. of Medicine

Dissertation Advisor: Donna Beer Stolz, PhD, Cell Biology

Podocyte Injury Causes Chronic Kidney Disease in the Ercc1 Deficient Mouse Model of Accelerated Aging

Kathryn E. Wack, PhD

University of Pittsburgh, 2014

ABSTRACT

In 2013, it was determined by the United States Renal Data System (USRDS) that 32% of the people over 60 had some form of chronic kidney disease (CKD)(1). CKD is often age-associated, but confounding factors make it difficult to separate age-related causes from other factors such as diabetes and hypertension. Animal models can be useful to evaluate aging nephropathy but are costly since they take years. The aim of this thesis was two-fold. First, I used the *Ercc1* deficient mouse model of accelerated aging to test the hypothesis that unrepaired DNA damage can cause CKD, similar to that seen as a result of natural aging. Second, I tested the hypothesis that inherent podocyte damage due to *Ercc1* deficiency causes the loss of kidney function associated with aging. In order to test this hypothesis, kidneys from the $Ercc1^{-/\Delta}$ mouse, a model of a human progeria, and old wildtype (WT) (2-3 yrs) mice were characterized and compared to elucidate the time-course and extent of injury. At one month after birth, $Ercc1^{-/\Delta}$ mice develop evidence of podocyte injury, autophagy induction, and a slightly elevated urine albumin-creatinine (ACR) ratio. Glomerular filtration rate (GFR) remained comparable to WT mice until 2 months, after which time albuminuria increased significantly, GFR decreased significantly, and podocytes began to display increased IKK expression and chronic NF-κB activation, as seen in old WT kidneys. At this same time, increased LC3 and p62 protein levels indicated a functional breakdown in autophagy. ICAM up-regulation in glomerular capillaries and tubule apical membranes occurred, followed by proximal tubule injury, an increase in myofibroblast-like cells,

and macrophage infiltration. A podocyte specific knock-out of *Ercc1* was created and the results support the hypothesis that inherent podocyte injury drives age-related kidney pathologies. In contrast, a proximal tubule cell specific knock-out of *Ercc1* showed no elevation in ACR, and no decrease in GFR throughout the time period tested. This thesis provides mechanistic information as to how aging nephropathy can occur over time as a result of endogenous DNA damage, and provides evidence that the podocyte should be a major target for therapeutic intervention.

TABLE OF CONTENTS

LIST OF TABLES

LIST OF FIGURES

PREFACE

This has been more than just four years of PhD research, teaching, and learning. My time here in the Center for Biologic Imaging in the Cell Biology program at the University of Pittsburgh has resulted in me becoming a stronger, healthier, and happier human being. Along with all of the members of my committee, for being so supportive and giving such practical and wise advice, I'd like to thank a few individuals in particular.

I thank you, Donna, most of all. You have been my mentor for the last 16 years in many ways. You lead by example, with creativity, enthusiasm, determination, and wisdom. Most importantly, you showed me how to be at peace no matter how rough the waves were. We've had a wild, exciting ride, and I hope it continues. You always made me laugh. You have a knack for putting things into perspective, and you shared such a wealth of knowledge about science and life in general. All of that has spilled over into other areas of my life… as a mother, a nature lover, a biological photographer, a partner in crime, etc. You taught me how to be brave enough to not just "get through," but to dance my way through. I hope to continue to create memories with you and enjoy all of the beauty that we've both been blessed enough to experience. Thank you.

To my Wacks (siblings and parents): you are the best family I could ask for. You stood by me through many, many tough times in the last decade or so, and I'm so happy to see you still standing by me to celebrate better times. We are connected in ways that non-Wacks can't understand, and I've learned just how unique this is during my wild 36 years on planet earth. I love you all completely and thank you sincerely.

To Adam: thank you for helping me to tackle things like a champ, take advantage of every moment, and love like I never have before. I'm so lucky you came into our lives. You have been

my rock in the last year, and you have certainly been more than wonderful to Sadie. I am incredibly excited to continue down this road with you. Thank you.

To all of CBI, especially Simon, Claudette, Katy, Jenny Mark, Morgan, Callen, Patricia, Lauren…. all of you: you were there every day to lend a hand, encourage me, give me sage advice, and make me laugh. Having started my journey at CBI and then stepping out for science and teaching adventures at MIT and in Rochester, I really do know just how lucky I was to be welcomed back and supported every step of the way. I'm very thankful to have been able to work in the "Disneyworld" of imaging. I literally grew up in your center, Simon! I hope to continue to be lucky enough to collaborate with you in any respect, my friends, as I move on. Thank you.

To Laura: thank you so much for making it possible to study such a valuable model of kidney aging, and for continuing to allow that to happen from Florida. I learned so much from spending time in your lab here at Pitt, and met some good friends and colleagues along the way. Your clever and innovative ways of thinking as a scientist are something I strive to implement in my own future career. You always encouraged me to go the distance and so I did! Thank you.

To my Sadie Rose: Thank you for being such a brave, clever, silly, optimistic, mature, and unique daughter. You are always right there by my side, supporting and cheering me on. You helped me every step of the way in this kidney adventure, and I'm proud to call you my firecracker of a daughter. This is for you.

1.0 INTRODUCTION

It is estimated that over 10% of adults and 32.2% of people over 60 in the U.S. have chronic kidney disease (CKD)(1, 2). Due to increased lifespan, the number of elderly people (65 years or older) is projected to increase from 420 million in 2000 to 550-973 million by 2030(3). As we age, our kidney function declines and other age-related diseases such as hypertension and diabetes compound the risk of CKD and end-stage renal disease (ESRD) (Figure 1). Medicare expenditure in 2011 for CKD patients was over $40 billion(1). It is imperative to learn about the process of aging nephropathy to discover preventative measures, better diagnostic tools, and more effective therapies. It has been very challenging to study the effects of kidney aging in humans since there are often many additional confounding factors and comorbid conditions that contribute to various age-related renal pathologies. Animal models have been useful in this respect, but remain costly and take years to manifest age-related diseases. As a result, the mechanisms of aging nephropathies, as well as the roles that specific kidney cell types play in these processes, remain largely unknown.

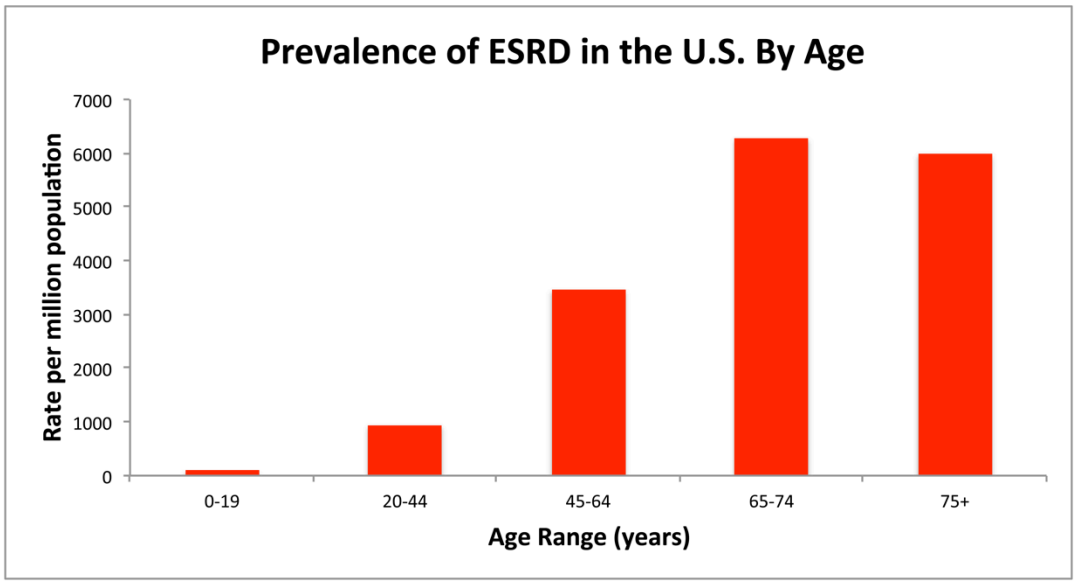

Figure 1. ESRD is largely a condition of the aged population

Data was extracted from the 2013 USRDS Atlas of CKD and ESRD in order to plot the prevalence of ESRD by age categories in the U.S(1).

The goal of this thesis is to utilize an animal model of accelerated aging to elucidate the mechanisms of age-related kidney disease, and specifically to determine the role of the glomerular podocyte in causing these pathologies. In Chapter 1, I will present the major findings in the field of chronic kidney disease with regard to factors that are known to be induced or enhanced by aging, in order to identify the knowledge gaps that remain and demonstrate areas of needed focus in order to identify new therapeutic targets. In Chapter 2, I test the hypothesis that accumulated DNA damage can cause accelerated kidney aging using the *Ercc1*$^{-/\Delta}$ mouse model and use this model to present new findings about the timing and progression of events that occur with renal aging. Finally, in Chapter 3, utilizing cell specific knock-outs of *Ercc1*, I test the hypothesis that it is the glomerular podocyte, not the proximal tubule cell, that causes chronic kidney disease with *Ercc1* deficiency, and I begin to elucidate the mechanism by which this injury occurs.

1.1 THE AGING KIDNEY

1.1.1 Kidney structure and function

The kidneys filter the entire volume of blood in the body every 30 minutes in order to remove excess liquid and wastes. In addition to removing toxins, the kidneys help to control fluid and ion levels in the body and also produce calcitriol, the active form of vitamin D, erythropoietin to stimulate red blood cell formation in the bone marrow, and renin to control blood pressure(4). Understanding how aging affects kidney cell homeostasis will help us to determine who is at risk for developing CKD with age and allow us to determine new and effective therapies for age-related kidney disease.

Blood flows into the kidney through the renal artery and then into a million nephrons, the functional unit of the kidney. The initial segment of the nephron is comprised of the glomerulus, the filtering unit, followed by a proximal tubule, where specific ions, water, and nutrients can be reabsorbed from the filtrate into the blood. Fine-tuning of water and ion balance occur downstream in the distal nephron and collecting duct, where filtrate eventually flows out of the kidney as urine to be stored by the bladder (Figure 2).

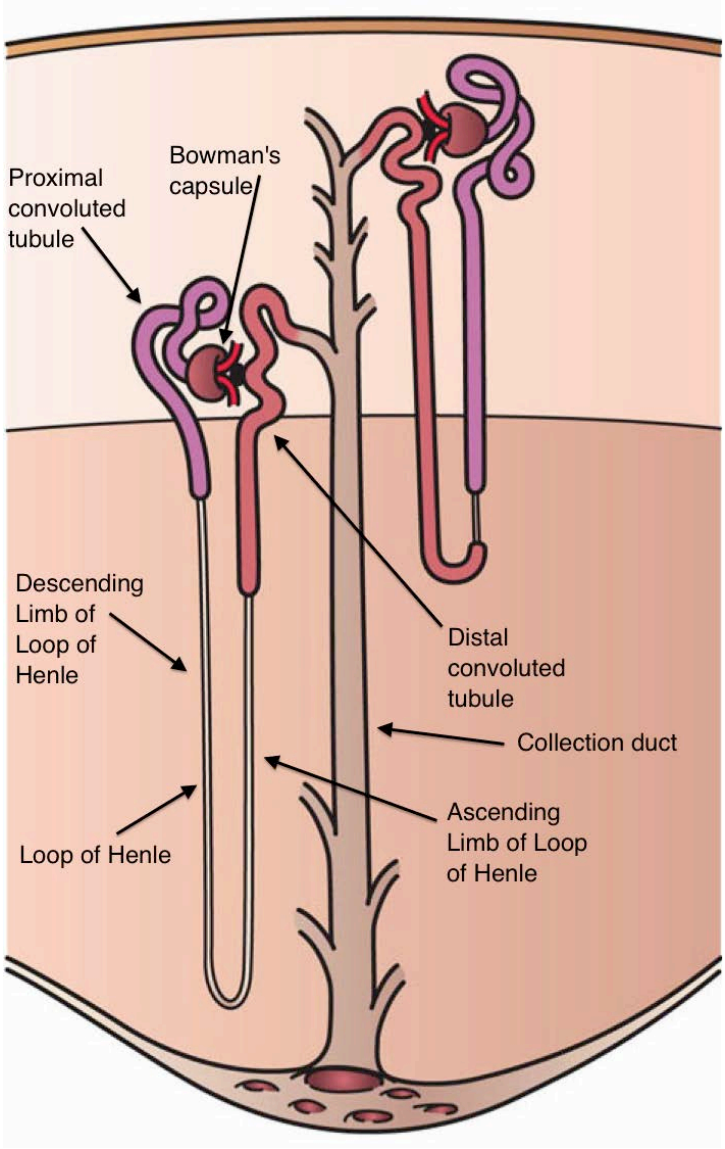

Figure 2. The kidney nephron

"Kidney Nephron" by Artwork by Holly Fischer - http://open.umich.edu/education/med/resources/second-look-series/materials - Urinary Tract Slide 20, 26. Licensed under Creative Commons Attribution 3.0 via Wikimedia Commons

The glomerular filtration barrier consists of the fenestrated, but undiaphragmed, endothelial cells that line the tortuous capillary clusters (Figure 3A, red asterisk) of the glomerulus. The endothelial cells (Figure 3B, red arrow) adhere to the glomerular basement membrane (GBM) (Figure 3B, asterisk). On the other side of the GBM, lies the terminally differentiated, complex architecture of the kidney podocyte (aka visceral epithelium). Each podocyte has primary

processes that extend from the cell body, which then branch into secondary and tertiary segments, called foot processes (Figure 3B, red arrowhead) or pedicels. Foot processes from neighboring podocytes interdigitate and are joined together by specialized junctional complexes, called slit diaphragms (Figure 3B, blue arrow). The slit diaphragm is a large, signaling protein complex, where the protein nephrin from adjacent podocytes homotypically binds on the lateral side of each interdigitating foot process, forming a selectively permeable barrier that prevents proteins larger than albumin (60kD) from leaving the bloodstream to enter the filtrate. The slit diaphragm is a highly complex and regulated signaling center that is tightly coupled to the dynamic podocyte actin cytoskeleton. Podocytes are derived from the metanephric mesenchyme and, after the capillary loop stage of development, become highly differentiated, post-mitotic cells with high levels of basal autophagy(5). Podocytes are under enormous mechanical and toxic stress and must deal with this stress throughout the lifetime of the organism, as there is little or no evidence that they can divide or be replaced with age or following injury(6, 7). Genetic diseases in humans and animal models have established that podocyte injury is the driving force for glomerulosclerosis(8-10). Podocytes are not bound on their apical side; rather filtrate flows through them and into the Bowman's Space (Figure 3A, blue asterisk). This space is lined by Bowman's capsule, which is comprised of the parietal cells (Figure 3A, blue arrow). These cells are thought to be the progenitors that can differentiate into either tubule or podocyte cells under certain conditions(11). Filtrate from Bowman's space then passes into the proximal tubule, where protein, water, and other substances from the blood can be reabsorbed. Podocyte injury can lead to disruption of the glomerular filtration barrier and an increase in the concentration of protein and other substances that flow into the filtrate. This can then affect proximal tubule uptake of proteins and eventually cause proximal tubule injury and proliferation as an adaptive response(12).

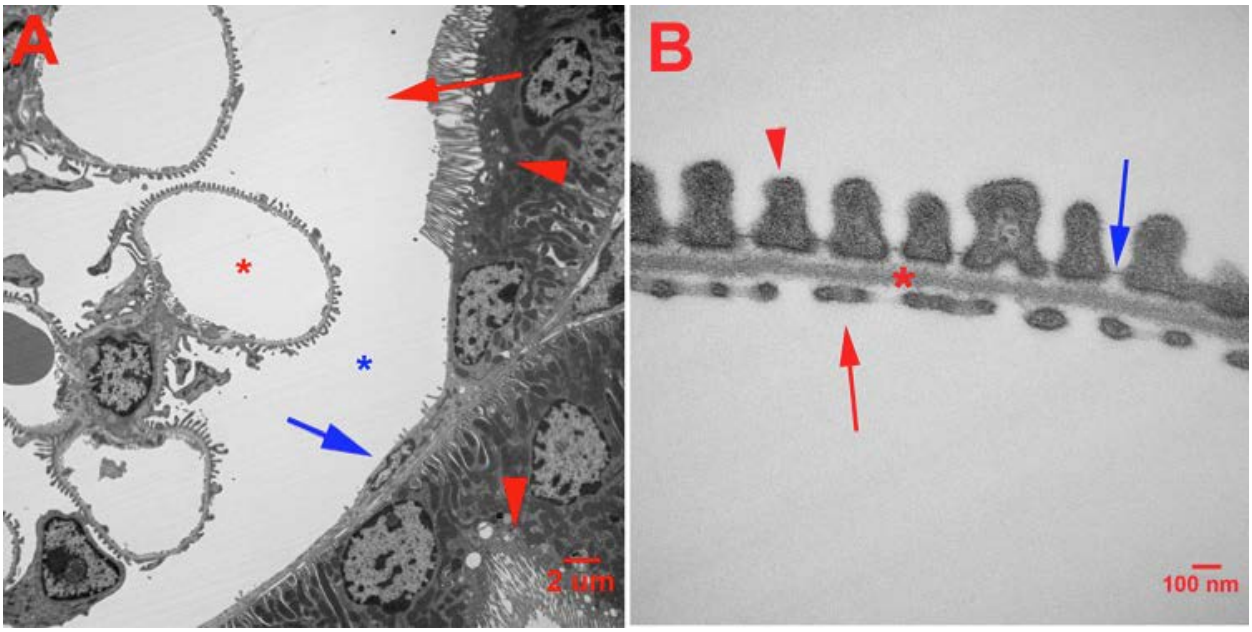

Figure 3. The Kidney Filtration Barrier

(A) TEM image of a healthy adult mouse glomerulus (red arrow indicates entire space with capillary loops). Capillary loops (red asterisk) are lined by fenestrated endothelium and podocytes, where materials from the blood are filtered into the Bowman's Space (blue asterisk). The glomerulus is surrounding by parietal epithelium (blue arrow), which then differentiate into brush border lined proximal tubule (red arrowheads). (B) TEM image of the glomerular filtration barrier, with fenestrated endothelium (red arrow) lining the capillaries, and the interdigitating foot processes of the podocytes (red arrowhead), connected the slit diaphragm protein complex (blue arrow). Both the endothelium and the podocytes adhere to and contribute to maintaining the GBM (red asterisk). Image taken by Donna Beer Stolz.

Podocytes must dynamically respond to changes in flow and, during health and injury states, must dynamically rearrange their actin cytoskeleton to maintain the filtration barrier. Therefore, it makes sense that signaling at the slit diaphragm complex affects actin cytoskeleton organization(13). This organization changes with injury and has been a target of study, as podocytes seem to take on a more migratory phenotype and this may play a role in podocyte loss with chronic kidney disease. Podocytes, being post-mitotic, must also manage damaged

macromolecules and organelles that accumulate over time, and they depend on a high-rate of basal autophagy(5, 14, 15). There is also evidence that podocytes may use autophagy to fuel their protein secretion, via content recycling, such as VEGF and glomerular basement membrane components, and to regulate the trafficking of slit diaphragm components(16).

1.1.2 Podocytes and autophagy

Macroautophagy, herein referred to as “autophagy” (Greek for “self-eating”) is the process by which damaged organelles and protein complexes are degraded and resulting materials supply nutrients for cell survival(5). In the first phase of autophagy, nucleation of double-membraned structure occurs in an unc-51-like kinase 1 (ULK-1)- and beclin 1-dependent process. Next, elongation of the double-membrane occurs in an autophagy related-5 and 12 (ATG5-ATG12) and light chain-3 (LC3) conjugation system. During this process, cytoplasmic LC3-I, is converted to membrane-bound LC3-II by conjugation with phosphotidylethanolamine. Next, damaged organelles and other substrates are enclosed by the double-membraned structure, the autophagosome. Unlike the other autophagy proteins mentioned thus far, LC3-II remains associated with the autophagasome until contents are degraded and machinery is recycled. Therefore, it is commonly used to mark autophagic structures in cells. In addition to labeling LC3-II, autophagy inhibitors must be used to differentiate between active autophagy and a functional block that results in LC3 accumulation(17). Autophagosomes fuse with lysosomes to form autolysosomes and the contents are then degraded(18, 19). Finally, contents are released and lysosomes are reformed from this structure upon completion of degradation in a mammalian target of rapamycin (mTOR)-dependent process(20, 21).

In addition to podocytes having the highest rate of autophagy among kidney cells, they also display the highest level of mTOR activation(22-25). mTOR is activated at the lysosomal cell membrane by various cues such as glucose and amino acids, growth factors, and oxidative stress. mTOR, through phosphorylation of various substrates, stimulates a wide variety of anabolic processes, such as protein and lipid synthesis, often involved in cellular hypertrophy(22). mTOR has been classically known for inhibiting the initiation of macroautophagy through inhibition of ULK-1, but it is necessary for lysosomal reformation after autolysosomal degradation, and therefore, necessary for autophagic flux(20, 21). Autophagic flux represents the cycling through of autophagy in which substrates are degraded, contents of the autolysosome are released, and lysosomes have reformed by budding away from the autolysosomal structure. mTOR also regulates slit diaphragm protein expression and podocyte cytoskeletal structure(26). So, how does the podocyte achieve both high levels of autophagy and mTOR activation? There is evidence of a Tor-Associated Spatial Coupling Compartment (TASCC) in the podocyte that provides a possible explanation. LC3-positive autophagosomes are located in a spatially separate compartment from mTOR-positive, LC3-positive, autolysosomes (co-localizing with LAMP-2)(16). In this way, podocytes achieve initiation of autophagy physically distant from mTOR activation, which occurs on the lysosomal membrane. The TASCC is located far from the foot processes in the cell body, peri-Golgi, and was also observed in Ras-induced senescent cells, regulating their senescence-associated secretory phenotype (SASP). Autophagic flux impairment and overall deficiency occurs with age(5, 27) and in diseases associated with oxidative stress such as diabetic nephropathy, as does an overall increase in mTOR activity(24, 25), Therefore, these two systems and their cross talk are likely key players during the process of glomerular aging. Large changes in podocyte cytoskeletal arrangement could also affect organization of the TASCC and may have

deleterious affects on regulating autophagy and mTOR-dependent processes. Because the TASCC was found to control secretion of growth factors and cytokines in cells(16), disruption of this structure and its function could contribute to disrupted secretion of GBM components and endothelial cell paracrine factors such as VEGF by podocytes.

1.1.3 Changes in human kidney structure and function with aging

Kidney function decline, often termed "renal senescence," is a multi-factorial, complex process that is influenced by genetics, gender, diet, activity, chronic inflammation, and other comorbid conditions. Kidney disease with aging often displays as glomerulosclerosis, interstitial fibrosis, and is defined functionally if an individual has an estimated glomerular filtration rate (eGFR) below 60ml/mi/1.73m^2, and a urine albumin creatinine ratio (ACR) of greater than or equal to 30mg/g (1, 28-33). Epidemiological studies are often performed on populations that have co-morbidities or confounding factors, such as living donors, making findings difficult to generalize. In addition, the method of measuring eGFR is inconsistent and includes serum creatinine measurements, inulin clearance, and iothalamate clearance. Serum creatinine levels can change with age and CKD-induced muscle deterioration, and often do not accurately reflect the GFR. A cross-sectional study in 2011 of 1203 adult living kidney donors, showed that there was a reduction in GFR of 6.3ml/min per decade of life(34). Poggio et al, in 2009, in a cross-sectional study of 1057 prospective kidney donors, found that GFR decreased at an average rate of 1.49 ml/min/1.72m^2 per decade of testing, but that a doubling in the rate of decline of GFR occurred in donors over the age of 45(35). The data from these cohorts indicate a progressive loss of renal function with aging. However, because a prerequisite of living kidney donation is the absence of

CKD and co-morbidities, these results may not accurately reflect the extent of decline in the general population.

The increase in proteinuria and the incidence of glomerulosclerosis, a scarring and thickening of glomerular capillaries, point to glomerular aging as a major driver of the loss of kidney function seen with age. However, there are also functional changes that indicate the tubules change with age. The elderly have increased susceptibility to volume handling, likely due to a reduction in sodium excretion in response to dietary salt deprivation(36). Proximal tubule function can be measured by lithium clearance and is reduced in elderly patients(37). Additionally, the aged are at risk for hyperkalemia, likely due to impaired potassium secretion in the distal nephron and collecting duct, which is linked to sodium reabsorption by Na-K-ATPase transporters, which are modulated by aldosterone in the tubules(38). Therefore, tubule atrophy or scarring could lead to a secondary problem with potassium handling. There is also a decreased capacity of the aged kidney to detoxify and metabolize drugs, likely due to a decline in kidney epithelial function(39). Similarly, tubule injury could be primary or secondary due to glomerular disease. As of yet, there is no clear understanding of the contribution of specific kidney cell types to age-related CKD, and the timing of events that occur with aging. It is important to identify this mechanism and target the primary cell type(s) involved in propagating aging nephropathy when discovering putative therapies.

Many structural changes have been shown to occur in humans with kidney aging (summarized in Table 1), and these are present with varying severity. Overall, the kidney loses mass and there is increased calcification and renal cysts(30). An overall decrease in glomerular number occurs, and those that remain display hypertrophy, glomerulosclerosis, increased mesangial area, thickened GBM(40), and podocyte loss and morphological changes (33, 41).

Moving down the nephron, there is tubular atrophy, decreased total tubule length, interstitial fibrosis, and increased diverticules(37, 42, 43). There is an overall decrease in vascularity and many cases of a-glomerular circulation in nephrons(44). There is an increase in intimal and medial hypertrophy, as well as an increase in atherosclerosis. Circulating factors such as Angiotensin II increase, and there is a decrease in plasma aldosterone as well as vitamin D activation. All of these changes result in an increase in oxidative stress and chronic inflammation(45), a decrease in kidney function and repair, and an increased susceptibility to further kidney disease(42).

1.1.4 Molecular changes that play a role in kidney aging

The molecular basis of renal aging is under extensive study. Theories of cellular senescence, genomic instability, accumulation of oxidative damage(46), and telomeric shortening(47) have been explored using both human and animal studies. On the gene expression level, kidneys of elderly individuals differentially express many important genes that could disrupt function. There is an over-expression of genes involved in inflammation and extracellular matrix synthesis, with a decrease in the expression of genes that regulate lipid and glucose metabolism and degradation of extracellular matrix. There is an increase in NF-κB (32, 45, 48) and mTOR activation, a decrease in longevity factors such as Klotho(37) and Sirtuin family proteins(42, 49). Interestingly, Angiotensin II receptor blockers have been shown to suppress oxidative stress and inhibit NF-κB activation and inflammation in aged rat kidneys(50). Many of these molecular modulators of kidney aging have been manipulated using genetics and pharmacology in animal models of aging, and these studies provide further evidence of their roles in maintaining kidney health and extending healthspan and lifespan.

Studies in animals have led to a wealth of information as to the changes in kidneys that occur with aging. This research takes years and is very costly to perform. Also, there is little mechanistic evidence of what drives these age-related changes. Further, different cell types are exposed to varying kinds of stress and some can divide or be replaced after damage while others cannot. Therefore, the oxidative stress and damage that occurs over time will have different outcomes for the various kidney cell types. What has become clear is that diet, exercise, and genetics make the rate of aging and the length of health-span variable for both animals and humans. In this section, I aim to present the major modulators of kidney aging uncovered by studying animal models of aging to date.

1.1.4.1 Calorie restriction extends lifespan and uncovers important molecular players for renal aging

Calorie restriction was the first method used to increase lifespan in animal models. In 1935, McCay et al established that a reduced calorie diet, without malnutrition, extended maximum and average lifespan in rodents(51). Since then, numerous studies in small organisms such as yeast and worms, rodents, and primates have been completed in order to identify molecular programs involved in extending lifespan during calorie restriction(52-54). Long-term calorie restriction (CR) has been shown to prevent glomerular hypertrophy, mesangial expansion, podocyte loss, and glomerulosclerosis(55), markers of senescence(56), and overall evidence of aging nephropathy(57). While calorie restriction may not be a viable option for prevention of renal aging in humans, it has allowed us to uncover important factors that may serve as therapeutic targets. One common thread is that CR changes animal metabolism, and decreases factors that increase oxidative damage. Recently it's been shown that even short-term (8 wks) CR lessens age-

associated decline in autophagic flux, increased AMPK and SIRT1, decreased age-associated mTOR activation and mitochondrial damage, compared to ad libitum fed old rats(56, 58).

1.1.4.2 Modulation of insulin-like growth factor signaling delays aging in the kidney

It has become clear that reduction of insulin-like growth factor (IGF-1) signaling is one way of extending lifespan and delaying age-related pathologies(59, 60). Interestingly, Klotho protein, discussed in the following paragraph, can inhibit IGF-1 signaling, both *in vitro* and *in vivo(61).* In rats whose Growth Hormone (GH) and subsequent IGF-1 signaling was suppressed by an anti-sense GH gene, renal aging was largely prevented. Twenty-four month old transgenic mice had significantly fewer sclerotic glomeruli, decreased macrophage infiltration, and decreased myofibroblast populations. Suppressing IGF-1 elicits almost identical effects, adding evidence to the theory that GH signals mainly through IGF-1(62). When combined with CR, GH suppression resulted in an even greater delay of renal aging and extended lifespan significantly(63), suggesting there are some additional mechanisms involved in CR-induced preservation of renal function in aging. Importantly, mice over-expressing GH, developed evidence of accelerated renal aging with diffuse renal glomerulosclerosis(64). Importantly, complete inhibition of IGF-1 or GF can have deleterious effects on growth and immune function. Thus there are studies using controlled suppression as more viable options for therapies(65).

1.1.4.3 Klotho maintains kidney health with age

Klotho is highly expressed in the distal nephron. Klotho protein is secreted by proximal and distal convoluted tubules, and mediates its effect by binding to a cell surface receptor and repressing insulin/insulin-like growth factor signaling. Klotho mutation in mice leads to a decrease in lifespan and accelerated kidney aging(66, 67). Conversely, overexpression of Klotho leads to

an extension of lifespan(68). There is evidence that oxidative stress leads to a decrease of Klotho in the kidney and this can in turn increase cellular senescence(69). Klotho can also be found as a membrane bound form, binding to the transient receptor potential vallinoid-5 (TRPV5) and as a cofactor for FGF23 signaling, and has many implications in calcium and vitamin D metabolism(70). Klotho mutation leads to accelerated aging disorders such as vascular calcifications, ataxia, hypoglycemia, osteoporosis, and hyperphosphatemia, similar to what is seen with CKD patients on dialysis. Many more studies are underway to determine the implications of Klotho on kidney function and on aging in general(67, 70).

1.1.4.4 Sirtuin1 modulates NF-kB activity and preserves cellular integrity in the kidney

Sirtuin1, the most studied member of a family of class III deacetylases, is induced during calorie restriction-dependent extension of lifespan(71). SIRT1 is involved in regulation of many cellular processes, including metabolism, autophagy, and apoptosis(72). Sirt1 expression is decreased in the kidney of aged mice. In addition, heterozygous knockout of the *Sirt1* gene causes mitochondria in *Sirt1*$^{-/-}$ mice to resemble those from a mouse two-times older, and CR restriction did not prevent this(73). This provides evidence that Sirt1 may be exerting its effects through the mitochondria. SIRT1 deacetylates histones and many transcriptional regulators, including NF-κB. In the kidney, SIRT1 seems to protect cells from hypoxia, induces autophagy, and lessens fibrosis and inflammation(72, 74, 75).

A common thread between both CR and Sirt1 as longevity factors is the preservation of functional autophagy. Autophagy gene products eventually decline with age. In addition to this, autophagy impairment occurs and cells seem to lose their capacity to degrade as seen by the build-up of autophagic substrates such as p62/Sqstm1, and damaged mitochondria inside of autolysosomes.

1.1.4.5 Longevity factors in the kidney help to reduce oxidative damage and preserve autophagy and degradation

Could these longevity factors aid in preserving autophagy due to their ability to reduce oxidative damage(76)? Antioxidants, such as resveratrol prevent chronic NF-κB activation seen with aging by increasing Sirt1, while also regulating the mTOR activation(77). Perhaps preservation of autophagic machinery is also a beneficial side effect of this antioxidant therapy. Importantly, studies have shown that antioxidants can prevent Ang II or high glucose-induced autophagy in podocytes by decreasing ROS, and thereby decreasing oxidative damage accumulation(78, 79). As mentioned above, the post-mitotic podocyte depends on a high-rate of basal autophagy to maintain its health. Hartleben et al, provided strong evidence that defective autophagy in podocytes causes accelerated kidney aging nephropathy, including accumulation of oxidized proteins and damaged organelles(27). In kidney injury states, autophagy is induced to reduce damage and restore homeostasis. However, at some point with aging, the degradative process fails to work adequately(5, 22, 80, 81), and this leads to proteinuria, glomerulosclerosis, and tubule damage(80). Many suggested therapies involve autophagy-activating drugs, some through mTOR inhibition. However, regulated mTOR activation, as discussed above, is important for podocyte health and necessary for autophagic flux in podocytes(20, 21). In addition, autophagy inducers may fail to work, if the autophagic machinery is no longer functional.

As we age, there is evidence of accumulation of lipofuscin and free radicals in the lysosome, as well as decreased LAMP2 expression(82). This contributes to a decrease in autophagy. In addition, mouse studies with inducible LAMP2 expression in the liver, showed restored levels of autophagy, restored healthy mitochondria, and clearance of damaged biomolecules that accumulate with aging(83). Additionally, compounds that activate TFEB, a

transcription factor that induces lysosomal and autophagy genes, restore autophagy and lysosomal reformation in LPS-induced septic hearts, ameliorating damage(84). Perhaps, since it is not always plausible to prevent age-related pathologies in the kidney, therapies that aim to restore autophagy-lysosomal function may be a more effective method to reverse aging pathologies.

1.1.5 Questions that remain

Research in animals has taught us a lot about the factors and genetic programs involved in renal aging, but these studies are lengthy and have yet to provide us with clear evidence of the mechanism of progression and the role of various cell types in propagating age-related CKD. The information provided here on changes that occur with kidney aging is summarized in Table 1. While it seems as though glomerular damage may be a key component, it is not clear as to whether this damage is causing subsequent tubule injury and CKD with aging. Perhaps damage accumulation in the tubules is playing a large role in causing functional decline. There is a need for better models that allow for timely studies of the progression of aging nephropathy, as well as tools with which we can separate out the roles of the various cells in the nephron. But, how is it possible to cause aging in one cell type while maintaining the inherent health of the others? This thesis utilizes a mouse model of human progeria and the power of genetic manipulation to begin to answer these questions.

Structural Changes	Functional Changes	Altered Genes/Factors
Decreased kidney mass, thinning cortex(31)	Decreased GFR(42)	Decreased Klotho(85)
Glomerulosclerosis(32)	Increased urinary ACR(5)	Increased NF-κB activation(32)
Thickened GBM(86), TBM(40)	Hyperkalemia(38)	Increased mTOR activation(87)
Interstitial Fibrosis(88)	Reduced sodium conservation(36)	Decreased autophagy genes, impaired autophagic degradation(27)
Tubule Atrophy, loss(89)	Decreased concentration of urine(90)	Decreased Sirt1(72)
Membranous nephropathy(28)	Impaired fluid balance(91)	Increased p16, p21, p53 protein
Increased calcification(70), cysts	Decreased capacity to decrease urinary pH(42)	Decreased antioxidant genes, e.g., ceroplasmin(92)
Decreased vascularity(93)	Decreased vitamin D activation(94)	Increased Ang II signaling(95)
Increased intimal/medial hypertrophy(42)		Decreased aldosterone in circulation(96)
Glomerular hypertrophy(55), decreased glomerular #(97)		Decreased plasma RA(96)
Podocyte effacement, loss(98)		Increased fibrotic factors(99)
Mesangial proliferation(28)		
Increased macrophage infiltration(62)		
damaged mitochondria(56), accumulating autolysosomes(81)		

Table 1. Summary of Kidney Changes with Aging.

Table of structure and functional changes in the aging kidney, as well as genes and other factors that are altered in aged kidneys and have been shown to play a role in kidney aging. Abbreviations used: Glomerular Basement Membrane (GBM), Tubular Basement Membrane (TBM), Glomerular Filtration Rate (GFR), Albumin Creatinine Ratio (ACR), Nuclear Factor Kappa-light-chain-enhancer of activated B cells (NF-κB), mammalian Target of Rapamycin (mTOR), NAD dependent deacetylase sirtuin-1 (Sirt1), Angiotensin II (Ang II), Renin-angiotensin (RA)

1.2 ERCC1 MODEL OF ACCELERATED AGING

Aging is a complex process that manifests differently in each cell type, and depends on the various levels of stress, replication, environmental factors, and genetic regulatory programs that are present in each tissue and cell. Endogenous DNA damage occurs in all cell types to various extents, and as our cells age, any damage not repaired may accumulate and promote the aging process. The ERCC1 (Excision Repair Cross Complementary Group 1) protein forms an endonuclease that, along with its obligate binding partner, XPF (Xeroderma Pigmentosum Group F), is involved in various kinds of DNA damage repair. It is most well known for its function in nucleotide excision repair (NER) of bulky chemical lesions, but is also important in the repair of some double-strand breaks (DSBs) and interstrand crosslinks (ICLs)(100, 101). Human disease is caused by deficiency of XPF or Ercc1, including xeroderma pigmentosum (XP)(102), an accelerated aging or progeroid disease called XFP progeroid syndrome, cerebro-oculo facioskeletal syndrome (COFS)(101), Cockayne Syndrome (CS), and Fanconi Anemia(103-105). These rare but serious diseases have led to the development of mouse models, and have illustrated that Ercc1 and XPF are important in preventing age-related pathologies.

1.2.1 ERCC1-XPF DNA repair enzyme in human health and disease

The XPF-ERCC1 binding pair is an endonuclease responsible for excision at the 5' end of various types of DNA lesions(106). The XPF protein contains the endonuclease catalytic activity and ERCC1, its binding partner, is necessary for binding to DNA. The pair excises UV damaged nucleotides, such as cyclopyrimidine dimers (CPDs) during nucleotide excision repair. Therefore, humans with ERCC1 or XPF deficiency (XP) have extreme photosensitivity and an extremely high incidence of cutaneous and ocular neoplasms(107). However, the Ercc1-XPF pair are also involved in repairing ICL's and DSB's, so deficiency of either protein has diverse effects in multiple tissues as cells divide and are exposed to different levels of oxidative damage.

Patients with XPF or Ercc1 mutations have a range of photosensitivity and onset of skin carcinomas, as well as severe neurodegenerative and ocular defects, and some patients have accelerated aging or progeroid syndrome(101), including neurodegeneration, renal insufficiency, loss of subcutaneous fat, liver disease, kyphosis, vision and hearing loss, appearing in prepubescence. Patients with various mutations display a variety of symptoms. One patient with an *Ercc1* mutation had severe COFS syndrome(108), and another had severe neurodegeneration that was progressive and resulted in cortical atrophy and dementia. Another patient had pronounced progeroid features, severe renal insufficiency (GFR: 17ml/min x 1.73 m^2 and proteinuria with levels of 1.8g/m^2/24hr) and extremely small and dense kidneys. As a result, he had hypoalbuminemia, anemia, and acidosis, as well as elevated liver enzymes, optic atrophy, ataxia, and many other aging pathologies. These symptoms are not usually seen in XP patients, who primarily have symptoms of UV-sensitivity and sometimes neurodegeneration. However, this patient cell's also displayed only 5% of the normal UV-induced DNA repair, consistent with

XP(102) and he had an *Xpf* mutation. This discovery led to a new progeroid syndrome called XFE, and another patient with strikingly similar symptoms was recently been identified(101).

The clinical manifestations and severity of disease likely depend on how each mutation affects the protein expression and subcellular localization of the XPF-ERCC1 complex. These accelerated aging symptoms are strikingly similar to what is seen in mouse models deficient in either *Ercc1* or XPF. Knock-out mice for *Xpf* or *Ercc1* have identical phenotypes of accelerated aging(101), supporting the evidence that XPF and ERCC1 are obligate partners and rely on each other for stability and function.

1.2.2 *Ercc1* deficient mouse models.

The *Ercc1* gene was first knocked out by McWhir et al(109) and by another independent laboratory, Weeda et al(110). Knock-out is lethal in true inbred mice, and therefore is studied in a mixed background of C57BL/6 and FVB/n. *Ercc1*$^{-/-}$ mice live approximately 28 days and display severe neurodegeneration and very accelerated aging phenotypes. Genome-wide mRNA expression levels were compared between *Ercc1*$^{-/-}$ mice and their wild-type (WT) littermates, to those that occur between young and old WT, and significant overlap was observed, providing some evidence that endogenous DNA damage may contribute to aging pathologies. XPF knockouts, first created by Tian et al., (111), have a strikingly similar phenotype to *Ercc1*$^{-/-}$ mice, displaying the same neurodegenerative and liver function defects. The *Ercc1* deficiency in a mouse was corrected in the liver only of knock-out mice improved many symptoms including growth and lifespan(112). However, these animals developed renal insufficiency by 7 weeks and progressive chronic kidney disease, suggesting that the kidney and liver cells in *Ercc1* -/- mice are some of the most sensitive to endogenous DNA damage.

In order to mirror some of the human diseases and study the progression in a longer lived *Ercc1* deficient mouse, a truncated *Ercc1* allele was created that results in reduced *Ercc1* message levels and only about 10% of the protein expression levels(110). When this allele is combined with a null allele, resulting in the *Ercc1*$^{-/\Delta}$ mouse, the phenotype is very similar in all organ systems to the *Ercc1*$^{-/-}$ mouse. However, they are born with Mendelian frequency, display progressive aging pathologies after development, and live 6-7 months (Figure 4)(101). Therefore *Ercc1*$^{-/\Delta}$ mice serve as a slower, more physiologically relevant, accelerated aging model(101). This model is then useful in studying the mechanism of aging in various tissues, as well as identifying new targets for therapy.

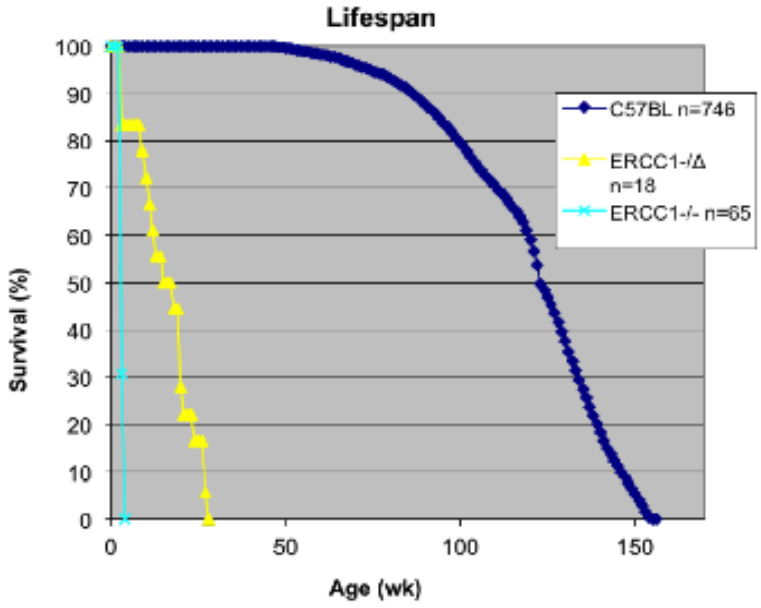

Figure 4. Lifespan of *Ercc1* Mouse Models

The liver of the *Ercc1*$^{-/\Delta}$ mouse exhibited characteristics of accelerated aging by 20-23 weeks of age(113). These included sinusoidal changes, such as thickening of endothelial cells, deposition of basement membrane and defenestration, inflammation, loss of liver regenerative capacity, and loss of function as indicated by serum markers. In addition, and similar to naturally aged WT livers, the *Ercc1*$^{-/\Delta}$ livers showed cell senescence, shown by

p16 expression, SA-β–galactosidase (SA-β–gal) activity and large nuclear size. Finally, there was evidence of oxidative damage, shown by increased lipid peroxidation and accumulation of lipofuscin and oxidative DNA damage(114), all characteristic of natural aging(82, 113, 115-117). This demonstrates that the *Ercc1*$^{-/\Delta}$ mouse is a useful tool to study liver aging. In this thesis, I will demonstrate that it is also a valuable and accurate tool to study the progression of kidney aging, which seems to occur at a younger age in the *Ercc1*$^{-/\Delta}$ than the detected liver age-related changes.

1.3 SUMMARY

Kidney aging likely plays a large role in the high incidence of CKD and ESRD that occurs in the U.S. and worldwide(28, 118). There is a wealth of descriptive information about the functional and structural changes that occur in kidney aging, but it is nearly impossible to decipher the progression and mechanism in humans who typically have multiple confounding factors. Therefore, we rely largely upon animal models. Rodent models have been useful because of similar changes observed with human kidney aging, and they allow for genetic manipulation. These studies have identified many factors involved in the aging process, as well as longevity factors that protect renal function from deleterious aging pathologies. In mice and rats, these studies take years and largely involve comparing old animals to young. It is very time-consuming and costly to try to learn about the timing and progression of events that occur over the course of 2-3 years. Additionally, it is difficult to separate out the roles of various kidney cells in driving aging nephropathy. The *Ercc1* deficient mouse models of human progeria provide an efficient and

accurate way of studying the aging process due to endogenous DNA damage. Secondly, they provide a way to determine cellular roles in driving aging diseases using cell specific knock out of the *Ercc1* gene. In this way, the mouse models presented in this thesis may facilitate discovery of targeted therapies. Finally, this accelerated aging model will also be useful in discovery of new aging biomarkers. It has become apparent that kidney aging does not occur at the same rate or to the same extent in all individuals, and this may impact what therapies are appropriate in CKD patients. In the following chapter, I will present the *Ercc1*$^{-/\Delta}$ mouse model of accelerated kidney aging, validating it by comparing it systematically to naturally aged mice. Finally, in Chapter 3, I will determine the timing and progression of pathological changes with aging, and I will use cell-specific knock-outs to show that the glomerular podocyte is the main renal cell responsible for driving age-related CKD in the *Ercc1* deficient mouse.

2.0 ACCELERATED RENAL AGING IN THE ERCC1 DEFICIENT MOUSE MODEL OF HUMAN PROGERIA

Chapter 2 is adapted from: **Kathryn E. Wack, M.S., Siobhán Q. Gregg, Ph.D., Tania A. Rozgaja, Ph.D., Amanda P. Beck, D.V.M., D.A.C.V.P., Sheldon Bastacky, M.D., Verónica Gutiérrez, M.Sc., Andria R. Robinson, Ph.D., Mark A. Ross, B.Sc., Lora H. Rigatti, D.V.M., Jing Zhao, B.S., Tyler Woodell, M.D., Jin Wang, Ph.D. Mohammad Fallahi-Sichani, M.S., Paul D. Robbins Ph.D., Yinsheng Wang, Ph.D., Donna Beer Stolz, Ph.D., Laura J. Niedernhofer, M.D., Ph.D. (2014) Accelerated renal aging in a murine model of progeria caused by a DNA repair defect.** Paper is currently in submission.

With aging, kidney structure and function are lost leading to increased risk of chronic kidney disease (CKD), end-stage renal disease and mortality. The incidence of CKD is rising, thus animal models of rapid renal aging are needed to accelerate research on causes and treatments of CKD. *Ercc1*$^{-/\Delta}$ mice model a progeria caused by low expression of the DNA repair nuclease ERCC1-XPF. *Ercc1*$^{-/\Delta}$ mice develop progressive multi-organ degeneration over a 7 month lifespan. To determine if *Ercc1*$^{-/\Delta}$ mice mimic natural renal aging, structural and functional changes in the kidneys from progeroid mice were compared to those of old wild-type (WT) mice. Renal development was normal in *Ercc1*$^{-/\Delta}$ mice but by 6 mo of age the animals exhibited glomerulosclerosis and tubulointerstitial fibrosis similar to 2-3 yr-old WT mice. *Ercc1*$^{-/\Delta}$ mice developed albuminuria and podocyte effacement by 1 mo. At 2 mo, the glomerular filtration rate was reduced 5-fold in *Ercc1*$^{-/\Delta}$ mice similar to 2 yr-old WT mice. At 5 mo, the blood urea nitrogen in *Ercc1*$^{-/\Delta}$ mice was doubled and the extent of podocyte degeneration matched 2 yr-old WT mice.

Both progeroid and old WT mice had increased intracellular adhesion molecule-1 and smooth muscle actin-positive cells, macrophage infiltration, senescence markers and endogenous oxidative DNA damage. These data demonstrate that renal aging is accelerated 5-6 fold in *Ercc1*$^{-/\Delta}$ mice and endogenous DNA damage plays a causative role in CKD.

2.1 INTRODUCTION

Chronic kidney disease (CKD) is a major health concern because its incidence is increasing, patient outcome is poor, and the costs associated with treatment are high (119). Aging is a major risk factor for CKD and other age-related conditions such as diabetes and hypertension compound this risk. CKD can lead to end-stage renal disease (ESRD) and it is also predictive of cardiovascular disease (120). Renal diseases are the ninth leading cause of death in the USA (121). Approximately 70 billion dollars is spent worldwide on medical costs associated with ESRD (122). Animal models of rapid kidney aging would dramatically accelerate research on the molecular basis of renal aging and susceptibility to CKD, as well as treatments.

Increased age is associated with a reduction in renal cortical mass(41). Renal senescence encompasses the age-related changes that occur in the kidney with aging and includes interstitial fibrosis, tubular degeneration and glomerulosclerosis and a linear decline in glomerular filtration rate (GFR) after the fifth decade of life (123). There is also up-regulation of ICAM in endothelium and macrophage infiltration with aging (45), indicative of inflammation. Shortened telomeres and increased expression of the senescence marker $p16^{INK4a}$ are observed in kidneys from elderly patients (47, 124).

The environmental and genetic variability in humans makes studying renal aging challenging. Mice are a useful model system because these variables can be controlled. However, it still requires a lengthy investment to perform studies on aged (2-3 yr old) mice. One approach to overcome this is to use mouse models of accelerated aging or progeria. Werner, Cockayne and XFE progeroid syndromes are examples of inherited diseases with accelerated aging of one or more tissues (125).

Patients with XFE progeroid syndrome display accelerated aging of all organ systems beginning in the second decade of life, including renal insufficiency and proteinuria (102). XFE is caused by mutations in *XPF*, which encodes one subunit of the DNA repair endonuclease Excision repair cross complementation group 1-Xeroderma pigmentosum group F (ERCC1-XPF). The enzyme is involved in the repair of DNA lesions including interstrand crosslinks, double-strand breaks and helix-distorting monoadducts (100, 106, 126). ERCC1 and XPF are obligate binding partners, stabilizing one another *in vivo* (127). Accordingly, *Ercc1*$^{-/-}$ and *Xpf*$^{-/-}$ mice have an identical phenotype (110, 111). *Ercc1*$^{-/-}$ mice die in the 4th wk of life with age-associated degenerative changes, including osteoporosis, neurodegeneration, bone marrow hypoplasia, epidermal atrophy, sarcopenia and liver and kidney dysfunction (102, 112, 128). We and others previously described *Ercc1*$^{-/\Delta}$ mice, a hypomorphic model of XFE progeroid syndrome that express approximately 5% of the normal complement of ERCC1-XPF and live longer than *Ercc1*$^{-/-}$ mice (28 vs. 4 wks) (113, 129-131). *Ercc1*$^{-/\Delta}$ mice are healthy into adulthood (8 wks) then begin to show progressive symptoms associated with aging. The aim of this study was to systematically compare the kidney of progeroid *Ercc1*$^{-/\Delta}$ mice to that of old wild-type (WT) mice (2+ yrs-old) to determine if the renal degeneration occurring in *Ercc1*$^{-/\Delta}$ mice is an accurate model of natural aging that could be used to accelerate research on the biology of kidney aging and therapeutic interventions to prevent, delay or ameliorate CKD in old age.

2.2 MATERIALS AND METHODS

Animal Care and Experimentation

Animal work was approved by the University of Pittsburgh and Scripps Florida Institutional Animal Care and Use Committees and is in accordance with NIH guidelines for humane care of animals. Ercc1$^{-/\Delta}$ mice were bred and genotyped as previously described (126). All mice were in a congenic f1 background generated by crossing inbred FVB/n and C57Bl/6 mice.

Histological analyses

Ercc1$^{-/\Delta}$ mice at 8 wks (pre-symptomatic adults), 16 wks (progeroid) and 23 wks (near terminal) were sacrificed by CO_2 inhalation with age-matched and old (25 and 36 mo) WT mice. Some animals were injected intraperitoneally with bromodeoxyuridine (BrdU; 50μL of a 10 mg/ml solution in sterile Dulbecco's phosphate-buffered saline (PBS); BD Pharmingen, San Jose, CA) weekly x 8 wks to label proliferating cells. Post-mortem, the kidneys were excised and fixed with 10% formalin and embedded in paraffin. Tissue sections (6 μm) were cut and stained with haematoxylin and eosin (H&E), Masson trichrome, and Periodic acid-Schiff stain (PAS). Alternatively, tissue specimens were cryopreserved by fixation in 2% paraformaldehyde in PBS for 2-4 hours, followed by 30% sucrose at 4°C overnight, then frozen in liquid N_2-cooled isopentane for sectioning on a Microm™ HM 525 cryostat (Thermo Scientific; Waltham, MA).

Quantification of cPu lesions as a measure of oxidative DNA damage

5'R and 5'S diastereomers of 8,5'-cyclopurine-2'deoxynucelosides in genomic DNA isolated from whole kidney lysates were measured by LC-MS/MS/MS as previously described (114).

Kidney perfusion and processing for ultrastructural analysis

For EM, the kidney of euthanized animals was cleared of blood by perfusion with PBS at 3 mL/min via cardiac puncture then perfuse-fixed with 2.5% glutaraldehyde and processed as described previously (113). 350 nm sections were cut and stained with Toluidine Blue. TEM images were captured with the JEOL JEM 1011 microscope and SEM images were taken with the JEOL JSM 6330F microscope (JEOL Ltd, Peabody, MA).

Immunohistochemical analyses

IHC was performed on deparaffinized kidney sections as previously described (113). Endogenous peroxidase activity was blocked with 3% H2O2. Sections were subjected to heat induced-epitope retrieval in sodium citrate buffer (10 mM, pH 6.0) for 30 min in a decloaker, followed by 30 min cool-down. Blocking was done with 5% rabbit serum for 20 min. Detailed information about antibodies is provided in supplemental information. Hematoxylin was used as a counterstain. Primary antibody (sheep anti-BrdU, Abcam, Cambridge, MA) was applied for 1 hr at room temperature (1:200). Biotinylated secondary antibody was applied for 30 min (1:1000) followed by VECTASTAIN avidin:peroxidase detection complex (ABC Elite, Vector Laboratories, Burlingame, CA) for 30 min. 3,3C Elite, Vector La (DAB) chromagen (Dako Cytomation, Carpinteria, CA) was applied for 6 min, followed by a two rinses with distilled water. Hematoxylin was used as a counterstain. Bright field images were captured using an Olympus BX51 fluorescent microscope.

Immunofluorescence analyses

IF was performed on frozen kidney sections as previously described (113). Briefly, kidneys were fixed in 2% paraformaldehyde in PBS for 2-4 hrs followed by 30% sucrose at 4°C overnight, then frozen in liquid N_2-cooled isopentane and sectioned (7 μm thick) on a Microm™ HM 525 cryostat

(Thermo Scientific; Waltham, MA). Primary antibody was incubated at room temperature for 1 hr (goat anti-CD68, Santa Cruz Biotechnology, Inc., Santa Cruz, CA; anti-SMA:Cy3, Sigma, St. Louis, MO; rat anti-CD45 or rat anti-CD31 (PECAM) both from BD Pharmingen, San Jose, CA; or hamster anti-ICAM, BD Biosciences, San Jose, CA) all at a dilution of 1:100. Sheep anti-BrdU (Abcam, Cambridge, MA) was 1:200. Anti-phospho-γH2AX (Ser139) (Millipore, Billerica, MA) was incubated overnight at 4°C at 1:200. The secondary antibodies (Invitrogen, Eugene, OR; Jackson ImmunoResearch Laboratories, West Grove, PA), were added for 1 hr in the dark at room temperature. Rhodamine-labeled wheat germ agglutinin was used at 2 μg/ml and incubated for 30 min at room temperature (Rhodamine Lectin Kit I, Vector Laboratories, Burlingame, CA). Nuclei were stained with Vectashield with DAPI mounting medium (Vector Laboratories, Inc., Burlingame, CA). Images were acquired using an Olympus Fluoview 1000 inverted confocal microscope.

Albumin/creatinine ratio measurement

Urine was collected first thing in the morning weekly and albumin levels measured using an Albumin Elisa Kit (Bethyl Laboratories, Montgomery, TX) normalized to creatinine levels using the Creatinine Urine Assay Kit (Cayman Chemical, Ann Arbor, MI). An n=3 was used for each time point and the average values plotted ± S.E.M.; significance was calculated using the Student's two tailed *t*-test; $*p < 0.05$.

Determination of GFR

GFR was measured using FITC-inulin clearance by modified protocol (132). Briefly, mice (n=3 per group) were given a bolus injection of a 2.5% FITC-inulin (Sigma-Aldrich, St. Louis, MO) solution retro-orbitally (2 μl per g body weight). Blood was collected from the tail tip before injection and 3, 5, 7, 10, 15, 20 and 40 min post-injection. Plasma was isolated and samples were

diluted 1:10 in 0.5M Hepes. FITC fluorescence was measured in duplicate for each animal using a Perkin Elmer EnVision 2104 Multilabel Reader. GraphPad Prism was used to plot FITC-inulin concentration using a two-phase exponential decay model. GFR was normalized using body weight and expressed as μl/min/g BW.

Renal function

Blood was collected by heart puncture from 6 animals per group and placed in plasma separator tubes coated with lithium heparin (BD Microtainer, Franklin Lakes, NJ). The plasma was sent to Antech Diagnostics (Pittsburgh, PA) for renal function tests. The average of values from 6-7 mice were plotted ± S.D. significance was calculated using the Student's two tailed *t*-test; $*p<0.05$.

Immunoblotting

Flash frozen renal tissue was weighed and homogenized in RIPA buffer (Thermo Scientific, Pittsburgh, PA) containing Complete mini-protease inhibitor cocktail (Roche, Branchburg, NJ). 25 □g protein was resolved on 4-20% Mini Protean TGX polyacrylamide gels (Bio-Rad) and proteins detected as previously described (113). p53 was detected with mouse anti-p53 (1:900, Cell Signaling, Beverly, MA). p21 was detected with rabbit anti-p21 (1:450, Abcam, Cambridge, MA). p16 was detected with mouse anti-p16 (1:100, Santa Cruz, Santa Cruz, CA). γ–H2AX was detected with mouse anti- γ-H2AX (1:1000, Millipore, Billirica, MA). Tubulin was used as a loading control and detected with rabbit anti-tubulin (1:7500, Abcam, Cambridge, MA). Secondary antibodies used were either anti-rabbit HRP (1:3000, Invitrogen, Carlsbad, CA) or anti-mouse HRP (1:3000, Cell Signaling, Beverly, MA).

Analysis of Gene Expression Data

The kidney Affymetrix dataset GSE43061 was downloaded from NCBI GEO database. The Mouse Gene 1.0 ST chip CEL files were imported into GeneSpring GX v12.1. The Robust Multi-

array Average (RMA) algorithm was utilized to calculate probe-set signals on each chip. The summarization algorithm was set to ExonRMA16 and the normalization parameter was set to quantile. Probe sets with signal higher than chip 20th percentile were selected for statistical analysis, which allowed one wildcard in each group of replicates. The Ercc1-/ □ 14 wk and V wk were compared to the WT 14 wk. To find differentially expressed probe sets in each comparison GeneSpring filter on the Volcano plot function was used. The unpaired t-test p-value cut-off was set to 0.05, the fold change cut-off was set to 1.5, and the p-value computation method was set to Asymptotic. Two lists of differentially expressed probe sets were created based on the above comparisons. The shared probe sets between these two lists were identified and annotated in GeneSpring. R programming language was used to calculate the overlap p-value between the two differentially expressed gene lists.

TUNEL Assay

To detect apoptotic cells, kidneys were fixed in 2% paraformaldehyde in PBS for 2-4 hrs followed by 30% sucrose at 4°C overnight then frozen in liquid N_2-cooled isopentane and sectioned on a Microm™ HM 525 cryostat (Thermo Scientific; Waltham, MA). The kidney sections were stained with the terminal deoxynucleotidyl dUTP nick ending labeling (TUNEL) kit (Roche, Indianapolis, IN), followed by an anti-streptavadin-Cy5 secondary antibody (Jackson Immunoresearch, West Grove, PA). Samples were co-stained with DAPI nuclear stain and mounted with gelvatol under coverslips. Samples were then imaged on an Olympus Fluoview 1000 confocal microscope at 200X and analyzed for co-localization of TUNEL stain and DAPI. The kidney from a 18 wk-old normal mouse isolated 1 month following exposure to 0.175 Gy of total body ionizing radiation weekly x 4 weeks was used as a positive control.

Detection of Senescence-Associated β-Galactosidase

Tissues fixed in 10% formalin for 4 hrs at 4°C were embedded in O.C.T. compound (Tissue-Tek, Sakura, Torrance, CA) then cryosectioned at 5 mM thickness using a Leica Cryostat. Slides were storedat -80°C until staining. Tissue sections were thawed by washing them in PBS and then stained for SA-bgal activity using X-gal staining solution (40 mM citric acid in sodium phosphate buffer, 5 mM K4[Fe(CN)6] 3H2O, 5 mM K3[Fe(CN)6], 150 mM sodium chloride, 2 mM magnesium chloride and 1 mg/ml X-gal dissolved in N,N-dimethylformamide) at pH 6 for 5-6 hours at 37°C as described previously (133). Slides were mounted with VectaShield (Vector Laboratories, Burlingham, CA) and visualized under bright field microscopy using an Olympus microscope at 10X magnification.

2.3 RESULTS

2.3.1 Histopathologic changes in progeroid *Ercc1*$^{-/\Delta}$ mouse kidney mimic normal aging

To investigate structural changes in the kidney of progeroid *Ercc1*$^{-/\Delta}$ mice, we compared renal tissue of 8, 16, and 23 wk-old *Ercc1*$^{-/\Delta}$ mice to age-matched and old (25 and 36 mo) WT mice (Figure 5A). Histologic evaluation of hematoxylin and eosin (H&E) stained sections revealed normal kidney architecture in 8 wk-old *Ercc1*$^{-/\Delta}$ mice demonstrating that their renal development is normal. In contrast, the kidneys from 16 and 23 wk-old *Ercc1*$^{-/\Delta}$ exhibited glomerular changes, including increased mesangial matrix and segmental thickening of capillary loops. Similar lesions were observed in much older WT mice (25 and 36 mo-old). Additionally, the 36 mo WT mice had multiple foci of tubulointerstitial mineralization, not observed in younger WT animals. None of

the above lesions were observed in 8 wk *Ercc1*$^{-/\Delta}$ or 16 and 25 wk WT mice, demonstrating that the lesions are degenerative in nature. Period acid-Schiff's (PAS) reagent staining revealed thickening of glomerular capillary loops in the 16 and 23 wk-old *Ercc1*$^{-/\Delta}$ and 25-36 mo-old WT mice, in addition to thickened glomerular and tubular basement membranes in the 23 wk-old *Ercc1*$^{-/\Delta}$ and 25-36 mo-old WT mice. Masson's trichrome staining indicated mild tubulointerstitial fibrosis in the 16 wk *Ercc1*$^{-/\Delta}$ mice and varying degrees of tubulointerstitial fibrosis and glomerulosclerosis in the 23 wk *Ercc1*$^{-/\Delta}$ and 25-36 mo-old WT mice. Sections from progeroid and aged kidney with glomerulosclerosis were stayed with Congo Red to detect glomerular amyloid deposition and all samples were negative. Interstitial fibrosis and glomerulosclerosis are common in kidneys of aged humans (30). These data suggest that normal aging-related degenerative changes occur spontaneously and rapidly in kidneys of *Ercc1*$^{-/\Delta}$ mice.

The degenerative changes that occur in *Ercc1*$^{-/\Delta}$ mice are presumed to arise as a consequence of failure to repair endogenous DNA damage (134). 8,5'cyclopurine-2'deoxynucleosides are oxidative lesions that occur endogenously (135). We previously demonstrated that the four diastereomers of cyclopurine lesions (5'*R* and 5'*S* of dA and dG cPu) accumulate with aging in WT and more rapidly *Ercc1*$^{-/\Delta}$ mice, but in a tissue specific manner (114). At 10 wks of age, when *Ercc1*$^{-/\Delta}$ mice do not have extensive histopathologic changes in the kidney, the level of cPu lesions in the kidneys of these mice is similar to that of WT littermates (Fig. 5B). By 21 wks of age, the level of cPu lesions increased 4-fold in the kidney of *Ercc1*$^{-/\Delta}$ mice. This was significantly higher than cPu levels in age-matched WT mice, but similar to 3 yr-old WT mice. Thus, identical oxidative DNA lesions accumulate with accelerated and normal aging, and there is a strong correlation between elevated levels of DNA damage and onset of CKD.

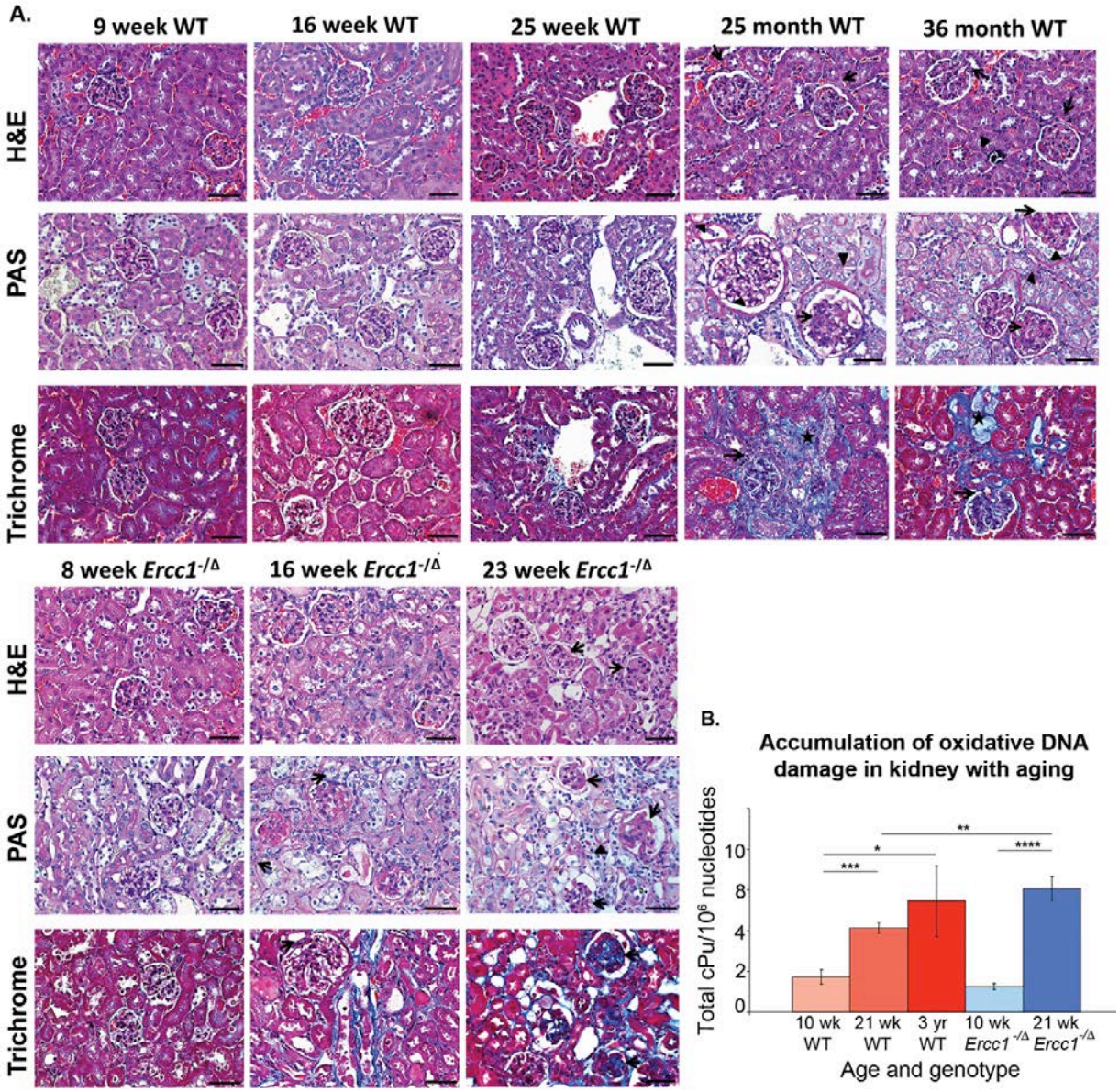

Figure 5. Histopathological changes in progeroid *Ercc1*$^{-/\Delta}$ and aged WT mouse kidneys

(A) Histologic evaluation of kidneys from *Ercc1*$^{-/\Delta}$ mice of increasing age as well as age-matched controls and old WT mice. Hematoxylin and eosin (H&E) stained sections from 16 and 23 wk *Ercc1*$^{-/\Delta}$ and 25 and 36 mo WT mice glomerular lesions, including increased mesangial matrix and segmental thickening of capillary loops (arrows). In addition, 23 wk *Ercc1*$^{-/\Delta}$, 25 and 36 mo WT mice display thickening of the glomerular basement membrane. The 36 mo WT mouse has multiple foci of tubulointerstitial mineralization (arrowhead). Period acid-Schiff's (PAS) reagent staining highlights the thickening of glomerular capillary loops (arrows) in the 16 wk and 23 wk *Ercc1*$^{-/\Delta}$ and 25 and 36 mo WT mice, in addition to thickened glomerular and tubular basement membranes (arrowhead) in the 23 wk *Ercc1*$^{-/\Delta}$ and 25 and 36 mo WT mice. Masson's trichrome staining revealed mild tubulointerstitial fibrosis (star) and glomerulosclerosis (arrow) in the 16 and 23 wk *Ercc1*$^{-/\Delta}$ as well as the 25 and 36 mo WT mice. In all panels, scale bar = 50μm. (B) Accumulation of oxidative DNA damage in kidney with normal and accelerated aging. Data from Wang

et al (114) were re-graphed to indicate the total number of cyclopurine lesions (5'*R*-cdA + 5'*S*-cdA + 5'*R*-cdG + 5'*S*-cdG) per 10^6 nucleosides. The values represent the mean and standard error from kidney of 3 animals per group. An unpaired two-tailed *t*-test was used to calculate *p* values. *p,0.05; **p<0.01;***p<0.001.

2.3.2 Functional changes in progeroid *Ercc1*$^{-/\Delta}$ mouse kidney mimic normal aging

Renal function can be assessed by examining clinical chemistries. High levels of urea, a nitrogenous waste product, in the serum can indicate decreased renal function (136). Blood urea nitrogen (BUN) levels were normal in 7-12 wk-old *Ercc1*$^{-/\Delta}$ mice, but by 20 weeks of age, the mutant mice exhibited significantly elevated BUN values compared to their normal siblings (Table 2). In mice, alkaline phosphatase (ALP) is found in the highest concentration in the kidney and intestine (137). Elevations in ALP may reflect acute renal damage due to increased cell death or reduced serum clearance of the enzyme (138). By 6-7 wks of age, *Ercc1*$^{-/\Delta}$ mice had significantly increased ALP values compared to age-matched controls indicating parenchymal injury. Serum lipase was also significantly elevated by 6-7 wks of age in *Ercc1*$^{-/\Delta}$ mice compared to age-matched controls. Though serum lipase is not renal-specific, it is excreted by the kidney
and may be elevated with renal disease due to decreased clearance (138).

Genotype	Age (wks)	BUN (mg/dL)	ALP (U/L)	Lipase (U/L)	Albumin (g/dL)	Creatinine (mg/dL)
WT	6-7	24 ± 5	146 ± 26	86 ± 25	3.1 ± 0.5	0.37 ± 0.12
	10-12	25 ± 6	112 ± 15	91 ± 15	3.4 ± 0.3	0.36 ± 0.05
	20-23	23 ± 4	56 ± 13	67 ± 3	2.9 ± 0.2	0.32 ± 0.04
	108-128	26 ± 16	48 ± 21	75 ± 32	2.8 ± 0.4	0.32 ± 0.04
Ercc1$^{-/\Delta}$	6-7	25 ± 6	208 ± 40*	120 ± 18*	2.7 ± 0.2	0.37 ± 0.16
	10-12	29 ± 8	207 ± 81*	132 ± 20*	2.5 ± 0.6*	0.32 ± 0.04
	20-23	60 ± 26*,**	316 ± 170*	132 ± 31*	1.9 ± 0.5*,**	0.42 ± 0.15

Table 2. Serum chemistries relevant to renal function

*p<0.05 between *Ercc1*$^{-/\Delta}$ and age matched controls (Student's two tailed t-test).

**p<0.05 between age groups of one genotype (Student's two tailed t-test).

Hypoalbuminemia may develop secondary to the loss of protein via the glomerular membrane and/or failure of tubular reabsorption (138-140). At 10-12 wks of age, *Ercc1*$^{-/\Delta}$ mice had significantly lower serum albumin levels than age-matched controls. By 21 weeks of age, *Ercc1*$^{-/\Delta}$ mice exhibited hypoalbuminemia. Serum creatinine levels did not differ significantly from controls at any age.

Glomerular filtration is a direct measure of renal function. GFR was measured by determining the rate of FITC-inulin clearance from the blood (Figure 6A). Adult WT mice had a GFR within normal range (141) (8-12 μl/min/g body weight. The GFR was within normal range for 4 wk *Ercc1*$^{-/\Delta}$ mice (9.2 μl/min/g). But by 8 wks of age, the *Ercc1*$^{-/\Delta}$ mice had a significantly reduced GFR of 2.4 μl/min/g. Old WT mice (25 mo) had a GFR of 3.1 μl/min/g, which was significantly reduced from adult WT mice but similar to the GFR of 12-16 w- *Ercc1*$^{-/\Delta}$ mice.

To determine the age at onset of proteinuria, the albumin/creatinine ratio (ACR) in urine was measured weekly in young WT and *Ercc1*$^{-/\Delta}$ mice (Figure 6B). The ACR increased dramatically between 4-5 wks of age in the *Ercc1*$^{-/\Delta}$ mice. The ACR remained modestly elevated from 5-14 wks in the *Ercc1*$^{-/\Delta}$ mice, then increased again at 16 wks of age. The ACR in 2 yr-old WT mice was significantly increased compared adult WT mice (16 wks) and similar to that of 5-14 wk-old *Ercc1*$^{-/\Delta}$ mice. Together, these functional markers indicate that the *Ercc1*$^{-/\Delta}$ mice have progressive renal dysfunction that culminates in ESRD by 16 wks of age and mimics functional and histopathological changes that occur in the kidney over 2-3 years in WT mice.

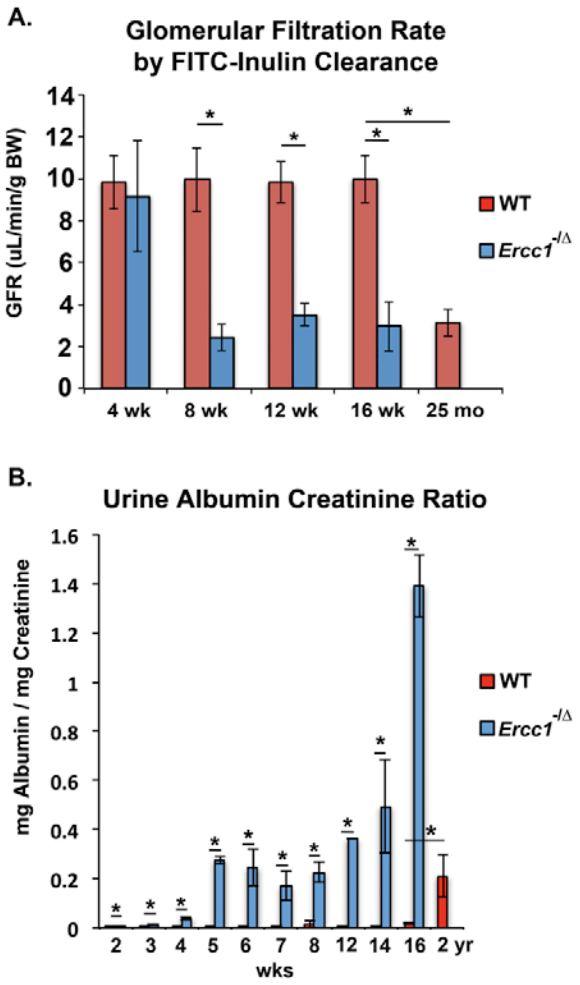

Figure 6. Changes in renal function in *Ercc1*$^{-/\Delta}$ and WT mice with aging

(A) Glomerular filtration rate (GFR) determined by FITC-inulin clearance from the blood after bolus injection. Data reflect the mean GFR in μL/min/g body weight from 3 animals per group ± S.E.M. Asterisk indicates $p<0.05$ as determined by a two-tailed Student's *t*-test. (B) Albumin/creatinine (ACR) ratio in the urine of WT and *Ercc1*$^{-/\Delta}$ mice. Data reflect the mean values from 3 mice per group ± S.E.M. Asterisk indicates $p < 0.05$ as determined by a two-tailed Student's *t*-test.

2.3.3 Cellular changes in progeroid *Ercc1*$^{-/\Delta}$ mouse kidney mimic natural aging

With renal aging, endothelial cells become activated, which is detected as an increase in intracellular adhesion molecule 1 (ICAM/CD54) expression on the cell surface and can result in macrophage infiltration (45). To evaluate this, kidney sections were co-stained with PECAM (CD31) to identify endothelial cells and ICAM to detect activation (Figure 7A). Sixteen wk-old *Ercc1*$^{-/\Delta}$ mice and old WT (26 mo) mice showed a significant increase in ICAM expression compared to adult WT mice not only in the vasculature but also lining Bowman's capsule and in the proximal tubules. Similarly, progeroid and old WT kidneys showed a significant increase in macrophage infiltration in and near the glomeruli, as detected by immunostaining for the pan-leukocyte marker, CD45, and the macrophage marker CD68 (Figure 7B).

With age-related renal fibrosis there is often an increase in smooth muscle actin (SMA)-positive cells (30, 31). In 4 mo-old *Ercc1*$^{-/\Delta}$ mice, there was a significant increase in SMA-positive cells scattered throughout the tubular interstitium, surrounding Bowman's capsule and extending from arterioles on either side of the glomerulus (Figure 7C). This periglomerular and interstitial increase in SMA was also significantly increased in 26 mo-old WT mice.

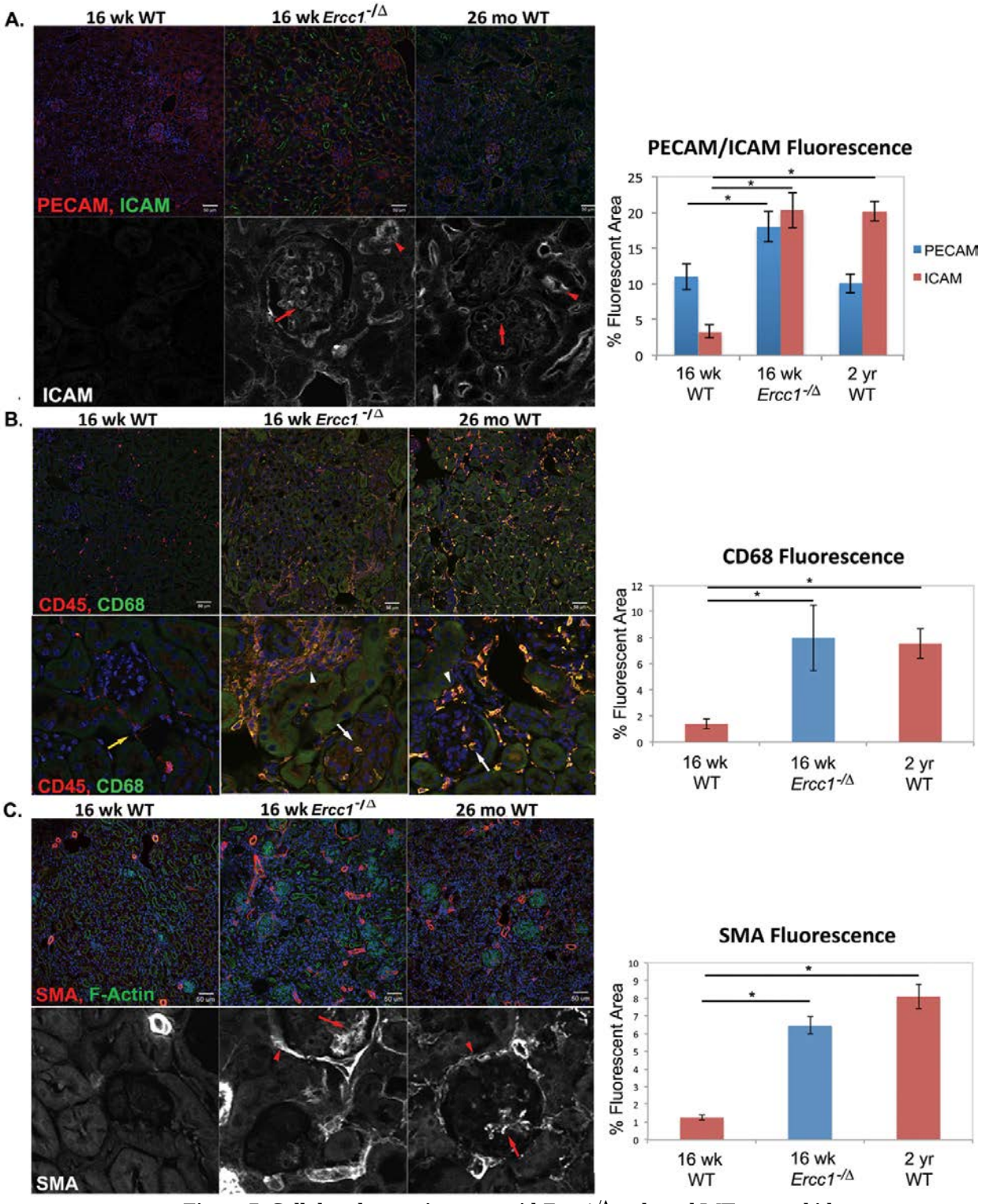

Figure 7. Cellular changes in progeroid *Ercc1*$^{-/\Delta}$ and aged WT mouse kidneys

(A) Immunofluorescence detection at 200X magnification of ICAM (CD54; green) a marker of endothelial activation and tubule injury, PECAM (CD31; red) to identify endothelial cells and Hoescht dye (nuclei; blue) in kidneys from 16 wk-old WT and *Ercc1*$^{-/\Delta}$ mice and old WT (26 mo) mice. The bottom row shows only ICAM staining (white) at

600X magnification. Red arrows show ICAM stained within the glomerulus and red arrowheads show ICAM staining at the apical border of the tubules. Changes are quantified in the graph to the right for both PECAM and ICAM. (B) Immunofluorescence detection at 200X of CD45 (red), a pan-leukocyte marker and of CD68 (green) a macrophage marker and Hoescht dye (blue) in kidney sections. The bottom row at 600X magnification shows the CD45+ and CD68+ fluorescence, highlighting a small CD45+ population in 16 wk-old WT (yellow arrow), and a widespread CD45+, CD68+ population in the 16 wk *Ercc1*$^{-/\Delta}$ mice and old (26 mo) WT animals, namely macrophage infiltration into the glomeruli (arrows) and clustered in infiltrates (arrowheads). Changes in CD68+ fluorescence are quantified in the graph to the right. (C) Immunofluorescence detection at 200X magnification of smooth muscle actin (SMA; red) a hallmark of aged kidney and the structural protein F-actin staining (green) in kidneys. The bottom row shows only the SMA fluorescence at 600X. Arrows highlight intraglomerular SMA^{+} cells and arrowheads point to periglomerular SMA^{+} cells. Changes in SMA fluorescence are quantified in the graph to the right. For all images, the scale bar = 50μm. For all graphs, n=3 animals per group and error bars represent the S.E.M. *p< 0.05, as determined by two-tailed Student's *t*-test.

2.3.4 Podocyte effacement in progeroid *Ercc1*$^{-/\Delta}$ and old WT mouse kidney

Due to early onset of albuminuria in *Ercc1*$^{-/\Delta}$ mice, we examined their podocyte structure using electron microscopy. Podocytes are highly specialized post-mitotic cells responsible for maintaining the filtration barrier and glomerular capillary loop structure (142). The foot processes that project from the cell body of podocytes form a highly organized meshwork that acts as a size and charge barrier to proteins. Podocyte effacement and thickening of the basement membrane are features of renal aging in kidneys of humans and mice (143). Scanning electron microscopy of murine kidney sections revealed that 5 mo-old *Ercc1*$^{-/\Delta}$ and aged (25 mo-old) WT mice exhibited a severe disruption of podocyte foot interdigitation, necessary for glomerular function (Figure 8A). Thin cytoplasmic finger-like projections were also seen extending out of the podocytes in these mice, similar to what is observed in aged rats (40). Four wk-old *Ercc1*$^{-/\Delta}$ mice had largely normal glomerular ultrastructure with only a few glomeruli displaying mildly disrupted interdigitation of the foot processes and largely normal interdigitation of podocyte foot processes by transmission

electron microscopy (Figure 8B). At 5 mo of age, there was substantial effacement of podocyte foot processes and thickening of the glomerular basement (quantified in Appendix B, Fig 25) in *Ercc1*$^{-/\Delta}$ kidneys, similar to changes in old WT mice. Therefore the structural changes observed with normal renal aging occur prematurely in *Ercc1*$^{-/\Delta}$ mice.

FIGURE 4

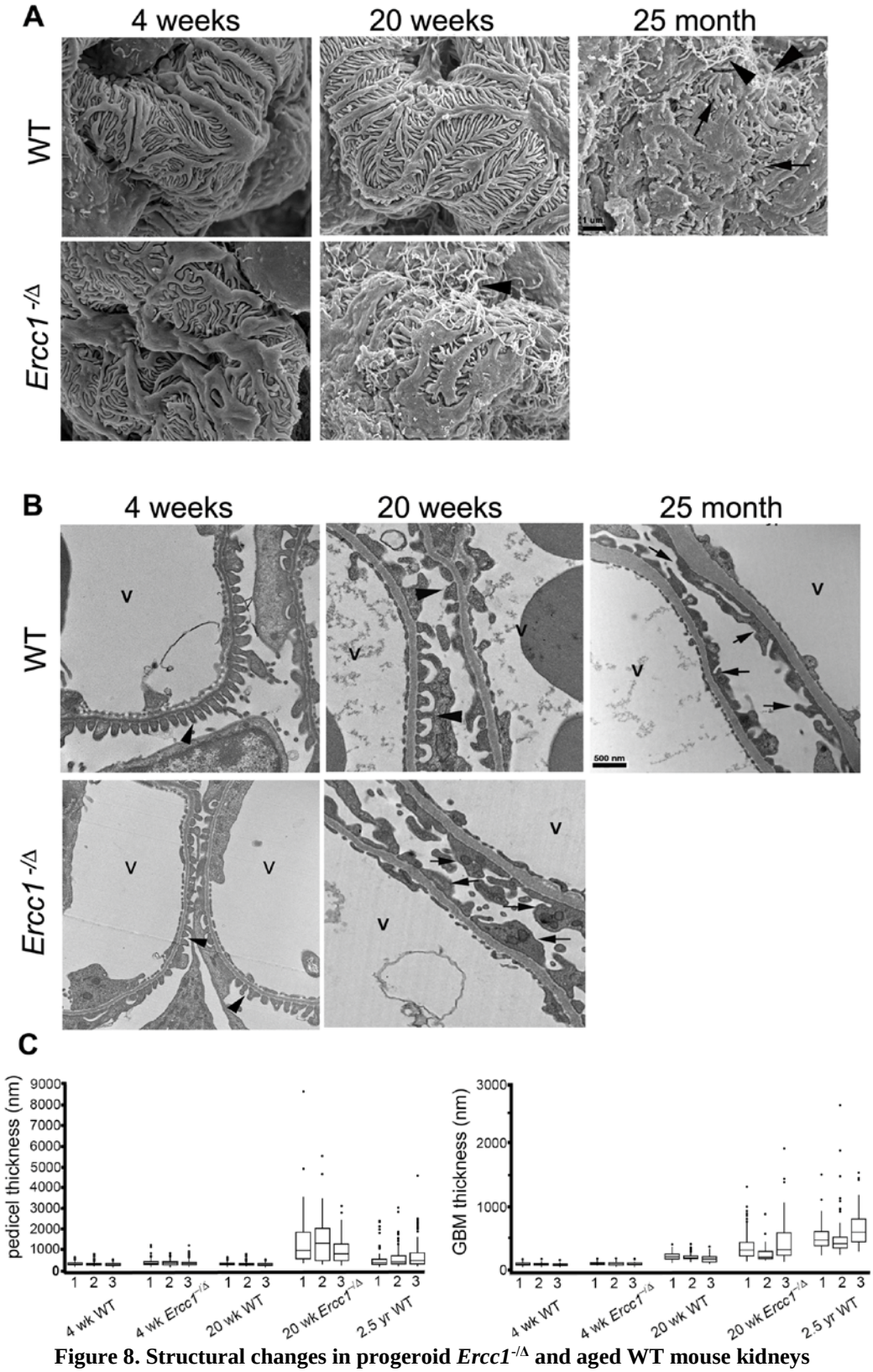

Figure 8. Structural changes in progeroid *Ercc1*$^{-/\Delta}$ and aged WT mouse kidneys

(A) Scanning electron micrographs (10,000X) of kidney illustrating progressive podocyte irregularities in mutant and WT mice with aging including loss of interdigitation (arrows), thickening of foot processes, and appearance of thin cytoplasmic projections (arrowheads). Scale bars = 1μm. (B) Transmission electron micrographs (20,000X) illustrating loss of podocyte architecture that is progressive in mutant and WT mice with aging. Arrowheads indicate interdigitating foot processes. Arrows indicate effacement and thickening of foot processes. V=vessel. Scale bar = 500nm.

2.3.5 Cell turnover in proximal tubules and collecting ducts of *Ercc1*$^{-/\Delta}$ mice

To investigate the mechanism by which renal degeneration occurs, we measured cleaved caspase-3, a marker of apoptosis. By immunoblot, there was no difference in the amount of cleaved caspase-3 in renal lysates from 5 wk-old *Ercc1*$^{-/\Delta}$ and WT mice (Figure 9A). Remarkably, cleaved caspase-3 levels were increased in all adult WT mice but dramatically lower in *Ercc1*$^{-/\Delta}$ mice. TUNEL staining of renal sections from 16 wk-old animals confirmed the lack of apoptotic cell death in *Ercc1*$^{-/\Delta}$ mouse kidneys (Figure 10). Transcriptional profiling of glomeruli from *Ercc1*$^{-/\Delta}$ and aged mice revealed a highly significant correlation and one of the processes dysregulated in both normal and accelerated renal aging is apoptosis (131). In contrast, many necrotic proximal tubule cells were detected in 5 mo-old *Ercc1*$^{-/\Delta}$ and 28 mo-old WT mice, but not in 5 mo-old WT mice (Figure 9B), as is observed in aged rats (40).

In response to cellular damage or loss, quiescent renal cells can re-enter the cell cycle (144). To test if this was the case, WT and *Ercc1*$^{-/\Delta}$ mice were chronically loaded with BrdU beginning at 5 wks of age to label replicating cells. At 13 wks of age, after 8 wks of BrdU exposure, there were significantly more BrdU-positive cells in kidneys of *Ercc1*$^{-/\Delta}$ mice compared to WT littermates (Figure 9C). Co-staining for wheat germ agglutinin (WGA) and BrdU revealed that the proximal tubules are the primary site of cell division (Figure 9D) and there is a significant increase

Ercc1$^{-/\Delta}$ mice compared to WT littermates (Figure 9E). These data indicate that proximal tubule cells are particularly sensitive to endogenous DNA damage, which leads to necrotic cell death and turnover.

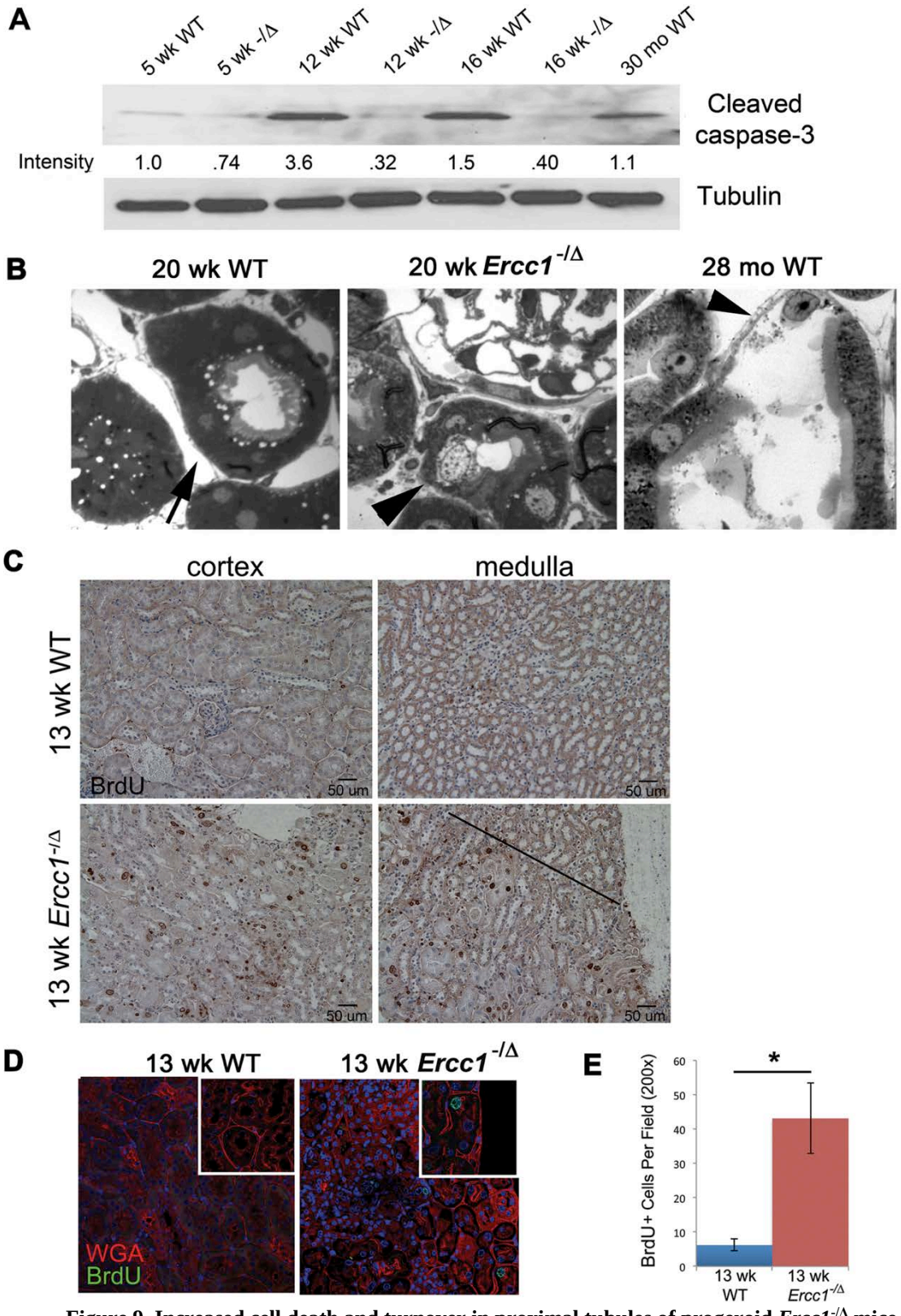

Figure 9. Increased cell death and turnover in proximal tubules of progeroid *Ercc1*$^{-/\Delta}$ mice

(A) Immunoblot detection of cleaved caspase-3. The blot is representative of data from 3 independent sets of mice. (B) Tissue sections (350 nm thick) stained with Toluidine blue. Arrowheads indicate necrotic proximal tubule cells in *Ercc1*$^{-/\Delta}$ mice and old WT mice compared to healthy tubule structure with brush border seen in young WT kidney (arrow). (C) Immunohistochemical detection of BrdU, a marker of replicating cells, in mice chronically administered BrdU 1x per wk x 8 wks total, beginning at 5 wks of age. Images of the cortex and medulla (above the diagonal black line in the *Ercc1*$^{-/\Delta}$ image) revealed increased proliferation primarily in the cortex of mutant animals. (D) Co-immunostaining of kidney sections for BrdU (green) and wheat germ agglutinin (red). Shown are 200X magnification images with 600X insets to show higher resolution of proximal tubule structure with characteristic brush border. The proliferating cells are localized in the proximal tubules. (E) BrdU uptake was quantified in WT and *Ercc1*$^{-/\Delta}$ kidney (n=3 mice per group and 5 sections per animal). Results are expressed as the average number of BrdU-positive nuclei per 20X field ± S.E.M. An asterisk denotes that $p<0.05$, as indicated by a two-tailed Student's *t*- test.

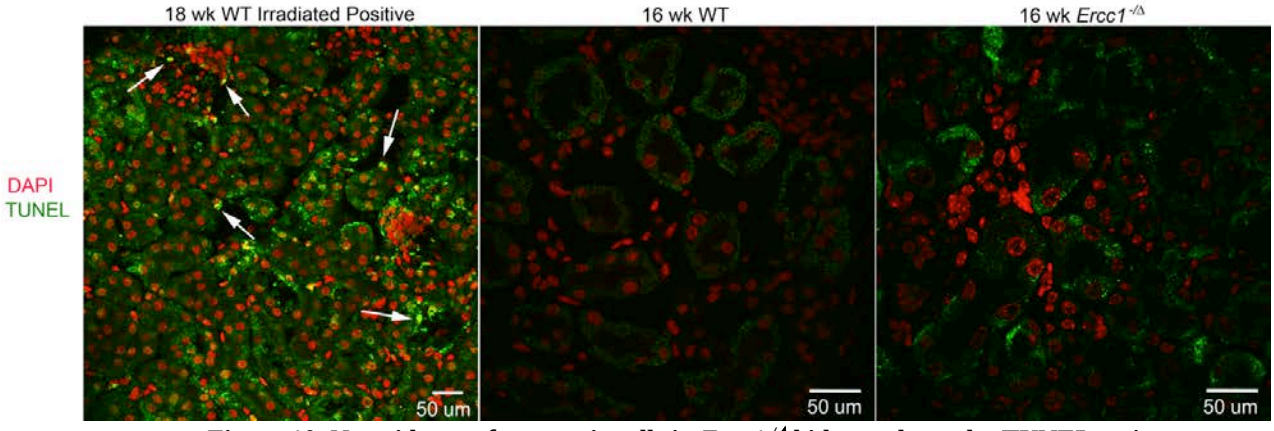

Figure 10. No evidence of apoptotic cells in *Ercc1*$^{-/\Delta}$ kidneys shown by TUNEL stain.

Kidneys from 18wk irradiated WT mice were stained with TUNEL (green) as a positive ctrl. Arrows indicate positive TUNEL stain colocalizing with nuclear stain, DAPI (red). No positively stained nuclei were detected in 16 wk WT or *Ercc1*$^{-/\Delta}$ kidneys, supporting the cleaved caspase-3 data in Figure 9.

2.3.6 Increased senescence in *Ercc1*$^{-/\Delta}$ and old WT kidney

Genotoxic stress is known to drive cellular senescence (145), which in turn drives age-related degenerative changes (146). Senescent cells are characterized by nuclear foci of the

phosphorylated histone variant, γH2AX (Ser139) (147), as well as increased expression of p53, p21 and $p16^{ink4a}$ and are thought to be largely protective in response cell damage or tissue injury (148). To further examine the mechanism by which renal aging is accelerated in *Ercc1*$^{-/\Delta}$ mice, senescence markers were measured by immunofluorescence and immunoblot. Kidneys from aged WT mice had more γH2AX foci compared to young animals (Figure 11A). Young *Ercc1*$^{-/\Delta}$ mice (6 wk) have a modest increase in γH2AX foci compared to littermate controls, which increased dramatically by 20 wks of age. This was confirmed by immunoblot, which revealed an approximately 2-fold increase in γH2AX protein in renal lysates of *Ercc1*$^{-/\Delta}$ and aged mice compared to young WT animals (Figure 11B). p53 protein expression was also substantially increased in *Ercc1*$^{-/\Delta}$ mice compared to WT littermates and increased with age. P53 expression was also dramatically increased in the kidneys of aged WT mice. A similar pattern of expression was observed for p16 (Figure 11B). P21 levels were also elevated in aged WT mice compared to younger animals and peaked at 3 mos in *Ercc1*$^{-/\Delta}$ mice. Finally, increased senescence-associated β-galactosidase activity was detected in 9 and 15 wk-old *Ercc1*$^{-/\Delta}$ mice compered to WT littermates (Figure 12). These data provide strong evidence that endogenous DNA damage promotes cellular senescence in the kidney and this contributes significantly to renal aging even in repair competent organisms.

As a final comparison between old and progeroid kidneys, we re-analyzed the transcription profiles recently created from glomeruli of 96 wk-old WT mice and 14 wk-old *Ercc1*$^{-/\Delta}$ mice (131). In our analysis, the *Ercc1*$^{-/\Delta}$ and aged mouse profiles were compared to that of 14 wk-old adult WT mice. 300 genes were discovered to be differentially expressed in *Ercc1*$^{-/\Delta}$ mice, defined as ≥1.5-fold change and $p<0.05$ (Figure 11C and gene list in Table 4 in Appendix A) and 147 genes were differentially expressed in aged mice. 69 genes overlapped between the *Ercc1*$^{-/\Delta}$ mice and

old WT mice, which was highly significant ($p<2.2x10^{16}$). This extends the strong parallels between accelerated renal aging in *Ercc1*$^{-/\Delta}$ mice and normal renal aging to molecular commonalities. Pathways discovered to change with aging include immune regulation, which was confirmed in Figure 7, cell fate, confirmed in Figure 9 and 10, and metabolism.

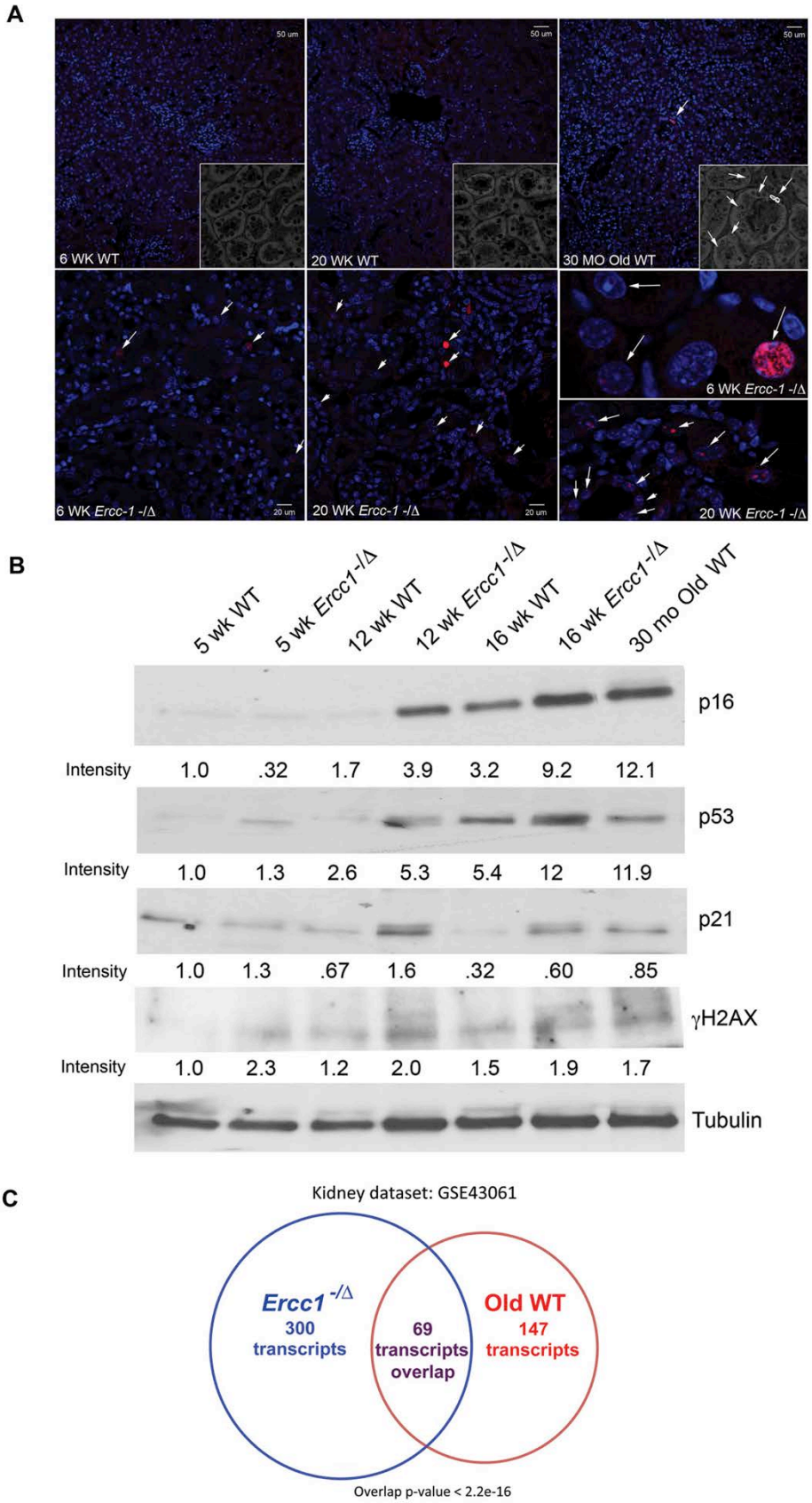

Figure 11. Increased cell senescence in old and progeroid *Ercc1*$^{-/\Delta}$ mouse kidneys.

(A) Immunofluorescence detection of γH2AX (200X, with higher mag insets to show foci), indicating a modest increase in foci in 6 wk *Ercc1*$^{-/\Delta}$ and 30 mo-old WT kidneys compared to young WT, and a large increase in foci in 20 wk *Ercc1*$^{-/\Delta}$ kidneys compared to young WT. γH2AX staining is red, DAPI highlights nuclei in blue. (B) Immunoblot detection of senescence markers γH2AX, p21, p53and p16^{INK4a} in whole kidney lysates. Tubulin was used as a loading control. The blot shown is representative of data obtained from 3 sets of mice. (C) Gene expression analysis of the published kidney dataset GSE43061. There were 369 transcripts differentially expressed in 14 wk *Ercc1*$^{-/\Delta}$ kidneys compared to 14 wk WT controls (≥1.5 fold change and p<=0.05) and 216 transcripts differentially expressed between 96 wk WT kidneys and the 14 wk WT control group. 69 genes overlapped between the two profiles, which is highly unlikely to be due to chance (p<2.2x10^{6}). The overlapping gene names are included in supplementary table 5 in Appendix C.

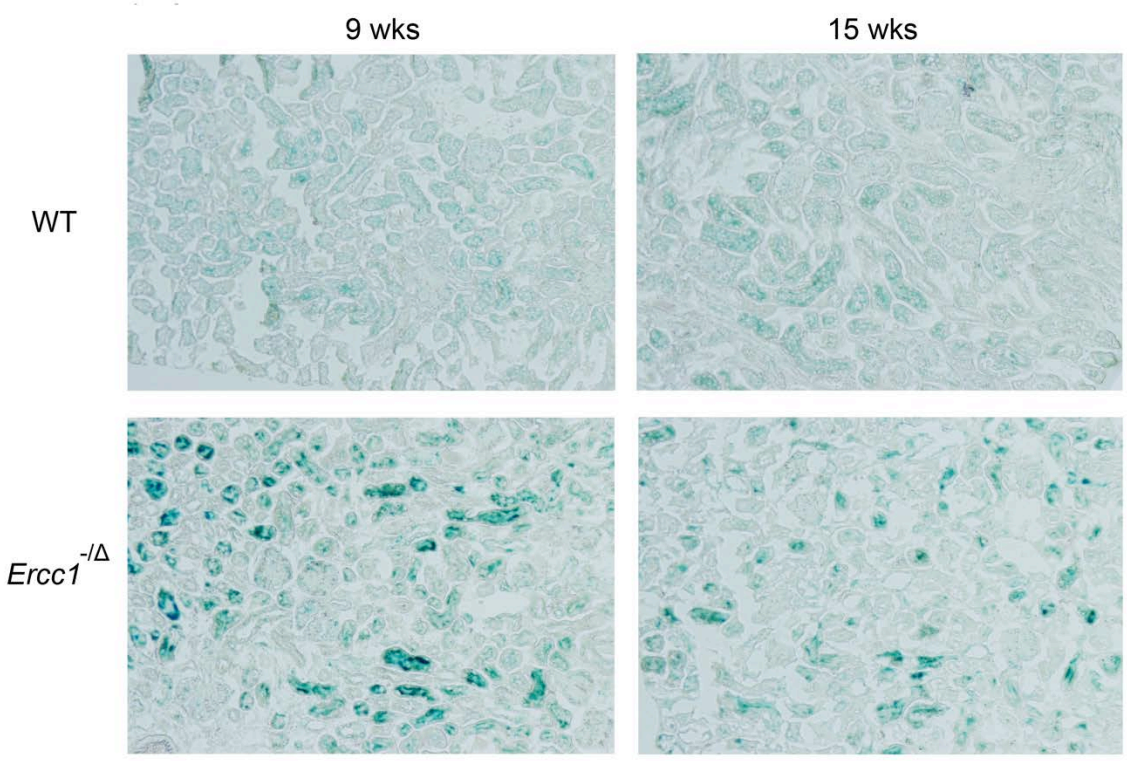

Figure 12. Senescence-associated-β-galactosidase (SA-β-gal) increase in *Ercc1*$^{-/\Delta}$ Kidneys

Frozen kidney sections from 9, 15 wk WT and *Ercc1*$^{-/\Delta}$ mice were stained to detect senescence-associated β−galactosidase (SA-β−gal) activity. SA-β−gal staining (blue) was increased in *Ercc1*$^{-/\Delta}$ kidneys at both 9wks and 15wks. In progeroid kidneys, as compared to 9 wks, there is a slight decrease of stained cells at 15 wks, possibly due to tubule cell loss and/or replacement, as detected in Figure 8.

2.4 DISCUSSION

Renal function declines with age leading to a decrease in GFR, glomerulosclerosis, macrophage infiltration and fibrosis (30, 31, 45). The underlying cause of age-related nephropathy is largely unknown. Herein, we demonstrate that the functional, structural, histological, cellular and molecular changes seen with renal aging in WT mice is recapitulated in DNA repair-deficient *Ercc1*$^{-/\Delta}$ mice, albeit the onset is accelerated 5-6 fold. This provides strong evidence that endogenous DNA damage, which accumulates in the kidney with aging (149), contributes to age-related nephropathy.

FAN1 codes for a DNA repair nuclease similar to ERCC1-XPF that is required for the repair of DNA interstrand crosslinks and other endogenous lesions (105). *FAN1* disruption in fish causes apoptosis and renal cysts. *FAN1* mutations in humans cause karyomegalic interstitial nephritis characterized by cystic dilation of renal tubules and widespread interstitial infiltrates and fibrosis (105). These studies further demonstrate that failure to repair spontaneous, endogenous DNA damage can lead to CKD and other degenerative changes associated with age-related nephropathy.

To determine how DNA damage promotes renal aging, markers of apoptosis, cell senescence, regeneration and necrosis were measured. Cleaved caspase-3 protein expression does not correlate between normal and accelerated aging. However, there is evidence of necrosis and regeneration in proximal tubule epithelia. Importantly, senescence markers γH2AX, p21, p53 and p16 were strongly up regulated in *Ercc1*$^{-/\Delta}$ mice. This suggests that cellular senescence, a programed cell fate associated with aging (146), plays a key role in promoting age-related nephropathy in response to endogenous genotoxic stress. Notably, p16, p53 and γH2AX levels were greatest in old WT mice, strongly supporting the conclusion that genotoxic stress-induced cellular senescence plays a

causal role in normal age-related nephropathy. Finally, transcriptome analysis of isolated glomeruli revealed highly significant overlap in gene expression changes in *Ercc1*$^{-/\Delta}$ old WT mice and point changes in immune regulation, cell fate and metabolism as contributing to renal aging in both natural and accelerated aging.

The urinalysis and structural studies indicate that podocyte foot-process thickening is one of the first changes detected in the *Ercc1*$^{-/\Delta}$ mice (Figure 2 and 4). It begins at 4 wks of age and progresses. The glomerular basement membrane also thickens. Podocytes are exposed to multiple sources of stress, including distending forces from high glomerular blood flow (27) and depend primarily upon mitochondrial oxidative respiration for energy (150), a source of damaging reactive oxygen species. Oxidative damage to macromolecules and organelles is cleared by autophagy, since podocytes are post-mitotic and not replaced. If the damage is overwhelming, podocytes are lost, which correlates strongly with ESRD (27).

Following podocyte injury at 4 wks of age *Ercc1*$^{-/\Delta}$ mice, at 8 wks, there is evidence of vascular and proximal tubule injury, including upregulation of ICAM, progressive increase in SMA^{+} cells, macrophage infiltration and proximal tubule epithelial cell necrosis and proliferation. In a toxin model, podocyte injury induces proliferation of renal tubule epithelium (12). Proximal tubule cell necrosis is seen in aged rats (40). Collectively, these studies suggest that podocytes are particularly susceptible to damage with aging, leading to loss of glomerular function, which in turn triggers other, subsequent renal pathologies.

In summary, data from both the progeroid model and aging WT mice indicate that endogenous DNA damage can drive renal aging. Glomerular injury appears to precede renal tubule necrosis, fibrosis and macrophage infiltration. The *Ercc1*$^{-/\Delta}$ mice offer a highly rapid and accurate spontaneous model of aging-related degenerative changes leading to CKD and ESRD.

3.0 PODOCYTE INJURY CAUSES SUBSEQUENT KIDNEY DISEASE IN ERCC1 DEFICIENT MOUSE MODEL

Because of the increasing elderly population, there is rising incidence of CKD and ESRD. Very little is known about the mechanism of or the contributions of various kidney cell types to causing aging nephropathy(28, 31, 118). It is difficult to separate out age-related kidney changes from other aging diseases such as diabetes or cardiovascular disease, which affect kidney function. Here, I provide mechanistic information as to the progression of CKD in the *Ercc1* deficient mouse, as well as evidence of the role of the glomerular podocyte in causing this disease. The *Ercc1*$^{-/\Delta}$ mouse model is an accurate tool in which to study the progression of age-related renal senescence in an accelerated manner. Podocyte injury, characterized by effacement of foot processes, an increase in IKK, and induction of autophagy, occurs at 4 weeks, along with an elevated albumin-creatinine-ratio (ACR). By 8 wks of age, autophagic flux in podocytes becomes impaired, chronic activation of the transcription factor, NF-κB, begins in podocytes, ACR rises significantly, glomerular filtration rate (GFR) decreases, and tubule injury occurs. This is followed by other global age-related kidney changes such as fibrosis and macrophage infiltration. Using a podocyte specific and a proximal tubule specific knock-out of *Ercc1,* evidence is provided here that damage accumulation in the *Ercc1* deficient podocyte, but not the *Ercc1* deficient proximal tubule, is the primary driving force in decline in kidney function, loss of structure, and early death. Finally, *in vitro* work in podocytes provides evidence that the IKK- NF-κB pathway and autophagy are intertwined, and that dis-regulation of each could be playing a role in age-related kidney disease.

3.1 INTRODUCTION

Renal function declines in adults and end stage renal disease (ESRD) occurs at peak incidence in the elderly. Glomerulosclerosis is the main cause of ESRD and this is accompanied by a decrease in glomerular filtration rate(32, 151, 152). Loss of kidney function with age is also an independent risk factor for cardiovascular disease and mortality(151). The elderly are at greater risk for glomerular disease. The aging population is rising and evidence of kidney functional decline is present even in otherwise healthy individuals. Also, the aged kidney is much more susceptible to injury and disease(32). Still, little is known about the mechanism of changes that occur in the aging glomerulus and the role of specific cell types in driving these age-related pathologies.

Podocyte loss occurs during glomerular disease and with aging, and there is little or no evidence that podocytes are replaced by proliferation or by bone marrow or parietal cells(6). It is known that this podocyte injury and loss predicts the severity of disease and eventual ESRD(151), but little is known about the mechanism of such injury and the role it plays in causing subsequent pathologies in the glomerulus, tubules, and interstitium. The cellular "aging" phenotype in patients with renal disease may determine what therapies may work and may be completely different than what is appropriate for a younger patient.

3.1.1 The aging glomerulus

Evidence from aging research in humans and animals show that 30% of glomeruli are lost by 75 years of age and the remaining have limited filtering capabilities. These studies suggest that

many factors contribute to aging nephropathy such as hypertension, obesity, and previous kidney injury(28). It is then difficult to tease out the contribution of inherent kidney damage in causing aging nephropathy, as well as to elucidate the role of the various kidney cells. Glomerular diseases associated with old age include membranous nephropathy, minimal change disease and focal segmental glomerulosclerosis. It is estimated that at least 90% of ESRD is subsequent to chronic glomerular damage and ESRD is strongly associated with aging(6, 33). Podocyte loss and glomerulosclerosis increases with age(13). Various factors can affect and accelerate this process, but the problematic outcome seems to remain the same. Loss of podocytes and failure of the glomerulus to compensate leads to age-associated kidney damage. While there is much in the way of describing age-associated glomerulosclerosis and other kidney pathologies, very little is known about the mechanism or the contributions of certain compartments and cell types.

3.1.2 NF-κB and autophagy

While there is a wealth of evidence in various cell types of a complex relationship between the NF-κB and autophagy pathways(153-158), very little is known about this relationship during aging, and even less is known about this relationship in the podocyte. It is clear from the literature that the IKK complex and NF-κB can enhance expression of autophagy proteins in a context specific manner, and that autophagy can degrade all subunits of IKK to negatively regulate the pathway after autophagy cycles through(157). However, it has also been shown that NF-κB activation can cause an increase in autophagy inhibitors such as Bcl-2/xL and inhibit activators such as reactive oxygen species (ROS)(157). Eventually with aging, there is a decrease in Beclin

1 and evidence of impairment of autophagic degradation. It is also known that there is chronic NF-κB activation in some tissues with aging(157, 158). Meng et al(159) showed that defective autophagy by Atg 7 knock-out in the hypothalamus caused inflammation and NF-κB activation, which resulted in a changed metabolism and weight gain in mice. The effects were reversed in mouse that also had a brain-specific IKKβ knock out. Along these lines, many investigators(155, 156)) have shown that the members of the IKK complex and active IKKβ are down regulated by autophagy, so it would make sense that defective autophagy could result in sustained levels of active IKK and subsequent sustained NF-κB activation.

Podocytes depend on a high level of autophagy to deal with the oxidative damage and stress that can build up during its long-lived, post-mitotic life, and also use autophagy to fuel their protein secretion and trafficking(5). This leads to the hypothesis that the dis-regulation of autophagy and NF-κB signaling could be related and play a role in propagating podocyte injury in the *Ercc1*$^{-/\Delta}$ mouse model of accelerated kidney aging.

3.1.3 The *Ercc1*$^{-/\Delta}$ mouse model of accelerated renal aging

As we have previously shown, the *Ercc1*$^{-/\Delta}$ mouse is a valuable tool in which to study the process of aging in the kidney in a timely manner. The transcriptional profile of the *Ercc1*$^{-/\Delta}$ kidney glomerulus and a naturally aged glomerulus share many differential gene expression changes when compared to young adult WT, including genes involved in inflammation, cell fate, and metabolism(131). These mice have a maximum lifespan of 7 months and develop widespread aging pathologies(102), including neurodegeneration, sarcopenia, and liver(113) and kidney

disease. As presented in chapter 2, mice develop albuminuria in the first 1-2 months of life and podocyte injury, followed by a decrease in GFR, tubule injury, fibrosis, and macrophage infiltration. Kidneys also show up-regulation of senescence markers, p16, p21, and SA-β–galactosidase activity. Histology studies demonstrate thickening of capillary loops, focal glomerulosclerosis, thickening of GBM and TBM, and widespread interstitial fibrosis. By creating cell specific knockouts of *Ercc1* in the kidney, it is possible to determine the contribution of various cell types in causing age-related kidney disease and to then study the mechanism by which this occurs in order to develop therapies for age-related CKD. Because podocytes are post-mitotic and loss of podocytes correlates with ESRD, could podocyte damage during the aging process be responsible for subsequent kidney injury and disease? Or, is it proximal tubule injury due to *Ercc1* deficiency that is primarily responsible for the aging pathologies and decrease in function?

The work here tests the hypothesis that podocyte injury causes the subsequent kidney pathologies seen in the *Ercc1* deficient mouse model of accelerated kidney aging, and possibly in natural aging as well. In order to test this hypothesis, it was necessary to first determine the time course and nature of podocyte injury as it relates to other age-related changes in the $Ercc1^{-/\Delta}$ mouse kidney. Secondly, a genetic approach was employed to determine the role of inherent podocyte injury caused by *Ercc1* deficiency in causing age-related chronic kidney disease. Specifically, a podocyte-specific knock out of *Ercc1* was created using a Podocin-cre mouse(160), crossed into a mouse with a floxed Ercc1 allele, allowing Ercc1 to be knocked out of podocytes only. Since proximal tubule injury also occurred in the $Ercc1^{-/\Delta}$ mouse kidney, a proximal tubule-specific *Ercc1* knock out was created, using a *gamma-glutamyltransferase-cre* (γ-GT-cre) mouse(161). The data presented here provide key insight into cellular and molecular pathways that should be targeted for development of effective therapies for age-related CKD.

3.2 MATERIALS AND METHODS

Animal Care and Experimentation

Animal work was approved by the University of Pittsburgh and Scripps Florida Institutional Animal Care and Use Committees and is in accordance with NIH guidelines for humane care of animals. Ercc1$^{-/\Delta}$ mice were bred and genotyped as previously described (126). All mice were in a congenic f1 background generated by crossing inbred FVB/n and C57Bl/6 mice. For the podocyte specific knock out of Ercc1, a C57/BL6 mouse expressing Cre recombinase under the NPHS2 (podocin) promoter (Pod-cre+/-, Jackson Laboratories, Bar Harbor, ME) and heterozygous knock-out of Ercc1 (Ercc1$^{+/-}$) was crossed with a FVB/n mouse carrying one loxP-flanked Ercc1 allele, termed "conditional," (Ercc1$^{+/c}$). Podocyte specific knock-out mice were bred and genotyped as above, displaying a genotype of Pod-cre$^{+/-}$; Ercc1$^{-/c}$. For the proximal tubule-specific knock out, a C57/BL6 mouse expressing cre recombinase under the Ggt1, gamma-glutamyltransferase 1, promoter (γGT-cre +/-, Jackson Laboratories, Bar Harbor, ME), Ercc1$^{+/-}$, was crossed with a FVB/n mouse carrying a loxP-flanked Ercc1 allele, termed "conditional," (Ercc1$^{+/c}$). Proximal tubule-specific knock out mice were bred and genotyped as above, displaying a genotype of γGT-cre$^{+/-}$; Ercc1$^{-/c}$. In order to monitor NF-κB activation, NF-κB^{EGFP} mice, containing the eGFP reporter under the control of NF-κB responsive elements(162), were crossed into Ercc1$^{+/-}$ and Ercc1$^{+/\Delta}$ lines to create an NF-κB^{EGFP}; Ercc1$^{-/\Delta}$□mouse. NF-κB^{EGFP} young and old "WT" mice were used as controls.

Kidney perfusion and processing for ultrastructural analysis

For EM, the kidneys of euthanized animals were cleared of blood by perfusion with PBS at 3 mL/min via cardiac puncture then perfuse-fixed or immersed in 2.5% glutaraldehyde in PBS and processed as described previously (113). 350 nm sections were cut and stained with Toluidine Blue for light microscopy analysis. Ultrathin sections were digitally imaged using a JEOL JEM 1011 transmission electron microscope (Peabody, MA) at 80 kV fitted with a side mount AMT 2k digital camera (Advanced Microscopy Techniques, Danvers, MA).

Immunofluorescence analyses

IF was performed on frozen kidney sections as previously described (113). Briefly, kidneys were fixed in 2% paraformaldehyde in PBS for 2-4 hrs followed by 30% sucrose at 4°C overnight, then frozen in liquid N_2-cooled isopentane and sectioned (7μm thick) on a Microm™ HM 550 cryostat (Thermo Scientific; Waltham, MA). Primary antibody was incubated at room temperature for 1 hr (goat anti-CD68, Santa Cruz Biotechnology, Inc., Santa Cruz, CA; anti-SMA:Cy3, Sigma, St. Louis, MO; rat anti-CD45 or rat anti-CD31 (PECAM) both from BD Pharmingen, San Jose, CA; or hamster anti-ICAM, BD Biosciences, San Jose, CA) all at a dilution of 1:100. Sections stained with rabbit anti-LC3 (1:200), Novus, Littleton, CO; guinea pig anti-p62 (1:100), Fitzgerald, Acton, MA; guinea pig anti-nephrin (1:100), Fitzgerald, Acton, MA; rabbit anti-pS6 (1:50), Cell Signaling, Danvers, MA; rabbit anti-IKK-β (1:100), Novus, Littleton, CO; rat anti-KIM-1 (1:100), R&D systems, Minneapolis, MN were incubated overnight at 4°C. The fluorescent secondary antibodies (Invitrogen, Eugene, OR; Jackson ImmunoResearch Laboratories, West Grove, PA), raised against the origin of each primary antibody, were added for 1 hr in the dark at room temperature. Nuclei were stained with DAPI and mounted with gelvatol under glass coverslips. Images were acquired using an Olympus Fluoview 1000, inverted confocal microscope or the Nikon 90i scanning microscope for whole section fluorescence image quantification.

Albumin/creatinine ratio measurement

Urine was collected from mice weekly as described in Chapter 2 and albumin levels quantified using the mouse Albumin Elisa Kit (Bethyl Laboratories, Montgomery, TX). Albumin levels were normalized to creatinine levels using the mouse Creatinine Urine Assay Kit (Cayman Chemical, Ann Arbor, MI). For each time point, an n=3 was used and the average albumin-creatine-ratio (ACR) values were plotted ± S.E.M.. Significance was calculated using the Student's two tailed *t*-test; $*p < 0.05$.

Determination of GFR

GFR was measured using FITC-inulin clearance by modified protocol (132). Briefly, mice (n=3 per group) were given a bolus injection of a 2.5% FITC-inulin (Sigma-Aldrich, St. Louis, MO) in HEPES retro-orbitally (2 μl per g body weight). Blood was collected from the tail tip before injection and 3, 5, 7, 10, 15, 20 and 40 min post-injection. Plasma was isolated and samples were diluted 1:10 in 0.5M Hepes. FITC fluorescence was measured in duplicate for each animal using a Perkin Elmer EnVision 2104 Multilable Reader. GraphPad Prism was used to plot FITC-inulin concentration using a two-phase exponential decay model. GFR was normalized using body weight and expressed as μl/min/g BW.

Cell culture of immortalized podocytes and glomerular isolation from kidney

Conditionally immortalized mouse podocytes (MP-1) cells were generously provided by Dr. Valerie Schumacher (Harvard Medical School). These podocytes were originally derived from the temperature-sensitive SV40 large T antigen transgenic mouse by subcloning outgrowths of glomeruli isolated using standard sieving and magnetic bead isolation(163). This podocyte cell line grows at 33^{o}C and in the presence of IFN-γ, and becomes differentiated and post-mitotic after switching to 37^{o}C with 10-14 days of culture. Cells were grown on 0.05mg/mL collagen IV

(Millipore, Temecula, CA) substrate and displayed primary and secondary branching and high levels of nephrin, similar to *in vivo* podocytes. Isolated glomeruli culture experiments were performed with glomeruli from freshly resected mouse kidneys, isolated by standard differential sieving as described previously(164, 165). Briefly, freshly isolated kidney cortex was minced into approximately 1 mm sized pieces in DMEM medium (Life Technologies, Grand Island, NY) plus 5% fetal bovine serum (FBS). Cortex pieces were then incubated at 37ºC for 30 min. in 1mg/mL collagenase II (Worthington, Lakewood, NJ) in DMEM medium. The digested suspension was then passed through a 100 μm sieve, followed by a 70 μm sieve to remove large tissue chunks and connective tissue. This suspension was then passed through a 40 μm sieve, and the material on top of the filter (>40 μm) was washed and used for glomerular culture. Few tubules remained and glomeruli were identified by nephrin expression during imaging experiments. Glomeruli were cultured overnight on 0.05mg/mL collagen IV (Millipore, Temecula, CA) with or without 5nM bafilomycin A (Sigma-Aldrich, St, Louis, MO), and fixed with 2% paraformaldehyde in PBS for staining and imaging. Images were acquired using an Olympus Fluoview 1000, inverted confocal microscope. Autophagic flux studies were performed using either 5nM bafilomycin A as mentioned above, or 25 μM chloroquine (Sigma-Aldrich, St. Louis, MO). For IKK inhibition, 300nM IKKi VII (EMD Millipore, Billerica, MA) was added to the culture medium for 3 or 6 hrs. For constitutively-active IKK expression, cells were transfected overnight with 100ng of the FLAG-IKK-2 plasmid (Addgene, originally from Dr. Anjana Rao, Scripps, La Jolla, CA) into the center well of a Mattek dish, using 0.2 uL of Lipofectamine 2000 (Life Technologies), on day 8 of differentiation. Experiments were performed and cells were fixed on day 10, 2 days post transfection. Transfection was confirmed with an anti-mouse FLAG antibody (clone M2, 1:100, Sigma-Aldrich, St. Louis, MO).

3.3 RESULTS

3.3.1 Time course of podocyte injury and age-related kidney pathologies in the *Ercc1$^{-/\Delta}$* mouse

Podocyte injury is detected as early as 4 wks in the *Ercc1$^{-/\Delta}$* mouse model, followed by endothelial cell activation, proximal tubule injury, macrophage infiltration, and fibrosis. Podocytes are post-mitotic and therefore must deal with accumulated damage or die during the aging process, where there is little or no evidence of replacement. Loss of podocytes correlates with ESRD. It is then possible that podocyte injury in the *Ercc1$^{-/\Delta}$* mouse model and during natural aging is largely responsible for causing subsequent pathological changes, such as tubule injury and macrophage infiltration. First, it was necessary to determine the time course of major changes that occur in podocytes with aging in the *Ercc1$^{-/\Delta}$* kidney, and how they relate to the time course of global kidney changes that occur.

3.3.1.1 Age-related chronic NF-κB activation occurs in the podocytes of *Ercc1$^{-/\Delta}$* mice

Since increased NF-κB activation occurs with aging(166-168), it is possible that dis-regulated NF-κB signaling could be responsible for propagating the inflammatory and senescence changes detected in Chapter 2. Therefore, we determined whether NF-κB activation, previously found in both old WT and 3 month old *Ercc1$^{-/\Delta}$* kidneys (but not young WT) (168), occurs chronically in *Ercc1$^{-/\Delta}$* kidneys and in which cell type(s). To achieve this, kidneys from old NF-κB^{EGFP} mice, as well as 1, 2, 3, 4, and 5 mo old *Ercc1$^{-/\Delta}$*; NF-κB^{EGFP} mice and their NF-κB^{EGFP} control littermates were examined. These mice contain the EGFP reporter under the control of NF-

κB responsive elements(162), and therefore display eGFP fluorescence in cells where NF-κB is activated. No GFP-positive cells were detected in young WT mice. However, low levels of GFP were detected in the glomerulus by 2 months of age in the *Ercc1*$^{-/\Delta}$ kidney and continued through 4 months of age, disappearing at 5 months, when severe cellular loss and overt pathologies occurred (Figure 13A). GFP fluorescence in the cortex was quantified in whole sections using a Nikon 90i, scanning microscope, and GFP levels were confirmed to increase significantly by 2 months of age, peaking at 3 months. Significant GFP-positive glomeruli were also detected in 2 year old WT kidneys (Figure 13B). This chronic NF-κB activation in the glomerulus was confirmed (n=3 mice), and the trend was the same, with varying levels of fluorescence between mice.

In order to determine in which cell type this chronic NF-κB activation was occurring, kidneys were stained with an antibody against nephrin, a podocyte marker (Figure 13C). Nearly all of the GFP fluorescence co-localized in single confocal sections with nephrin. Nephrin levels also decreased significantly over time, indicating a functional breakdown of the podocyte filtration barrier. Of note, GFP fluorescence did not ever co-localize with endothelial or tubule markers.

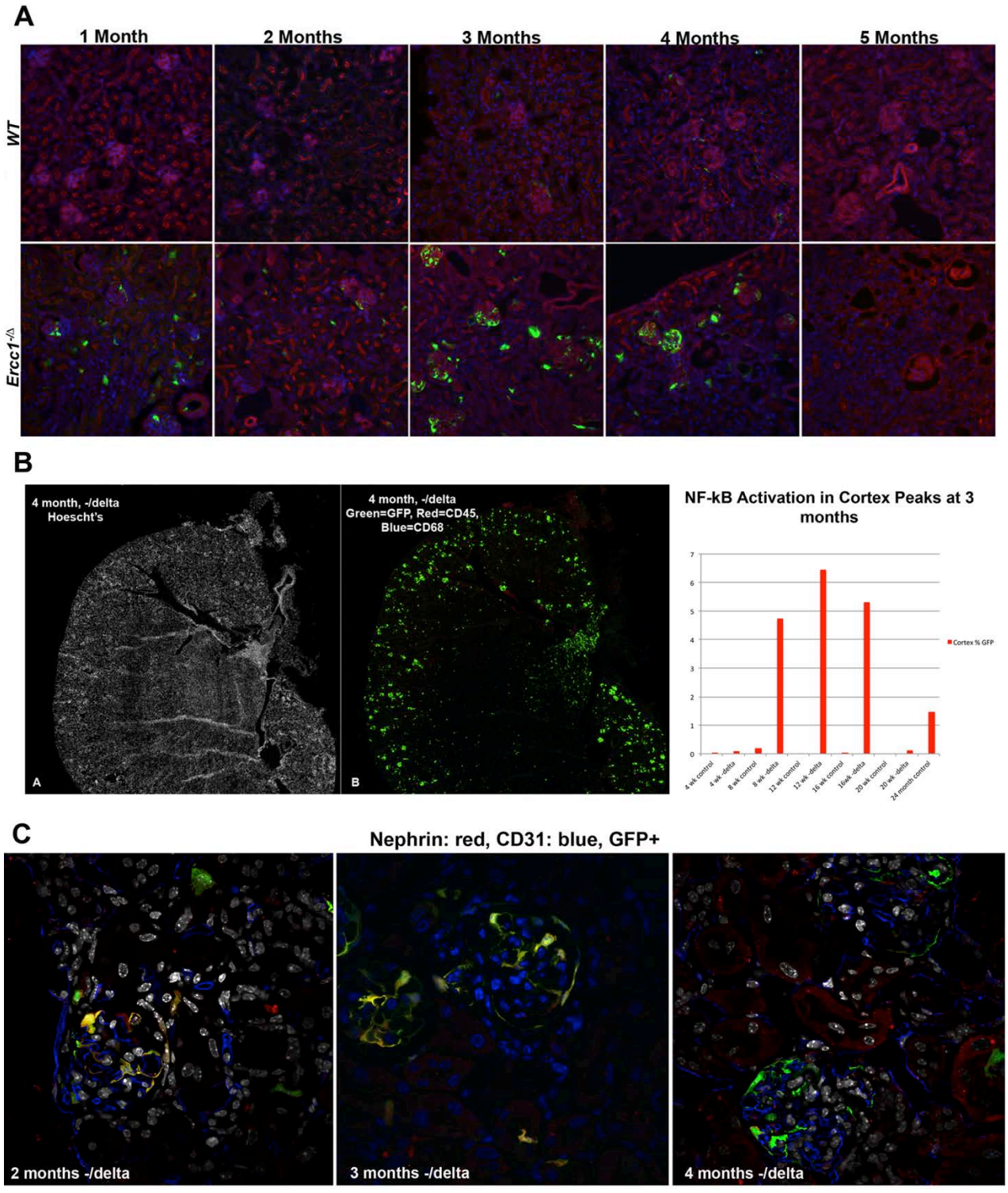

Figure 13. Chronic NF-κB activation in podocytes in the *Ercc1*$^{-/\Delta}$ and old WT kidney

(A) Epifluorescent images of NF-κB-eGFP; *Ercc1*$^{-/\Delta}$ and their age-matched controls at 1, 2, 3, 4, and 5 months of age show chronic NF-κB activation in glomeruli from 2-4 months. (B) Representative image of whole section, high

resolution fluorescence image and quantification of GFP fluorescence. NF-κB activation begins at 2 months, peaks at 3 months, and eventually decreases to null right before death. Old WT kidneys also display high levels of glomerular NF-κB activation. (C) Single optical section confocal images of 2-4 months old NF-κB-eGFP; *Ercc1*$^{-/\Delta}$ kidneys, co-stained for podocyte marker, nephrin and endothelia cell marker, CD31 (PECAM). eGFP co-localizes primarily with nephrin and never with PECAM, SMA, or CD68 (Fig 10), providing evidence that the podocyte is the main cell type where NF-κB is chronically activated in the accelerated aging model and with natural aging. Nephrin expression decreases with time in the Ercc1$^{-/\Delta}$ kidney podocyte, indicating functional breakdown.

The work in Chapter 2 provided evidence of up-regulation of ICAM, smooth muscle actin, and CD68 (macrophage infiltrates) at 16 weeks of age in the *Ercc1*$^{-/\Delta}$ kidney, as well as with naturally aged WT mice. In order to determine whether chronic NF-κB activation in the podocyte is upstream or downstream from these other aging pathologies, the time course of up-regulation of these markers was determined, using high-resolution whole slide imaging. The age of onset of the aging markers was compared to the onset of chronic NF-κB in podocytes, relative to WT controls. Representative confocal images show an increase in ICAM in capillaries and the apical border of tubules at 2-4 months in the *Ercc1*$^{-/\Delta}$ kidney, NF-κB-eGFP kidneys compared to controls. Quantification of whole sections shows that the onset of up-regulation occurs early, by 1 month of age in the capillaries (Figure 14A). It is likely that initial podocyte injury affects the endothelium, located on the other side of the GBM, and causes activation. Quantification of smooth muscle actin (Figure 14B), show that SMA up-regulation over controls begins at 2 months of age, around the same time NF-κB becomes chronically active in podocytes. CD68 quantification provides evidence that macrophage infiltration occurs after NF-κB activation in podocytes (Figure 14C). Therefore, it is possible that podocyte injury and chronic NF-κB activation may contribute to the

other inflammatory and fibrotic changes detected both in the accelerated aging model and with natural aging.

A

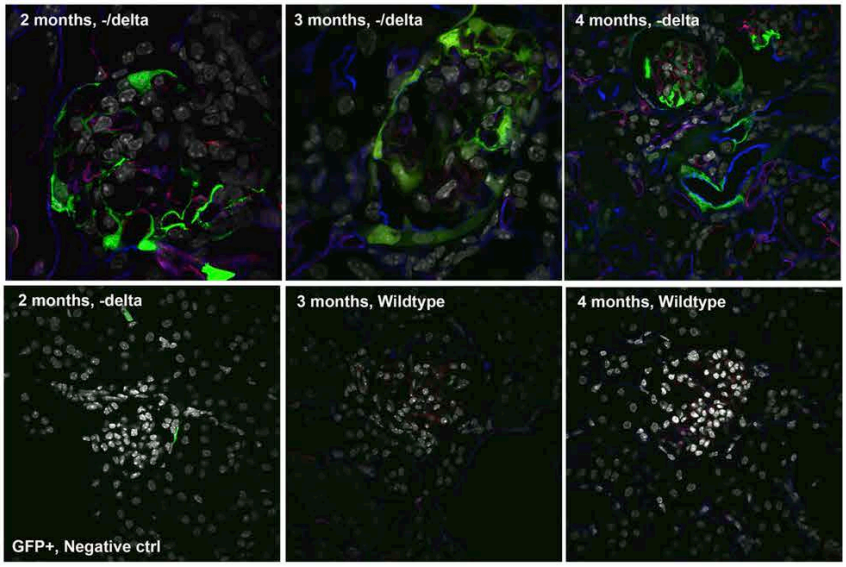

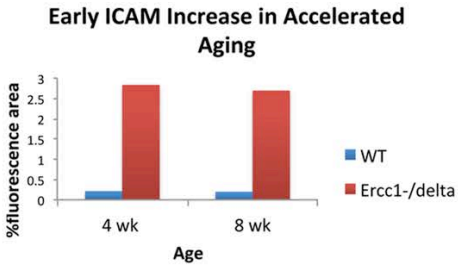

Smooth Muscle Actin Staining in Red

B

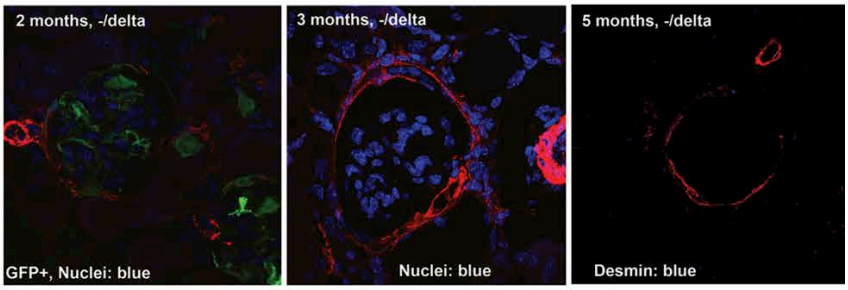

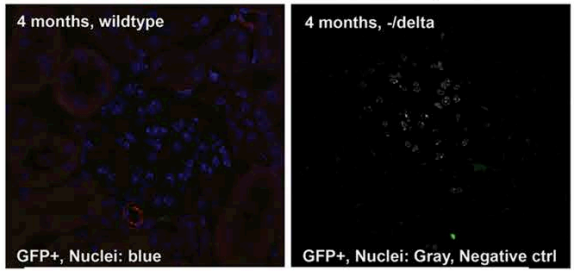

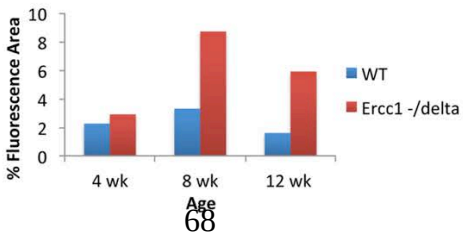

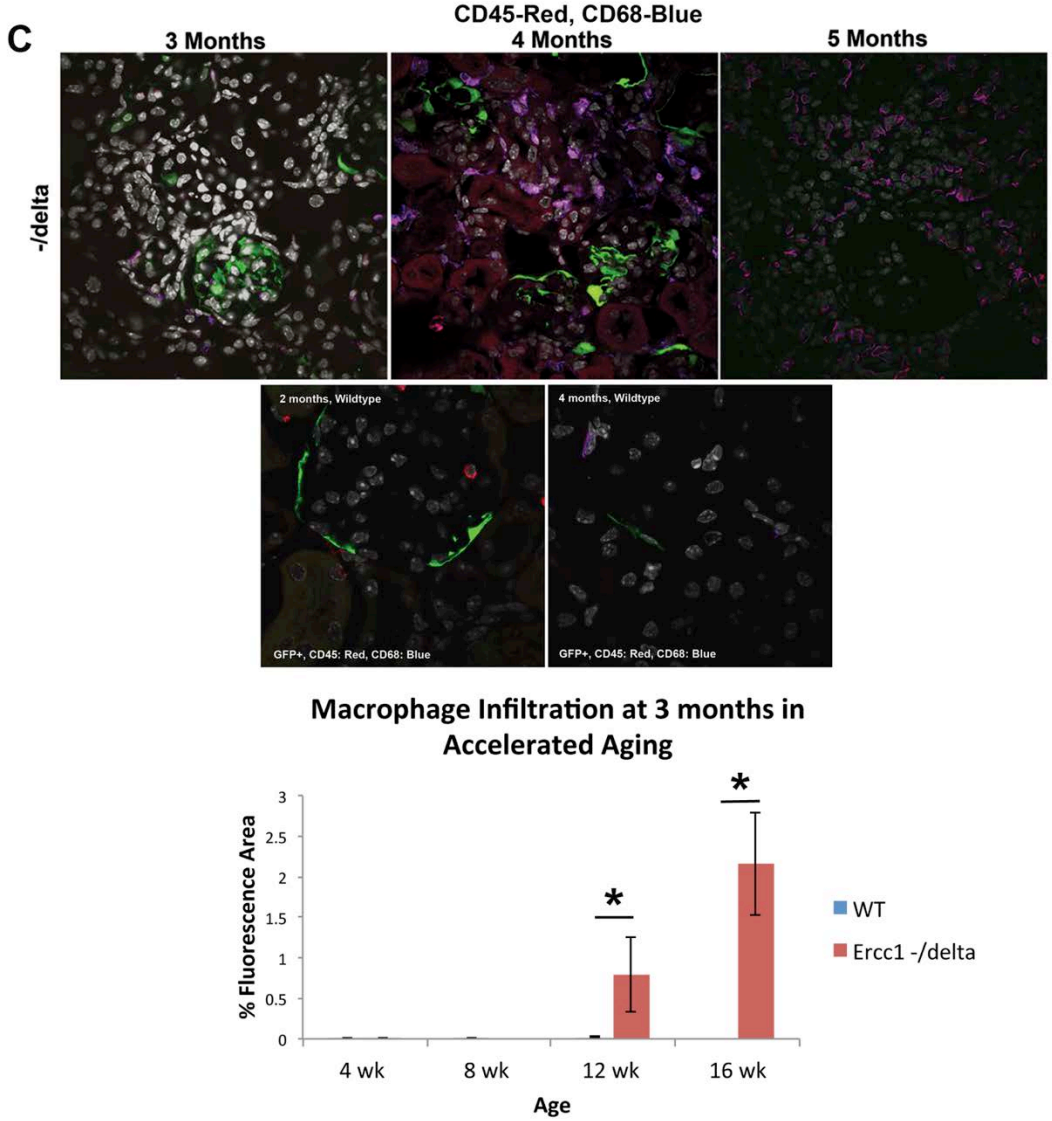

Figure 14. Time course of chronic NF-κB activation in podocytes in relation to other changes

(A) Representative confocal images of NF-κB-eGFP; *Ercc1*$^{-/\Delta}$ and their age-matched controls, stained for PECAM(red), ICAM(blue), and DAPI (white) in 2-4 mo old kidneys. Quantification of whole slides using high-resolution scanning epi-fluorescence imaging shows age of onset of ICAM increase in progeroid kidneys to be at 1 month of age. (B) Representative confocal images of NF-κB-eGFP; *Ercc1*$^{-/\Delta}$ and their age-matched controls, stained for smooth muscle actin (SMA), and DAPI (blue or white). Quantification of whole slides shows age of onset of SMA increase to begin at 2 months of age. (C) Representative confocal images of NF-κB-eGFP; Ercc1$^{-/\Delta}$ and their age-matched controls, stained for CD45 (pan leukocyte, red), CD68 (macrophage, blue). In progeroid kidneys, virtually

all CD45 co-localizes with CD68 fluorescence (purple), indicating immune cells are primarily macrophages. Quantification of whole slides shows age of onset of macrophage infiltration to begin at 3 months of age.

3.3.2 Chronic NF-κB activation onset coincides with autophagic flux impairment and induction of kidney pathologies at 2 months

Podocytes depend on a high rate of basal autophagy for their health and during times of stress, and it is known that autophagy impairment occurs with age and in CKD(5, 27). In agreement with evidence from the literature, isolated glomeruli from young WT mice display high levels of active autophagy, whereas glomeruli isolated from 2.5 yr WT mice display accumulation of LC3-positive and p62 (a protein constitutively degraded by autophagy)-positive puncta and less active autophagy (Appendix D, Figure 27). This leads to the question as to whether autophagy induction occurs at an early time point in the accelerated aging model, as well as to when autophagic flux impairment occurs during the aging nephropathy process.

Imaging was employed to measure levels of the autophagy markers, LC3 and p62, in the glomerulus. If functional autophagy is induced, LC3 fluorescence should increase, while p62 levels remain low or decrease due to increased degradation. As autophagic impairment progresses, LC3 puncta accumulate, and p62 levels increase as well, due to lack of effective degradation.

LC3 was shown to increase as early as 4 weeks in the *Ercc1*$^{-/\Delta}$ glomerulus and LC3 puncta continued to increase with age (Figure 15a). P62 levels at 4 weeks show a slight decrease, and therefore the increased LC3 most likely represents functional autophagy induction in the glomerulus. However, by 8 weeks (Table 3), p62 levels increase above controls and continue to remain high, often localized to puncta, as shown at 12 weeks (Figure 15b). IKK levels show a slight increase at 4 weeks (Table 3) and continue to increase with age, often localized to puncta

(Figure 15c). Finally, it has been shown in mouse embryonic fibroblasts that IKK-β can cause increased mTOR activation by inhibiting the TSC complex(169). pS6 kinase, a marker of mTOR activation, is increased by 2 months (Table 3), in the *Ercc1*$^{-/\Delta}$ glomerulus, and remains high to 4 months (Figure 15d).

There is extensive evidence in other cell types and tissues that IKK and NF-κB activation are tightly involved with autophagy regulation and vice versa(153-155, 157). Further, it has recently been shown that defective autophagy in the hypothalamus in mice causes inflammation and obesity through IKK-beta-NF-κB pathway(159). If the dysregulation of these pathways is related, the timing of autophagy impairment and chronic NF-κB activation in podocytes during aging should coincide. Table 3 provides a summary of all markers measured during the aging process in the *Ercc1*$^{-/\Delta}$ kidney and old WT. Markers measured in the glomerulus specifically are shown in red. From 1-2 months (Table 3, yellow), there is evidence of a large phenotypic shift in podocytes, where autophagy becomes defective and chronic NF-κB activation occurs in podocytes, followed by onset of global kidney pathologies and functional indications of CKD, indicated by large increase in ACR and decrease in GFR. This data leads to the question as to whether inherent podocyte injury, due to accumulating damage, could cause the age-related CKD observed in the *Ercc1* deficient mouse kidney and possibly during natural aging.

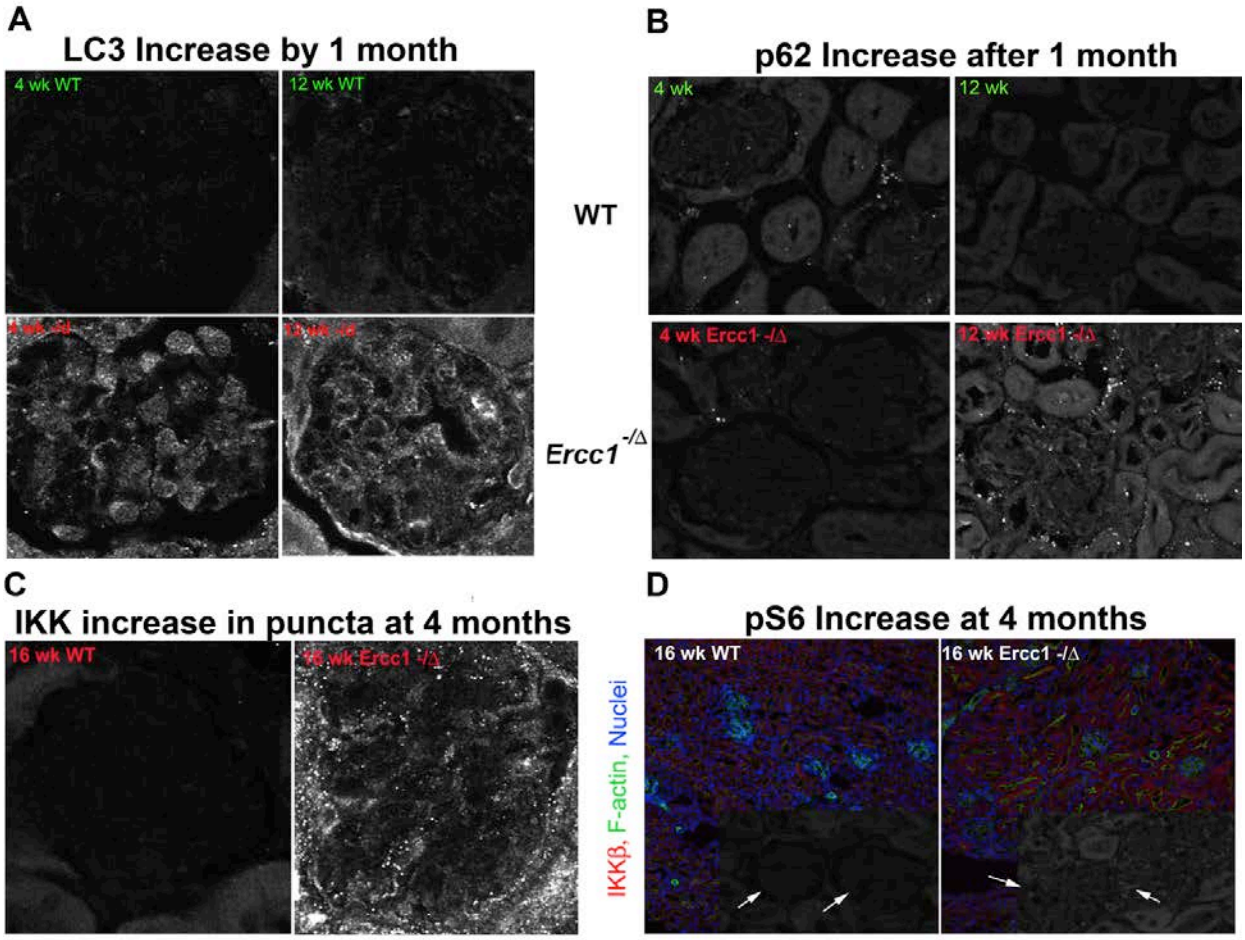

Figure 15. Glomerular autophagy and IKK changes in the *Ercc1*$^{-/\Delta}$ kidney

(A) Representative confocal images show LC3 increase by 4wks in the *Ercc1*$^{-/\Delta}$ glomerulus, maintained with increased puncta at 12 wks, compared to WT controls. (B) p62 levels remain low at 4wk during LC3 increase, indicate functional induction of autophagy. Subsequent increase in glomerular p62 levels, present in puncta, indicate autophagy impairment. (C) IKK increase shown at 16 wks in the *Ercc1*$^{-/\Delta}$ glomerulus, compared to WT controls. (D) pS6 increase, shown at 16 wks in the *Ercc1*$^{-/\Delta}$ glomerulus, indicate increased mTOR activation.

	1 mo	2 mo	3 mo	4 mo	Old WT
LC3	+	+	+ (puncta)	+ (puncta)	+(puncta)
p62	-	+	+	+	+
IKK	+ (slight)	+	+	+	+
NF-κB Activation	0	+	+	+	+
pS6	0	+	+	+	+
SMA	0	+	+	+	+
CD68	0	0	+	+	+
ICAM	+	+	+	+	+
GFR	0	-	-	-	-
ACR	+	++	++	+++	+

Table 3. Summary of age-related changes in the *Ercc1*$^{-/\Delta}$ kidney.

Autophagic flux impairment coincides with chronic NF-κB activation. Markers were quantified by either confocal or whole slide scanning, n=3. "0" denotes no change from young WT control. "+" denotes an increase compared to young WT controls. "-" denotes a decrease compared to young WT controls. Changes measured in the glomerulus specifically are written in red font. Major transition occurs from 1-2 months (highlighted in yellow).

3.4 INHERENT PODOCYTE DAMAGE DUE TO ERCC1 DEFICIENCY CAUSES SUBSEQUENT TUBULE INJURY, CHRONIC KIDNEY DISEASE, AND DECREASED LIFESPAN

3.4.1 Functional Changes in Podocyte specific knock-out and Proximal Tubule specific knock-out of *Ercc1*

Since there is evidence of podocyte injury by 4 weeks in the *Ercc1*$^{-/\Delta}$ kidney, before other pathological changes become apparent, it is possible that inherent damage in the podocyte, due to ERCC1 deficiency, is causing the subsequent global kidney pathologies, impaired function, and perhaps decreased lifespan. In order to test this, a podocyte specific *Ercc1* knock-out, (*Ercc1*-pod-KO) was created. Because there is also evidence of subsequent proximal tubule injury and replacement (discussed in Chapter 2) in the *Ercc1*$^{-/\Delta}$ kidney, and since there is much controversy over the role of the podocyte versus the proximal tubule in preventing albuminuria(170), a proximal tubule specific knock-out was also created using a gamma-GT-cre mouse (*Ercc1*-PT-KO). The podocyte specific Ercc1 knock-out has a significantly reduced average lifespan of 37 +/- 9.7 weeks (Figure 16A), which is slightly longer than the Ercc1$^{-/\Delta}$ mouse (16 +/- 2.3), possible due to additional systemic effects in the *Ercc1*$^{-/\Delta}$ mouse or variability in the degree of knock out in the *Ercc1*-pod-KO (Figure 1). Currently, 100% of the *Ercc1*-PT-KO knock-out group is alive (has not died of natural causes), at 11 months of age, with no overt pathological phenotype. Urine albumin creatinine ratio (ACR) was determined for both cohorts. The *Ercc1*-pod-KO had a significantly elevated ACR compared to controls by 12 weeks of age, and the ACR decreased dramatically until death (Figure 16B). The *Ercc1*-PT-KO never displayed elevated ACR above

controls, even up to 48 weeks of age (Figure 16C). Next, the glomerular filtration rate (GFR) was determined by FITC-inulin clearance. At 8 months of age, the *Ercc1*-pod-KO mice had a severe decrease in GFR to levels compared to control mice (Figure 16D). At 7 months of age, the *Ercc1*-PT-KO did not display any decrease in GFR compared to controls (Figure 16E). These data demonstrate that *Ercc1* deficiency in podocytes, but not proximal tubule cells, can cause a decreased lifespan, extreme albuminuria, and a large decrease in the GFR. In conclusion, podocyte injury due to unrepaired, endogenous DNA damage causes a significant decline in renal function, culminating in end stage renal disease (ESRD).

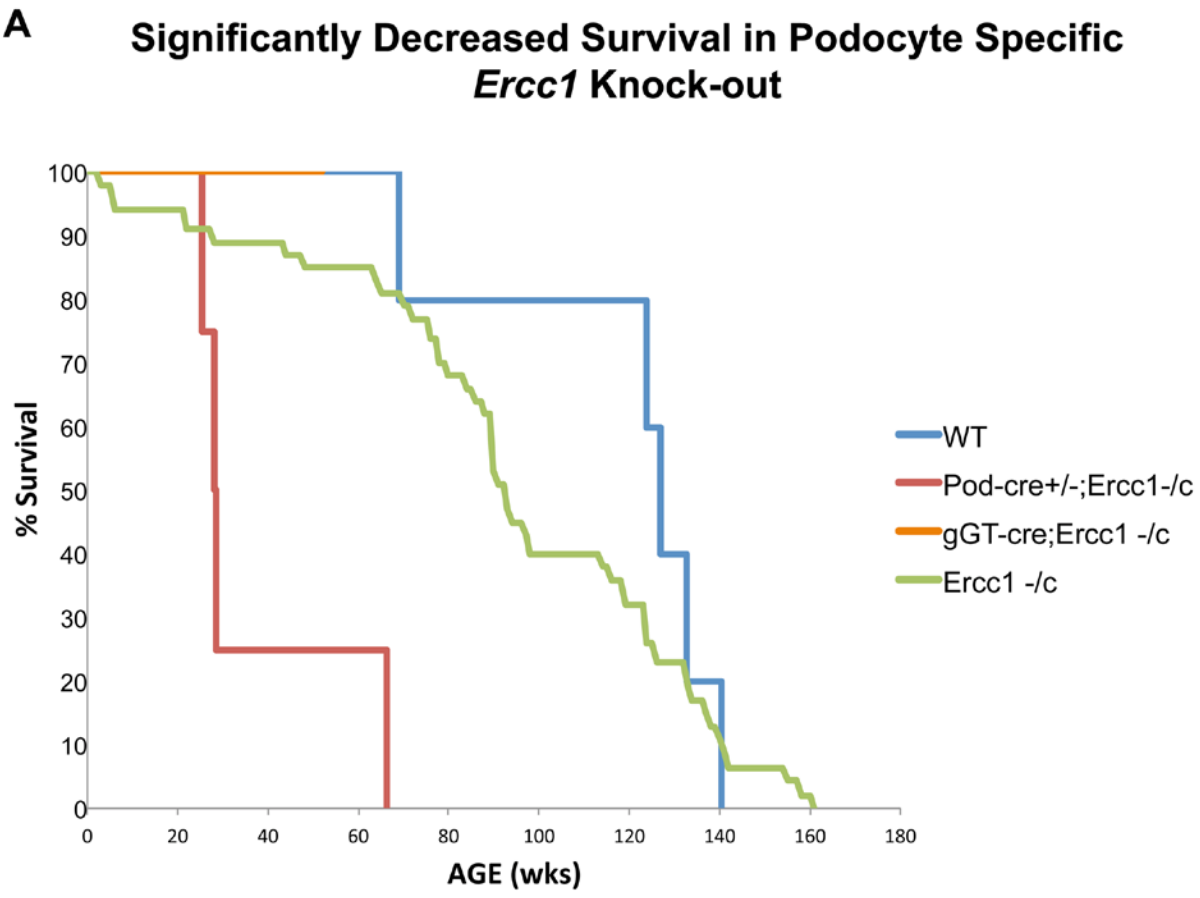

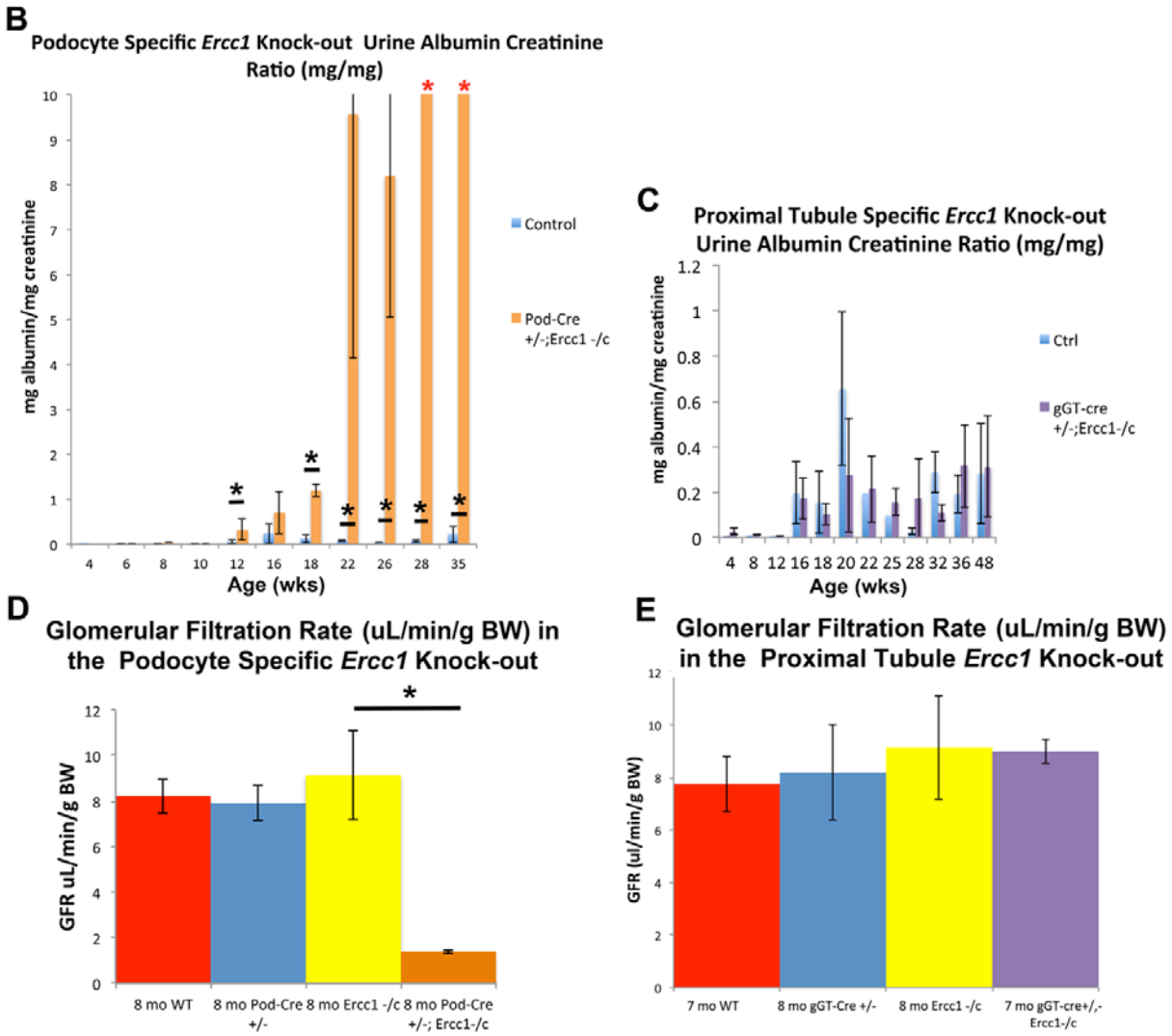

Figure 16. Podocyte, but not proximal tubule specific knock-out of *Ercc1*, results in impaired kidney Function and decreased lifespan.

A) Kaplan-Meyer curve compares lifespan of WT (blue), Ercc1$^{-/c}$, heterozygous for the floxed *Ercc1* as a control (green), *Ercc1*-Pod-KO (red), and *Ercc1*-PT-KO (orange, *=cohort has not died of natural causes yet, at the age of 11 months). (B) Urine albumin-creatinine ratio (ACR) of the *Ercc1*-Pod-KO mice compared to Pod-cre and Ercc1 -/c controls. Data reflect the mean values from 3 mice per group ± S.E.M. Asterisk indicates $p < 0.05$ as determined by a two-tailed Student's *t*-test. ACR values from 28, 35 wks are extremely elevated (red asterisks) with values of 78.97+/-0.08 and 85.39+/-0.22 respectively. (C) Urine ACR of the *Ercc1*-PT-KO compared to gGT-cre and Ercc1-/c controls. Data reflect the mean values from 3 mice per group ± S.E.M. Asterisk indicates $p < 0.05$ as determined by a two-tailed Student's *t*-test. (D) Glomerular filtration rate (GFR) for the *Ercc1*-Pod-KO, determined by FITC-inulin

clearance from the blood after bolus injection. Data reflect the mean GFR in μL/min/g body weight from 3 animals per group ± S.E.M. Asterisk indicates $p<0.05$ as determined by a two-tailed Student's *t*-test. (E) Glomerular filtration rate (GFR) for the *Ercc1*-PT-KO determined by FITC-inulin clearance from the blood after bolus injection. Data reflect the mean GFR in μL/min/g body weight from 3 animals per group ± S.E.M. Asterisk indicates $p<0.05$ as determined by a two-tailed Student's *t*-test.

3.4.2 Ultrastructural changes in Podocyte Specific Knock-out Only

In order to determine whether podocyte injury occurs early in the disease process in the *Ercc1*-Pod-KO as it does in the *Ercc1*$^{-/\Delta}$ glomerulus, the ultrastructure at early and late time points was examined in the knock-out versus the Pod-cre+/- control. At 6 weeks, as seen in the *Ercc1*$^{-/\Delta}$ glomerulus, thickening and effacement of podocyte foot processes (arrow) was evident in some glomeruli, while others appeared to be normal (Figure 17A). The GBM appeared to be of normal thickness, but as observed in the *Ercc1*$^{-/\Delta}$ kidney, it thickened substantially by 7 months of age (arrowhead). Very few healthy podocytes were evident and those that remained were hypertrophied, with large flattened areas against the GBM (asterisk). There was no observed difference in the glomeruli of the *Ercc1*-PT-KO at 7 months, compared to controls.

In the *Ercc1*$^{-/\Delta}$ kidney, subsequent tubule necrosis and replacement was evident. This could be due to inherent damage due to *Ercc1* deficiency, or it could be secondary to podocyte injury. In all controls and the *Ercc1*-PT-KO, some proximal tubules appeared to be healthy with basolateral membrane folds containing columns of mitochondria (Figure 17B, arrows) and an apical border of microvilli (arrowheads). Other tubules appeared to have increased autolysosomal structures and disruption of structure, but this did not lead to decreased GFR or albuminuria. Conversely, in the 7 month *Ercc1*-pod-KO, there was major damage to the tubule ultrastructure

compared to control, with scattered mitochondria and lack of membrane folds at the basolateral side (arrow), disruption of the apical microvilli, extensive debris in the lumen (asterisk), and evidence of many double membrane structures and necrotic tubules (arrowhead). This structural data and the functional data in Figure 16 provides evidence that early podocyte injury and disruption of the glomerular filtration barrier *Ercc1* deficient mice is causing the observed proximal tubule injury. In Chapter 2, extensive evidence was provided to show that the *Ercc1*$^{-/\Delta}$ mouse serves as an accurate model of accelerated kidney aging. The evidence presented here with the cell specific knock-outs of *Ercc1* leads to the hypothesis that early podocyte injury could be responsible for causing kidney disease in natural aging as well.

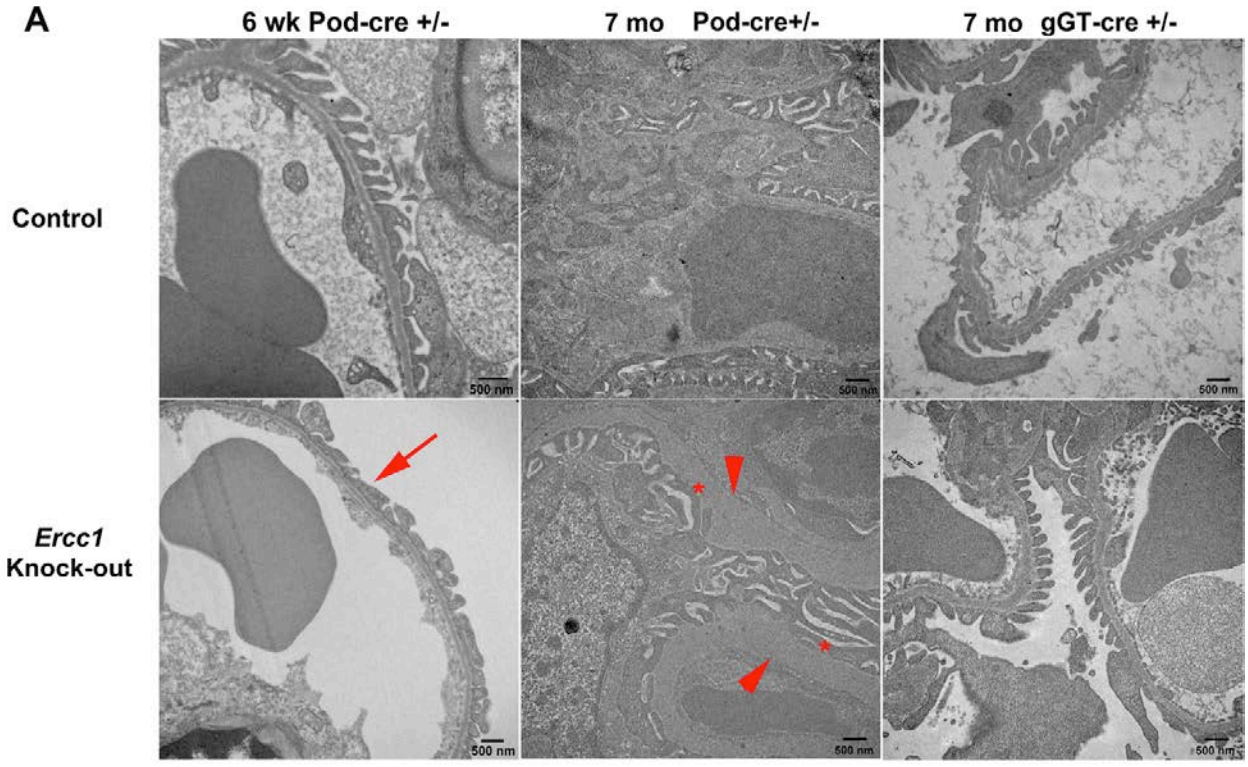

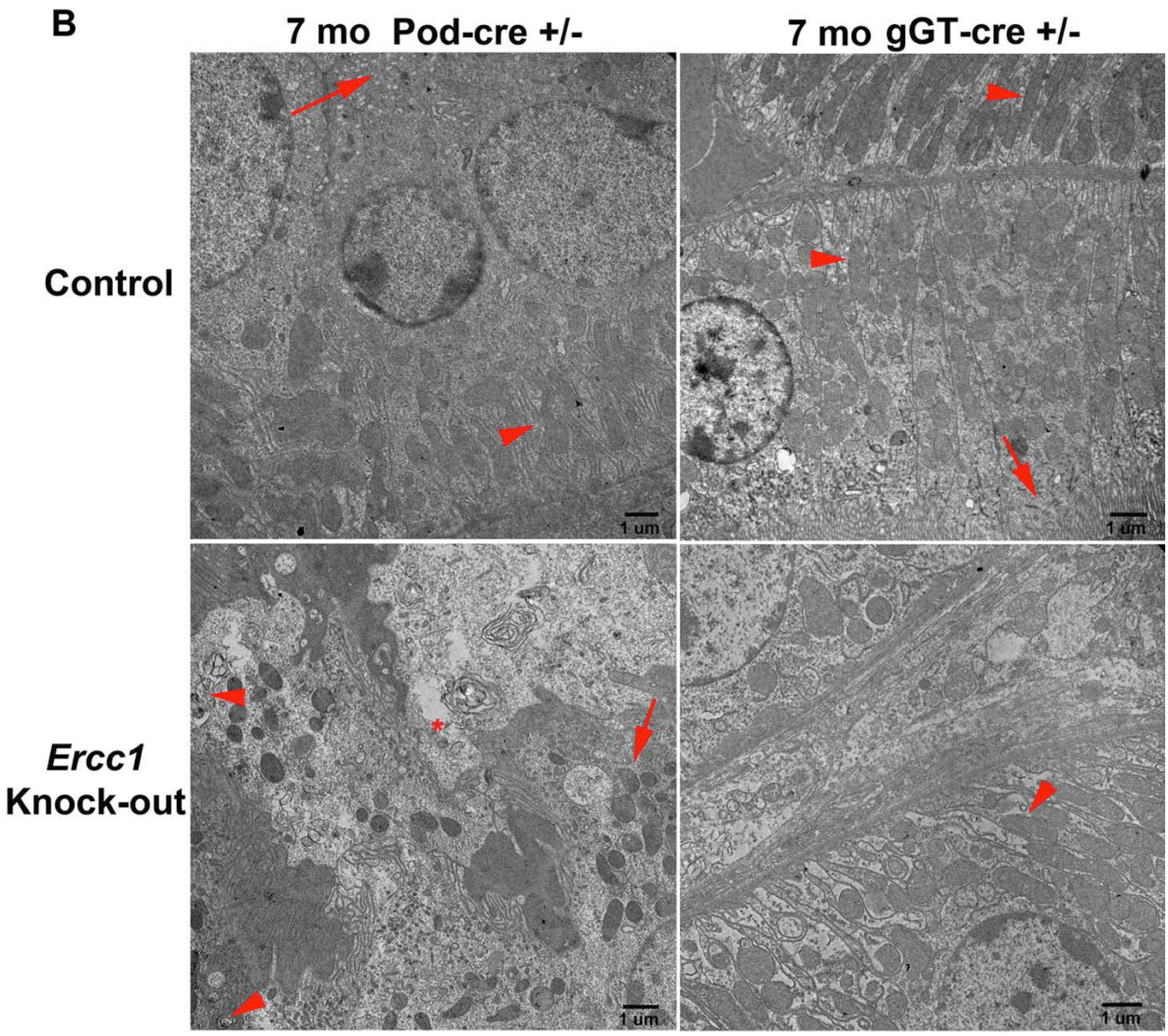

Figure 17. Ultrastructural evidence of podocyte and tubule injury in the *Ercc1*-pod-KO

(A) TEM micrographs at 20,000X of 6wks and 7mo Pod-cre +/- control and *Ercc1*-pod-KO glomeruli, as well as 7mo gGT-cre +/- control and *Ercc1*-PT-KO glomeruli. Normal foot process interdigitation and GBM thickness can be seen in all control glomeruli, as well as in the *Ercc1*-PT-KO. In the 6 wk *Ercc1*-pod-KO, some glomeruli display effacement and thickening of foot processes (arrow), but normal GBM thickness. By 7 months, few healthy glomeruli remained, and many podocytes appeared to be hypertrophied, with flattened foot processes (asterisks) and extremely thickened, irregular GBM (arrowheads). (B) In control kidneys and the *Ercc1*-PT-KO, normal basolateral membrane folds and organized mitochondria are seen (arrowheads), as well as the apical brush border (arrows).

3.4.3 Podocyte knock-out of *Ercc1* mirrors age-related cellular changes observed in Ercc1$^{-/\Delta}$ mouse kidney

3.4.3.1 Tubule injury is secondary to inherent podocyte damage

There is much evidence that glomerular injury and proteinuria can cause tubule injury(171), and the evidence presented thus far here, leads to the hypothesis that this can also occur during accelerated kidney aging. Kidney Injury Molecule-1 (KIM-1) has been well established as a marker for proximal tubule injury, and up-regulation of KIM-1 leads to fibrosis(171, 172). In order to test the hypothesis that tubule injury occurs subsequent to podocyte injury, immunofluorescence for KIM-1 was examined in both Ercc1$^{-/\Delta}$ and *Ercc1*-pod-KO kidneys at 1 month and 4 months of age. There was no evidence of KIM-1 at 1 month in either mutant when podocyte injury initially occurs, but it was evident by 4 months in tubules, both diffusely and at the apical border (insets), as well as increased diffusely in 2 yr old WT kidneys (Figure 18).

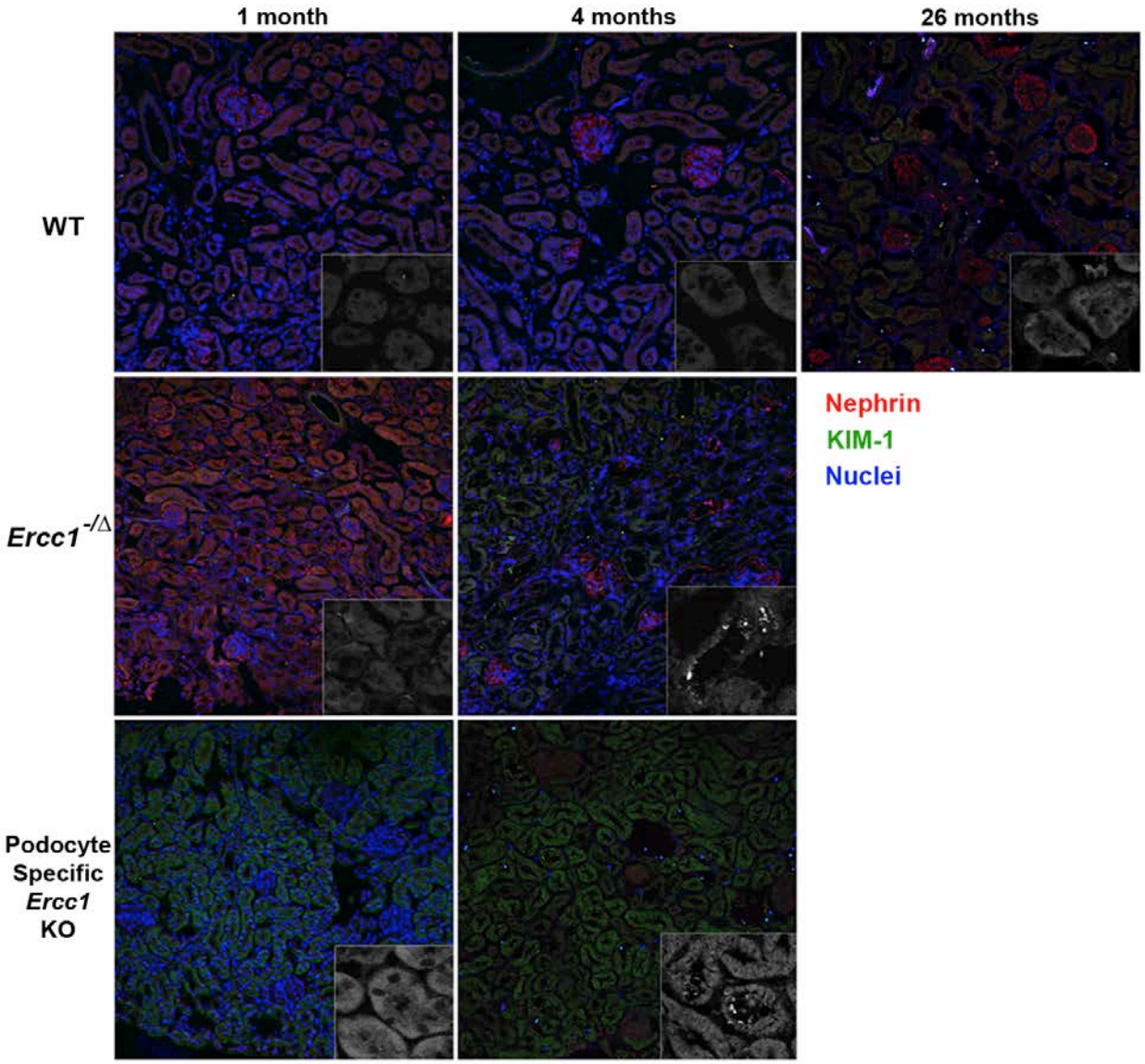

Figure 18. KIM-1 increase indicates tubule injury after 1 month due to podocyte damage.

Confocal images at a magnification of 200X, showing 1 mo and 4 mo WT, Ercc1 $^{-/\Delta}$, and *Ercc1*-pod-KO kidneys, as well as 26 mo WT. Nephrin (red), KIM-1(green), and nuclei (blue). Higher magnification insets, show KIM-1 channel only and highlight KIM-1 increase at apical border in *Ercc1* deficient kidneys by 4 months and to a lesser degree in old WT.

3.4.3.2 Vascular changes, myofibroblast accumulation, and macrophage infiltration is caused by Podocyte *Ercc1* deficiency

In the *Ercc1*$^{-/\Delta}$ and naturally aged mouse kidney, ICAM up-regulation, SMA actin-positive cell increase, and macrophage infiltration occurs. In order to see if these changes can be caused by inherent podocyte damage, the same markers were measured in the *Ercc1*-pod-KO kidneys using immunofluorescence. As in the Ercc1$^{-/\Delta}$ kidney, an increase in ICAM expression, both in glomerular capillaries (glomerulus labeled with nephrin) and at the tubule brush border, occurs early, shown at 6 and 16wks in the *Ercc1*-pod-KO compared to pod-cre +/- control kidneys (Figure 19A). ICAM was also measured in 7 mo old *Ercc1*-pod-KO and 8 mo old *Ercc1*-PT-KO kidneys and their controls (Figure 19B). By 7 mo, in the *Ercc1*-pod-KO kidney, ICAM expression is not as pronounced in the glomerulus (arrows), but is still largely increased in the tubules. A significant disruption of glomerular vascular beds, labeled with PECAM, is evident (arrowhead) at this time. No change in ICAM or PECAM is observed in 8 month *Ercc1*-PT-KO kidney.

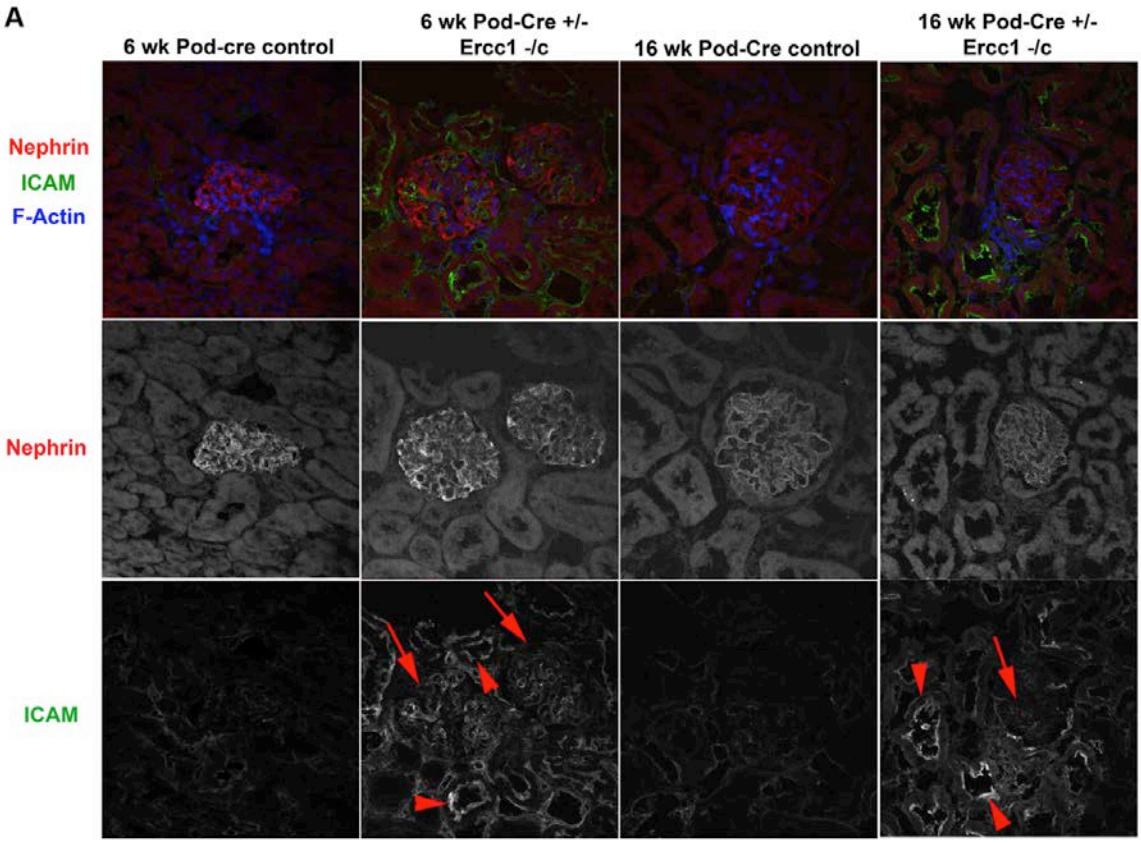
A
6 wk Pod-cre control
6 wk Pod-Cre +/- Ercc1 -/c
16 wk Pod-Cre control
16 wk Pod-Cre +/- Ercc1 -/c
Nephrin
ICAM
F-Actin
Nephrin
ICAM

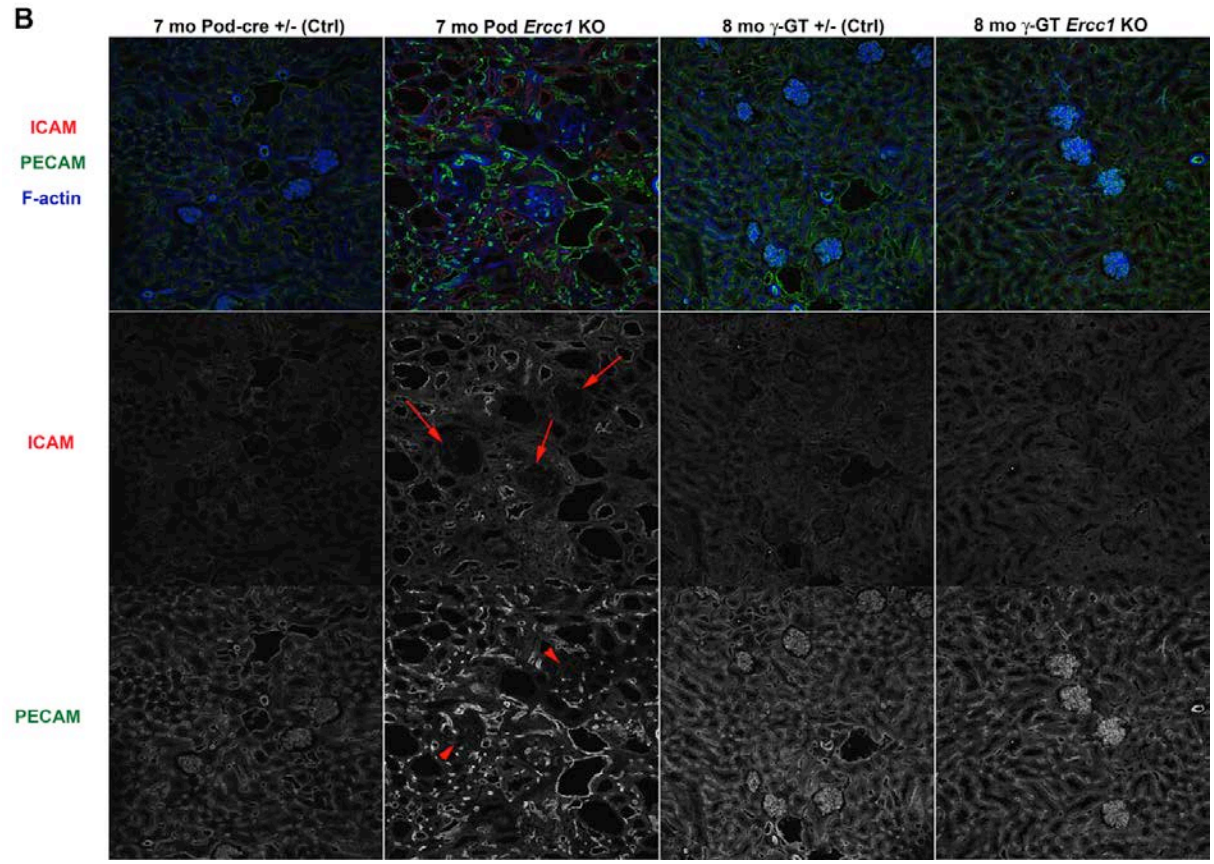

Figure 19. Early ICAM increase occurs in *Ercc1*-pod-KO, but not in *Ercc1*-PT-KO kidneys

(A) Confocal images at 600x magnification of 6 wk and 16 wk *Ercc1*-pod-KO kidneys and their pod-cre +/- controls. First row shows glomeruli marked by nephrin (red), ICAM (green), and F-actin (blue). The second row shows the nephrin channel only. The third row shows the ICAM channel only to highlight the increase in *Ercc1*-pod-KO's. (B) Confocal images at 200x of 7 month *Ercc1*-pod-KO and control, and 8 month *Ercc1*-PT-KO and control. ICAM increase is visible only in *Ercc1*-pod-KO, with irregular vascular architecture (PECAM).

An increase in SMA-positive cells in the $Ercc1^{-/\Delta}$ kidney is observed surrounding the glomerulus and within the interstitium by 2 months of age. This is also observed in the old, naturally aged mouse. In the 7mo *Ercc1*-pod-KO kidney, there is a dramatic increase of SMA+ cells, not only surrounding the hypertrophied glomeruli, but also inside of the glomeruli (Figure 20A, arrows), in the tubulointerstitial space and surrounding injured tubules (Figure 20A, arrowheads). These images also highlight the largely dilated tubule space, lined by epithelium,

which have lost their brush border and normal epithelium morphology. None of these SMA+ increases occur in any of the control age-matched animals, nor do they occur in the 8 month *Ercc1*-PT-KO.

With natural aging and in the *Ercc1*$^{-/\Delta}$ kidney model of accelerated aging, there is extensive macrophage infiltration. In the *Ercc1*$^{-/\Delta}$ kidney, this does not occur until 3 mo of age, after podocyte injury, NF-κB activation, and other global kidney changes. Similarly, there is severe macrophage infiltration in 7 mo *Ercc1*-pod-KO kidneys, compared to control. There is no significant F480 increase in 8 mo *Ercc1*-PT-KO kidneys compared to control (Figure 20B). The lack of global kidney pathologies or change in function in *Ercc1*-PT-KO indicates that *Ercc1* deficiency in proximal tubule cells does not likely cause age-related kidney disease.

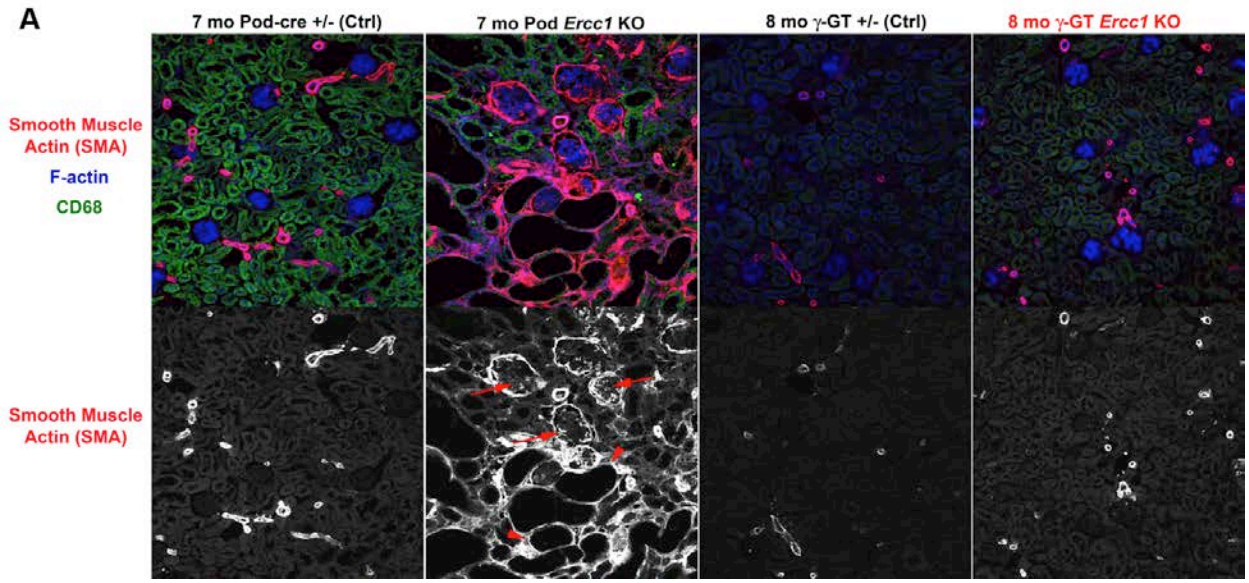

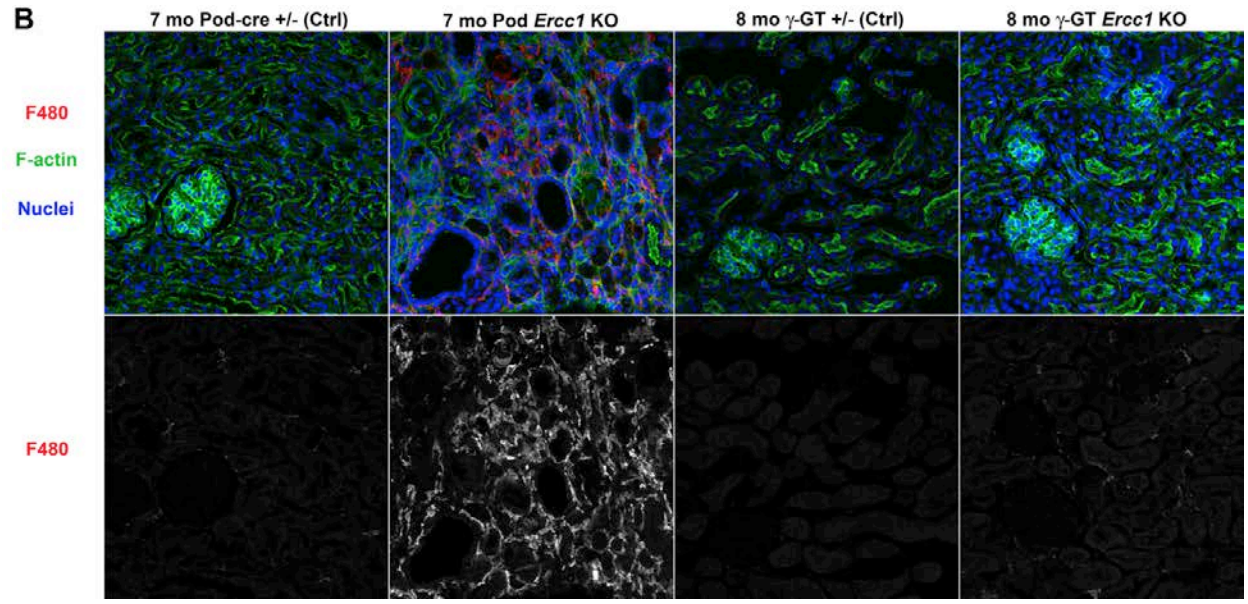

Figure 20. Dramatic SMA increase and macrophage infiltration at 7 mo in the *Ercc1*-pod-KO

(A) Confocal images at 200x magnification, demonstrating a large increase in smooth muscle actin-positive (SMA+) cells in 7 mo *Ercc1*-pod-KO compared to controls and 8 mo *Ercc1*-PT-KO. SMA increase is evident surrounding and within glomeruli (arrows), as well as interstitially and surrounding injured, dilated tubules. (B) Confocal Images at 400x magnification of F480 staining in 7 mo *Ercc1*-pod-KO and Pod-cre+/- controls, as well as 8 mo *Ercc1*-PT-KO and γ–GT+/- controls.

3.4.3.3 Ercc1 deficiency in podocytes causes autophagy impairment, chronic increase in IKK expression and mTOR activation

Finally, in order to characterize the changes within the glomerulus compared to *Ercc1*$^{-/\Delta}$ glomeruli and to gain an insight into which cellular processes may be contributing to this injury, autophagy markers and IKK-β were examined. In the *Ercc1*-pod-KO, as in the *Ercc1*$^{-/\Delta}$ glomeruli, there is an early increase in LC3 at 6wks of age (Figure 21A), compared to control. At this time, p62 levels remain low, demonstrating a functional induction of autophagy. However, at 4 months, there is an increase in p62 overall and in puncta in the *Ercc1*-pod-KO, comparable to

that seen in the *Ercc*1$^{-/\Delta}$ glomerulus (Figure 21B). This represents a breakdown in autophagic flux that occurs with aging, but in an accelerated manner in the *Ercc1* deficient podocyte. By 7 months, in the *Ercc1*-pod-KO, there is an accumulation of large puncta that are both LC3 and p62 positive. No significant changes were detected in the 8 month *Ercc1*-PT-KO compared to its control (Figure 21C).

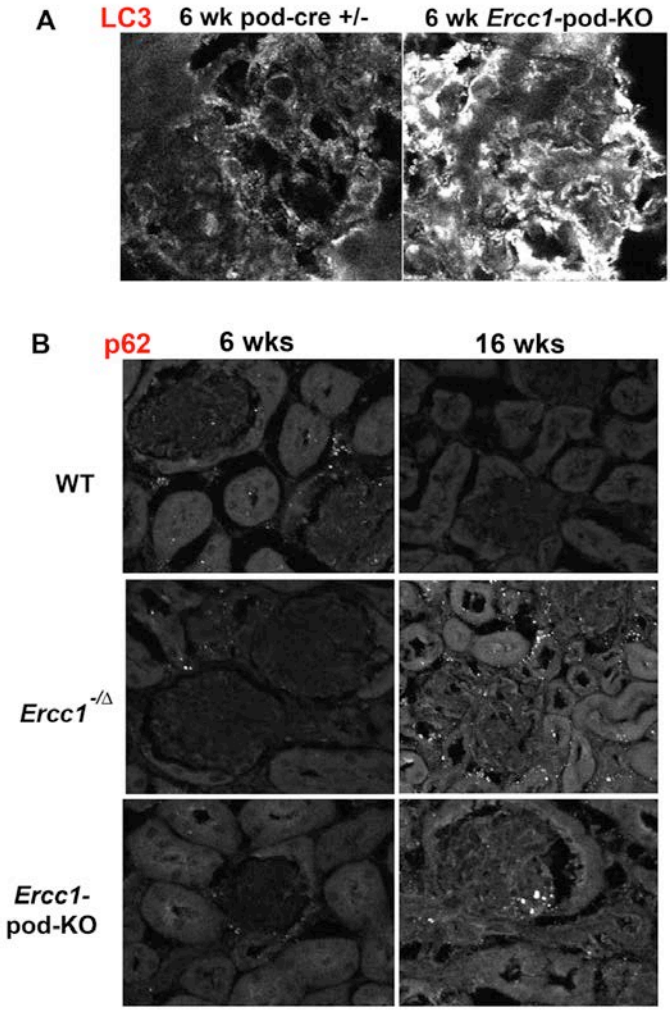

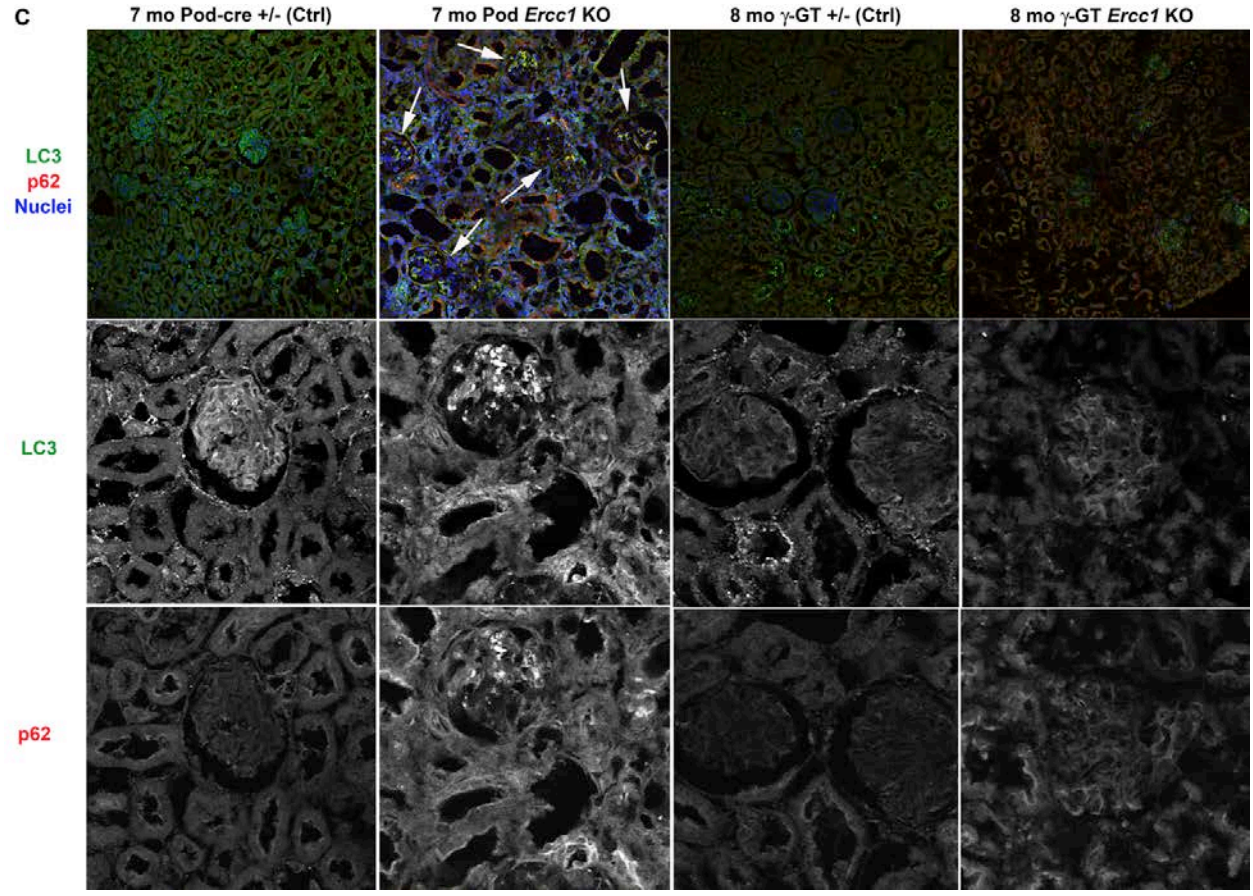

Figure 21. Early induction of autophagy followed by autophagy impairment in the *Ercc1* deficient glomerulus

(A) Representative confocal image of single glomeruli, highlighting the increase in LC3 at 6wks in the *Ercc1*-pod-KO vs. the pod-cre+/- control. (B) Representative confocal images of p62 levels in glomeruli from 6wks and 16wks from *Ercc1*-pod-KO and pod-cre+/- controls. P62 levels remain low at 6wks in the *Ercc1*-pod-KO and $Ercc1^{-/\Delta}$ glomerulus, demonstrating effective autophagy induction. P62 levels increase significantly by 4 months, demonstrating an impairment in autophagic degradation. (C) First row: Representative confocal images at 200X with LC3 (green), p62(red), and nuclei (blue). Arrows indicate significant build-up of LC3 and p62 positive, large puncta in glomeruli of 7 mo old *Ercc1*-pod-KO compared to Pod-cre +/- control. This change was not detected in 8 mo *Ercc1*-PT-KO, compared to its gGT-cre+/- control. Second and third row: higher magnification of glomeruli, showing only LC3 and p62 channels respectively.

Chronic NF-κB activation occurred in the podocytes of the $Ercc1^{-/\Delta}$ mouse, as did the activator of NF-κB, IKK, at an early age. In order to test the hypothesis that this sustained signaling

was a result of inherent podocyte damage, IKK expression in the *Ercc1*-pod-KO and the *Ercc1*-PT-KO was compared to their appropriate control kidneys. IKK levels were increased as early as 16wks in the *Ercc1*-pod-KO compared to controls (Figure 22A). At 7 months, IKK levels had significantly increased in glomeruli of the *Ercc1*-pod-KO, often localizing to large puncta (arrows). IKK levels did not increase in 8 month *Ercc1*-PT-KO kidneys compared to their gGT-cre+/- controls (Figure 22B). Also, as in the $Ercc1^{-/\Delta}$ mouse glomeruli, pS6 levels were increased in podocytes (arrows) in 7 mo *Ercc1*-pod-KO's, but not in 8 mo *Ercc1*-PT-KO's, compared to control. As stated earlier in this chapter, there is much evidence that IKK can result in increased mTOR activation, represented here by pS6 increase, as a result of inhibition of the TSC1 complex(169). Also, increased mTOR activation can lead to the hypertrophy that is observed in the *Ercc1*-pod-KO glomerulus. At 7 months, there are increased levels of pS6 in the glomerular podocytes of the *Ercc1*-pod-KO (arrows, Figure 22C), but not in the *Ercc1*-PT-KO, compared to controls. Also evident is the increased size of the glomerulus in the *Ercc1*-pod-KO, compared to controls and the 8 month *Ercc1*-PT-KO (Figure 22C, third row).

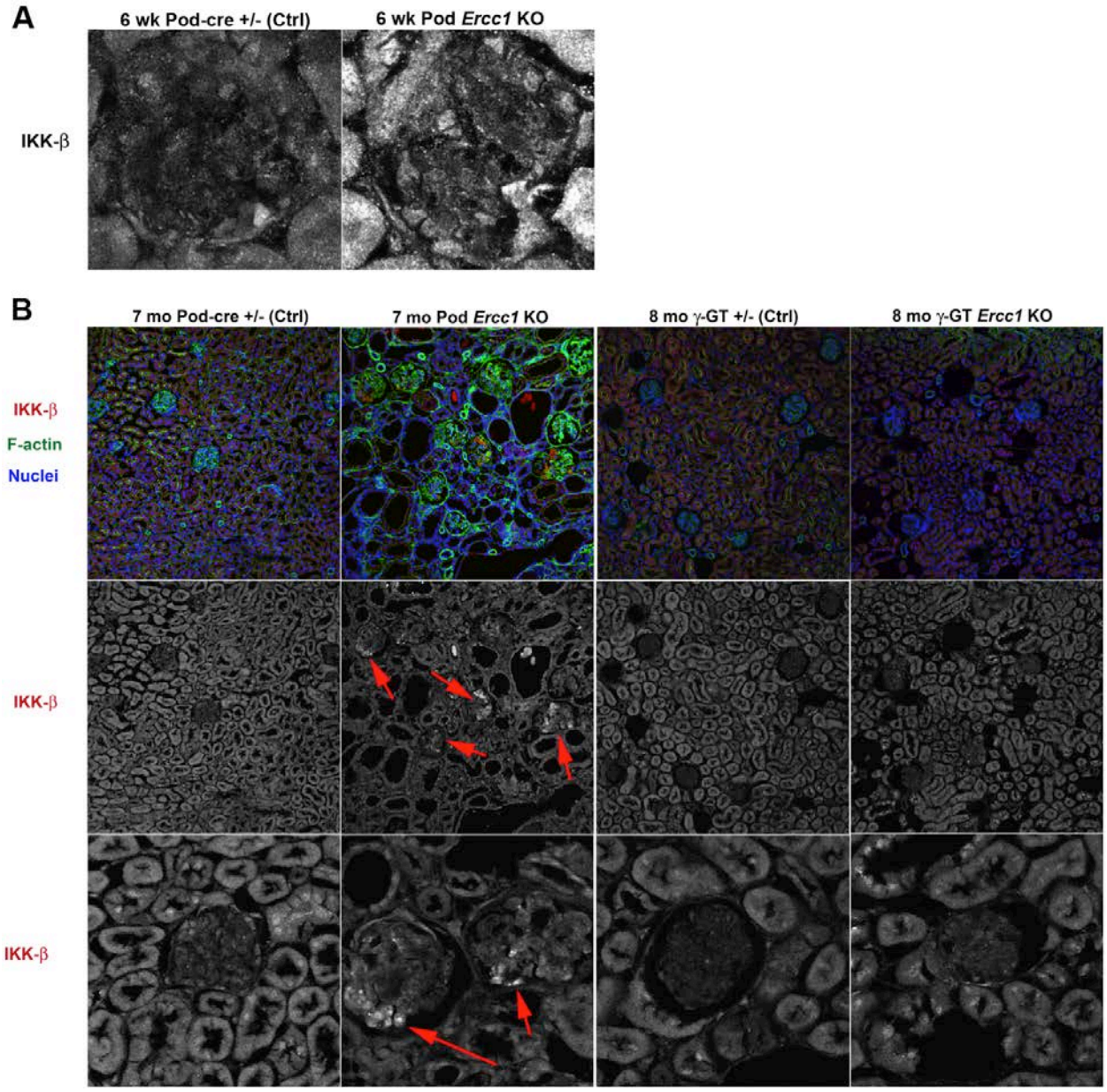
A
6 wk Pod-cre +/- (Ctrl)
6 wk Pod Ercc1 KO
IKK-β
B
7 mo Pod-cre +/- (Ctrl)
7 mo Pod Ercc1 KO
8 mo γ-GT +/- (Ctrl)
8 mo γ-GT Ercc1 KO
IKK-β
F-actin
Nuclei
IKK-β
IKK-β

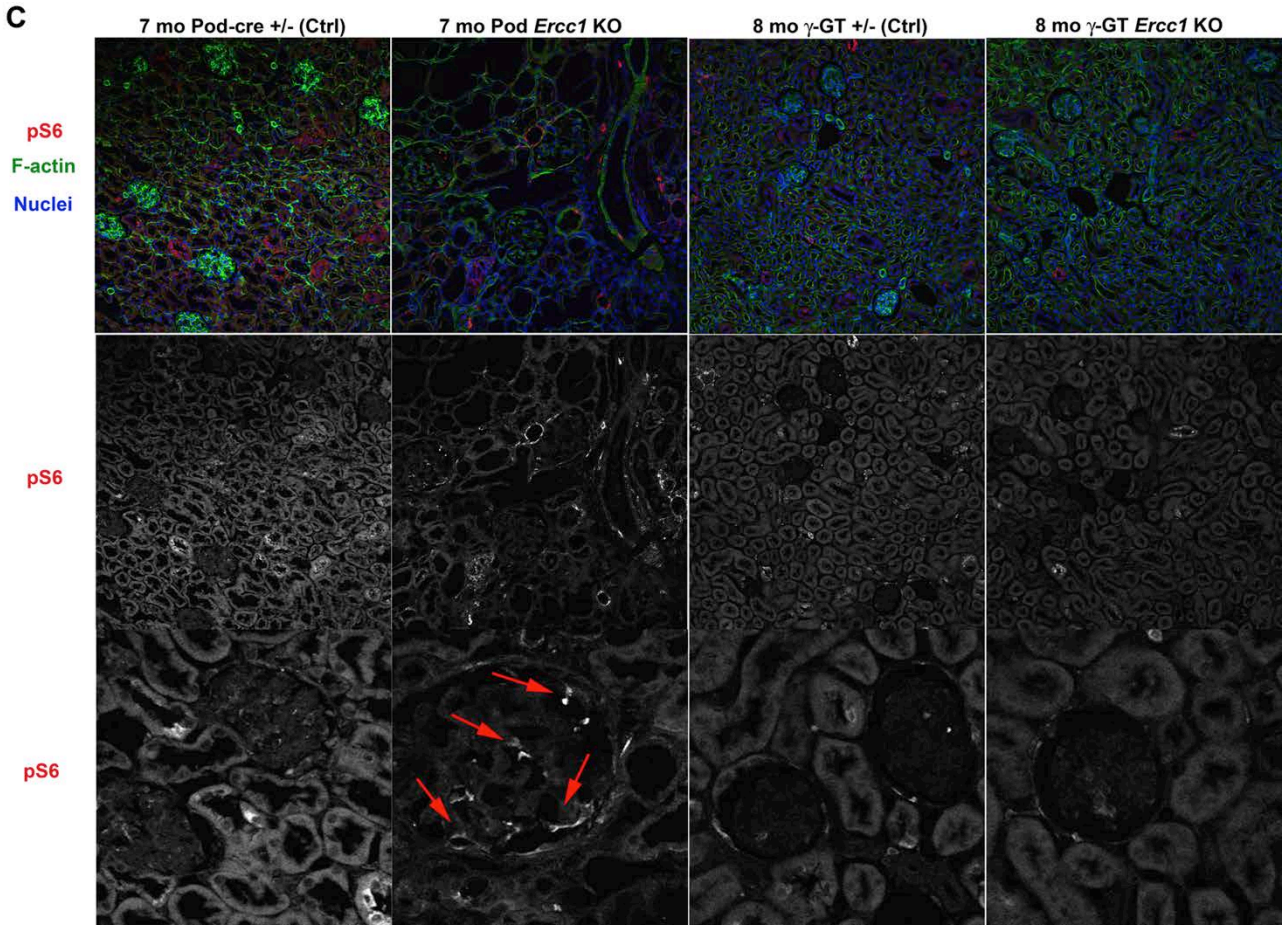

Figure 22. Sustained IKK increase and mTOR activation in *Ercc1*-pod-KO glomeruli

(A) Representative confocal images of a glomerulus showing IKK-β increase at 16 wks in the *Ercc1*-pod-KO vs. the pod-cre+/- control. (B) Confocal images at 200x stained for IKK-β. First row: IKK-β , red; F-actin, green; nuclei, blue. Second row: IKK channel only. Third row: higher mag images of IKK in glomeruli. The increase of IKK-β in the glomeruli of *Ercc1*-pod-KO (red arrows) is highlighted here. No change is seen in the *Ercc1*-PT-KO compared to control. (C) Confocal images at 200x stained for pS6 to represent mTOR activity. First row: pS6, red; F-actin, green; nuclei, blue. Second row: pS6 channel only. Third row: higher mag images of pS6 in glomeruli, highlighting pS6 increase in the enlarged glomeruli of the 7 mo *Ercc1*-pod-KO.

3.4.4 Crosstalk between IKK-NF-κB and autophagy systems in normal mouse podocyte cell line

There is abundant evidence of a closely-knit relationship between the IKK-NF-κB signaling network and the autophagy network in various tissues and cell types(153-158). As presented in the introduction of this chapter, IKK-NF-κB can induce autophagy in some cells, but has also been shown to inhibit autophagy in other systems(157). It is clear that the relationship is context- and tissue dependent. There is also evidence that all three subunits of IKK are degraded by autophagy(154, 155). Little to nothing is known about this relationship in normal or aged podocytes. Given the above *in vivo* data presented thus far, it is possible that podocytes, due to accumulated oxidative damage during aging, up-regulate autophagy through IKK(153, 154). When autophagic flux is in tact in the healthy podocyte, it would degrade IKK in a negative feedback mechanism. However, as damage accumulates and autophagic degradation becomes impaired, less IKK would be degraded, likely contributing to chronic NF-κB activation(159). Before these hypotheses can be tested in aging, it was first necessary to establish a relationship between IKK and autophagy in a normal, differentiated mouse podocyte cell line.

In a differentiated mouse podocyte cell line, grown for 10 days on a collagen IV substrate, autophagic flux studies were performed using 25 μM (27, 173) chloroquine, with and without a small molecule IKK inhibitor, IKKi VII. This cell line contains a mutant SV40 antigen which is degraded at 37^{o}C, at which point the cells are no longer "immortalized," and proceed to differentiate over a period of 10-14 days, when they express high levels of podocyte-specific markers such as nephrin, as well as high levels of LC3, both in diffuse and punctate staining patterns indicating a high level of basal autophagy (Figure 23A). This high level of basal autophagy

was demonstrated by chloroquine addition to show build-up of LC3+ autophagosomes and autolysosomes (Figure 23B, first row, last panel). In order to see how basal autophagy and autophagy induction are affected by IKK inhibition, I examined LC3 staining patterns with and without serum (to induce autophagy) in control podocytes or with IKK inhibition for 6 hours. Less LC3 was detected in cells with IKK inhibition and this effect was pronounced in cultures with serum starvation (Figure 23B, second row). Cell number and overall morphology was not affected (as measured with DAPI and F-actin staining, data not shown). These results could indicate that autophagy induction in podocytes may in part depend on IKK. In order to demonstrate this further and to reduce off-target effects from long-term inhibition, IKK inhibitor was added for only 3 hours, with and without chloroquine addition for the final 2 hours. Interestingly, there was less LC3 in the cytoplasm of cells with IKK inhibition (Figure 23C, first row), but more puncta along cell-cell junctions. This LC3 staining at cell-cell junctions was also detected in control cells to a lesser extent, independent of cell culture density, as well as in freshly isolated glomeruli, where it co-localized with nephrin and F-actin (Appendix D, Figure 26). This is the first report of this pattern and could represent a new role for LC-3 in podocytes. Upon the addition of chloroquine, it is clear that with IKK inhibition, there is less active autophagy, indicated by significantly less build-up of LC3+ vesicles (Figure 23C, row 2).

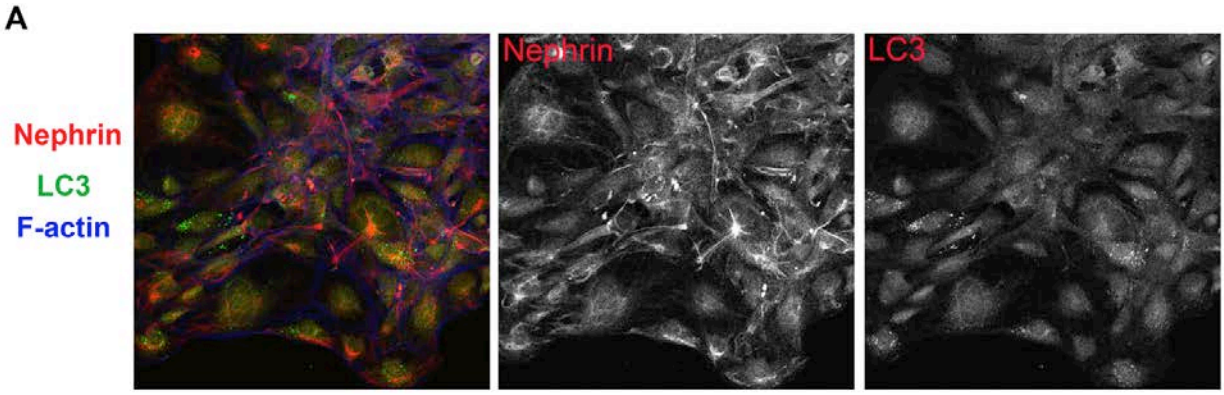

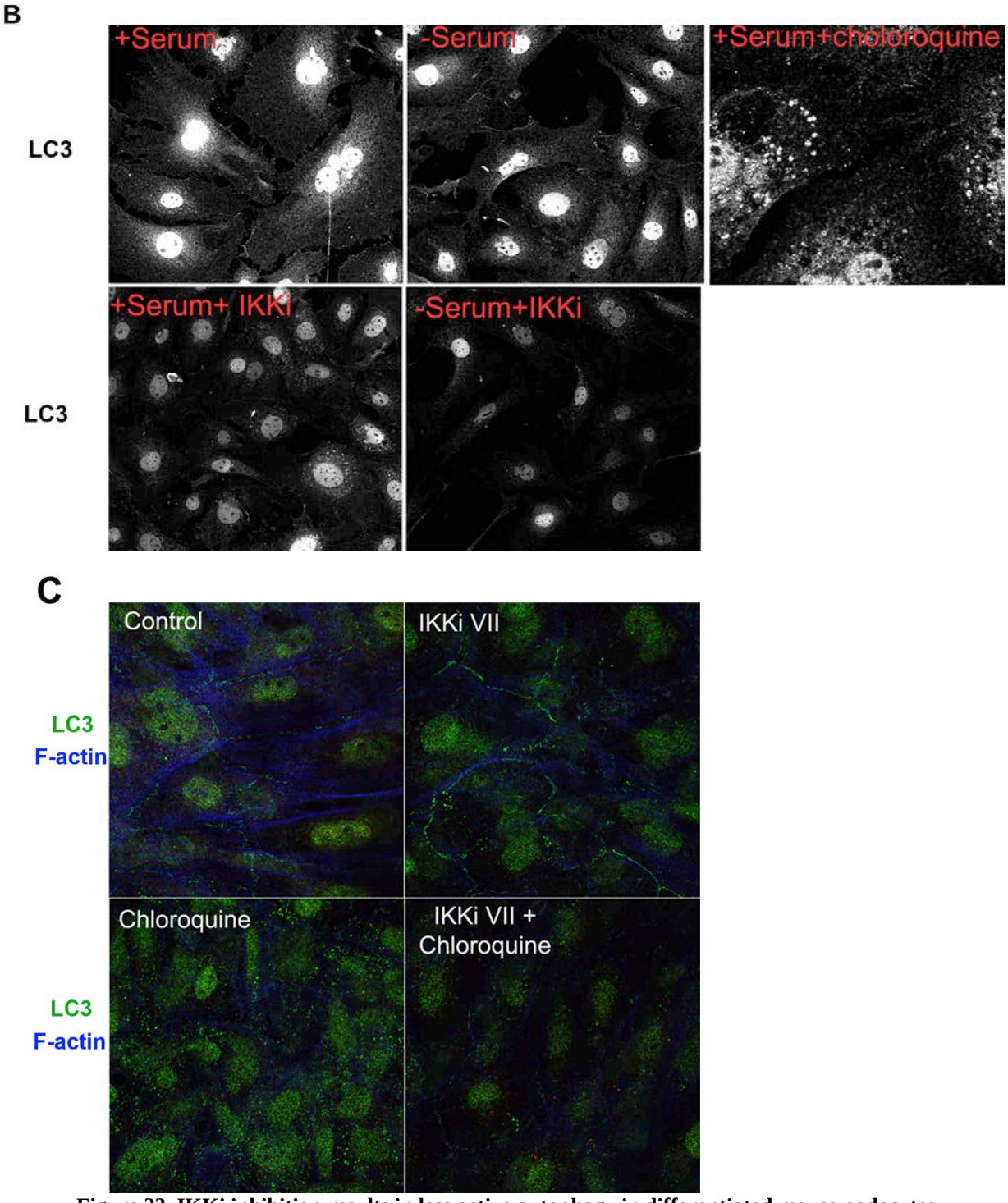

Figure 23. IKKi inhibition results in less active autophagy in differentiated mouse podocytes

(A) Mouse podocyte cell line, differentiated for 10 days at 37°C on collagen IV. High nephrin and LC3 expression, diffuse and in puncta, demonstrates differentiation and high basal autophagy. (B) First row: Control, differentiated podocytes, displaying high levels of LC3 with serum (basal levels) and without serum (6 hrs) to induce autophagy.

Addition of 25 μM chloroquine for 2 hours results in LC3-positive puncta build-up, demonstrating high levels of active autophagy. Second row: IKK inhibition with 500nM IKKi VII small molecule for 6 hrs results in less LC3 staining, and significantly less LC3 staining with serum starvation, demonstrating an inhibition of autophagy induction. (C) First row: short-term IKK inhibition (3 hrs) results in less cytoplasmic LC3 but more LC3 puncta at cell-cell junctions. Second row: 25 μM chloroquine addition for 2 hrs with IKK inhibition results in significantly less LC3 puncta build-up, compared to controls, demonstrating significantly less active autophagy with IKK inhibition.

With IKK inhibition in podocytes, there is less active autophagy. Therefore, with increased IKK activity, there could be an increase in autophagy. In order to test this hypothesis, the differentiated mouse podocytes were transiently transfected with a FLAG-tagged, constitutively active IKK mutant, termed IKK-2. Transfected cells displayed NF-κB activation, indicated by nuclear p65 localization, compared to non-transfected cells (Figure 24A). Transfected podocytes maintained their nephrin expression and displayed significantly increased amounts of IKK protein (Figure 24B). Transfected cells, labeled for the FLAG-tag, displayed increased LC3 and active autophagy, shown by LC3 puncta accumulation after chloroquine treatment (Figure 24C). Interestingly, LC3 was also localized to distinct spots that resemble focal contacts, as well as cell-cell junctions. The podocytes in which IKK was constitutively active took on a different morphology with more F-actin stress fibers, possible undergoing an actin cytoskeleton rearrangement. The work presented here in a differentiated mouse podocyte cell line shows that there is a distinct relationship between the IKK/ NF-κB pathway and autophagy in podocytes.

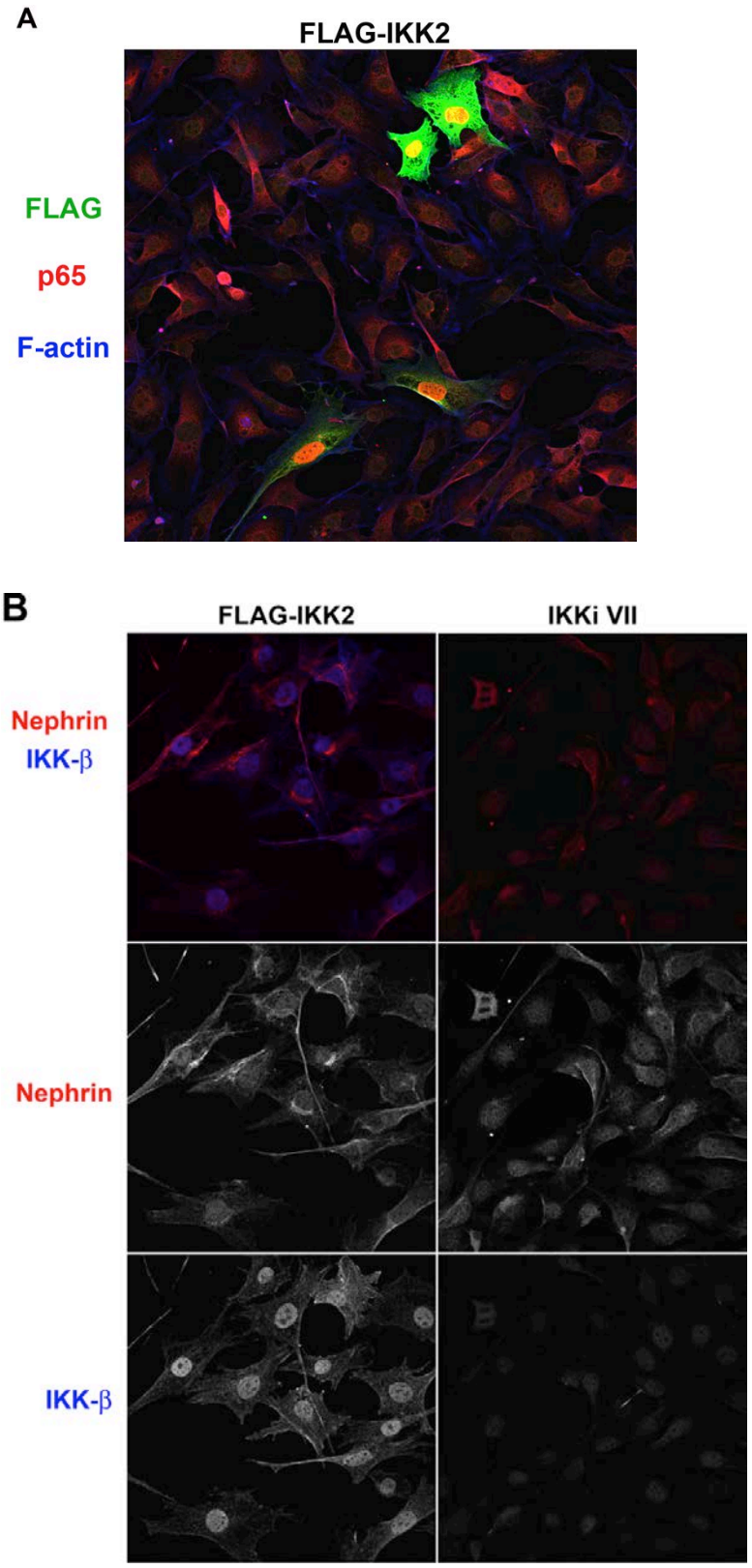
A
FLAG-IKK2
FLAG
p65
F-actin
B
FLAG-IKK2
IKKi VII
Nephrin
IKK-β
Nephrin
IKK-β

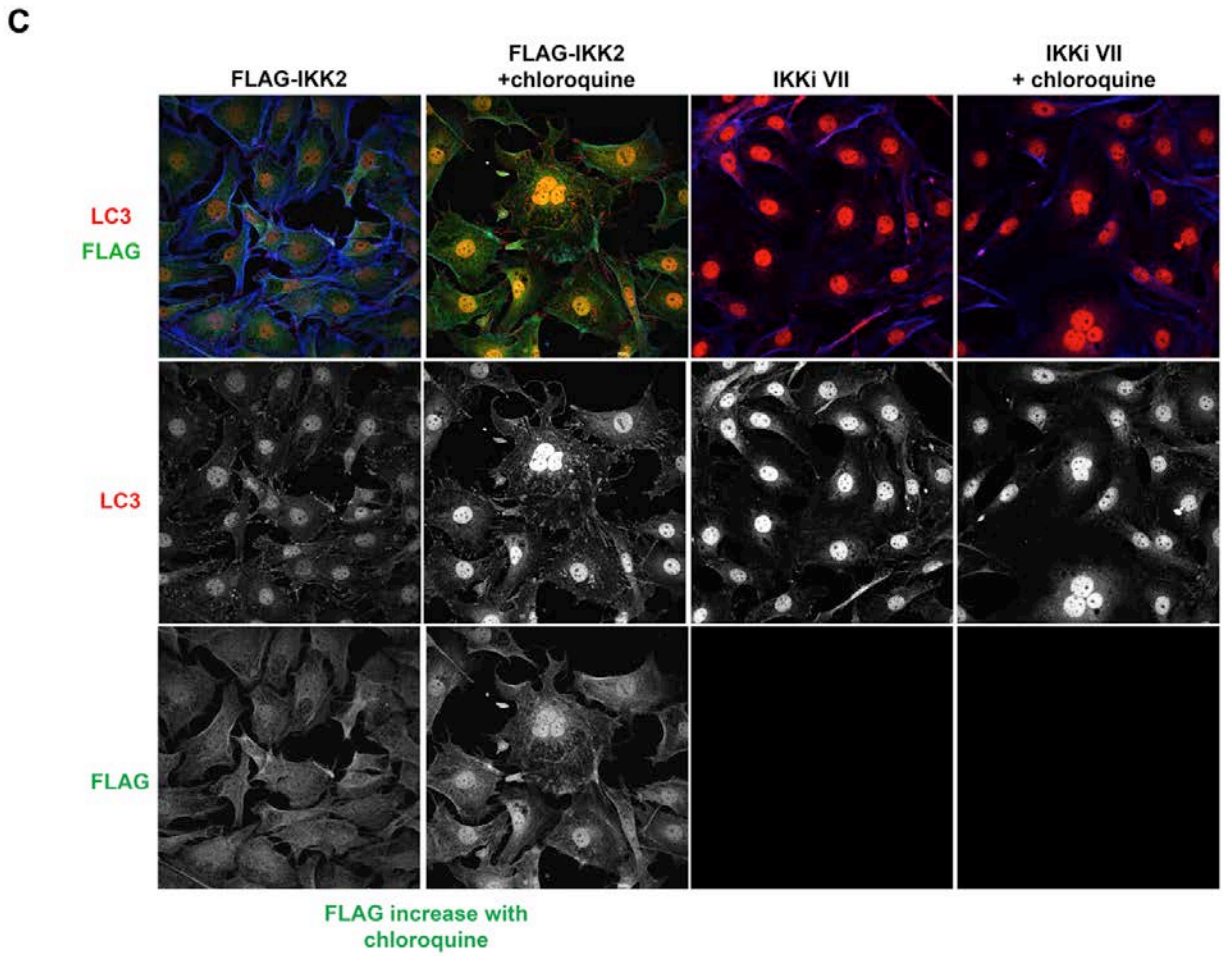

Figure 24. IKK increases autophagy in podocytes

(A) Example of IKK-2, transfected cells labeled with FLAG (green) next to neighboring cells with little to no transfection, highlighting p65 nuclear localization (NF-κB activation) with constitutively active IKK. (B) IKK-2 transfected cells continue to express nephrin (red) and display high levels of IKK-β (blue), compared to cells in which IKK has been inhibited. (C) Increased LC3 (red) and puncta accumulation with chloroquine administration in IKK-2 transfected cells (green), compared to those with decreased IKK activity.

3.5 DISCUSSION

Age-related CKD is a major healthcare problem in the U.S., as well as worldwide. It is imperative then to study the contribution of aging in order to identify new therapeutic targets and determine appropriate therapies for patients depending on their progression of aging nephropathy. Previously, we identified the *Ercc1*$^{-/\Delta}$ mouse as an accurate model of accelerated renal aging and provided evidence that DNA damage accumulation can drive the kidney aging process. Podocyte injury and albuminuria occurred before tubule injury and other global kidney changes. In this chapter, I have determined the time-course and nature of major glomerular changes and how they relate to the subsequent loss of kidney structure and function, in order to gain mechanistic information concerning renal senescence. For the first, time, I present evidence here that damage accumulation in podocytes, rather than proximal tubule cells, causes age-related chronic kidney disease in mice,

NF-κB has been found to be the major transcription factor in humans and mice most closely associated with aging(174, 175), and likely may be causing the subsequent changes such as endothelial cell activation, macrophage infiltration, coagulation, and fibrosis in rats(45). Wiggins et al identified NF-κB activation in an aging rat model in the glomerulus by chromatin immuno-precipitation (CHIP) assay. Rats that had extended lifespan by calorie restriction had smaller glomeruli than the hypertrophied glomeruli of ad libitum fed rats, less proteinuria, and fewer upregulated genes associated with NF-κB activation. In another study, researchers found that angiotensin receptor blockers (ARBs) prevented the NF-κB activation seen in aged rat kidneys, while also reducing oxidative stress and inflammation(50). Here, we show the time course of chronic NF-κB activation in the *Ercc1*$^{-/\Delta}$ mouse model and identify podocytes as the primary cell type in which this dis-regulated signaling is occurring. While evidence of initial podocyte injury

and autophagy induction occurs before this, the onset of chronic NF-κB activation coincided with autophagy impairment, a large increase in ACR, decrease in GFR, and the onset of global kidney pathologies.

Dis-regulated autophagy was found to contribute to the podocyte damage seen in a mouse model of Fabry's disease. ESRD is the leading cause of death in males with Fabry's disease, and there is apparent podocyte injury, proteinuria, hematuria, and hypertension(176). Fabry's disease is X-linked and is due to a deficiency in the lysosomal enzyme, hydrolase α–galactosidase A. Knockdown with RNAi technology of this gene product in podocytes, results in accumulation of autophagosomes and a decrease in subsequent degradation through the autophagy pathway. With aging, there is also a persistent decline in degradation and clearance of mitochondria and other damaged organelles and macromolecules(19). It is possible that the same oxidative damage that affects autophagic substrates, also eventually damages the degradative machinery itself. Elevated ROS induces autophagy, but eventually, the system breaks down as the components become defective. In the data presented here, there is evidence of oxidative DNA damage, accumulation of LC3 and p62-positive compartments, and this likely contributes to a phenotypic transition in the podocyte from a stressed but "coping" state to a permanently injured state, which leads to loss of a functional glomerular filtration barrier, as well as NF-κB inflammatory signaling.

The *in vitro* work presented here shows that the relationship between IKK-NF-κB and autophagy exists and warrants further exploration. One question is how is this cross talk achieved? Does IKK affect gene expression and/or post-translational modification of autophagy proteins? Is IKK affecting autophagy through the mTOR pathway? Finally, further studies using the podocyte cell line MP-1 will help determine whether defective autophagy, achieved by autophagy gene knock-down or increased ROS, can cause chronic NF-κB activation. Finally, can we facilitate

autophagy impairment and IKK/ NF-κB activation with stable knock-down of *Ercc1 in vitro* in order to better elucidate the mechanism of injury and find effective therapies?

In the hypothalamus of mice, high autophagy activity was detected, and autophagic decline correlated with decreased metabolic activity and obesity and insulin resistance(159). In a mouse model with hypothalamic autophagy inhibition, IKK-β protein expression increased, and introduction of a brain-specific IKK-β knock-out into the model prevented the obesity and insulin resistance changes. Therefore, defective autophagy can cause IKK-β dependent inflammatory signaling, which can result in metabolic change *in vivo.* The evidence presented here, in both in the mouse models and *in vitro*, shows that a similar pathological signaling may be occurring in the aging podocyte, which could result in loss of normal kidney structure and function with age.

The creation and characterization of the podocyte-specific *Ercc1* knock-out mouse presented here, provides strong evidence that the inherent injury due to accumulated damage in the podocyte is directly responsible for the age-related chronic kidney disease that results. Although, there was some evidence of ultrastructural damage in tubules seen by EM in the proximal tubule-specific knockout, this did not result in any measurable deficit in kidney function, nor did it activate any of the pathological changes detected in the accelerated, kidney aging model. Podocyte damage due to *Ercc1* deficiency causes early induction of IKK and autophagy, as a stress response. Ultrastructural studies show GBM thickening and podocyte effacement, followed by a functional increase in the ACR above controls by a few months of age. By 7 months, EM studies show an extremely thickened GBM, indicating a change in glomerular secretory behavior, and dis-regulated extracellular matrix maintenance. Eventually, p62 protein accumulates in LC3-positive puncta, indicating an impairment in autophagic flux. Interestingly, mTOR activation also increases in the glomerulus, as indicated by increased pS6 protein levels. There is also evidence of proximal

tubule injury by increased KIM-1 expression by 4 months, indicating that tubule injury is likely secondary to podocyte injury. ICAM upregulation is an early event, as in *Ercc1*$^{-/\Delta}$ mouse model, indicating that podocyte stress causes endothelial cell activation early in the process. ICAM expression on the apical border of the proximal tubule cell may occur in response to the increased protein passing into the filtrate. As in the *Ercc1*$^{-/\Delta}$ mouse model, a large increase in smooth muscle actin expression and macrophage infiltration occur, with populations infiltrating the glomerulus, as well as virtually every interstitial space.

Extreme albuminuria develops after 16 weeks and the GFR at 7 months has decreased below levels seen in the *Ercc1*$^{-/\Delta}$ mouse model. It is important to note that podocytes in the *Ercc1*$^{-/\Delta}$ mouse model have some *Ercc1* protein, whereas the podocytes in the cell-specific knock-out have none, likely causing the more extreme kidney phenotype. It will be important to determine the extent of knock-out in the podocyte-specific model, as different animals displayed varying degrees of severity of structural changes, which correlated to ACR levels. Currently, *Ercc1* antibodies are being tested and laser capture methods are being developed in order to measure *Ercc1* expression in the glomerulus and other tissues. Importantly, none of these structural or functional changes were detected in the proximal tubule specific knock-out animals. Some damage accumulation was seen in autolysosomal-like structures in the tubules of these knock-out animals, but this damage did not result in any elevation of the ACR or change in GFR, and there was no increase in ICAM or SMA expression, macrophage infiltration, or overt glomerular damage. In the *Ercc1*$^{-/\Delta}$ mouse model, proximal tubule cells do show some necrosis and division was detected, indicating efficient cell turnover. Perhaps this mechanism is enough to compensate for damaged cells while still maintaining kidney function. It will be interesting to study the serum levels of sodium, glucose, and other ions to determine whether there is any change in tubule-dependent

reabsorption/secretion in the *Ercc1* deficient proximal tubule. Additional, the extent of *Ercc1* knock-out in the proximal tubules must be verified.

With the evidence presented here, it is clear that accumulated DNA and cellular damage during aging affects various cell types differently, likely due to each cell's ability to replace itself or degrade damaged material in order to maintain its structure and function. Different cells are exposed to varying levels of stress that may cause faster accumulation of damage. The complexly differentiated, post-mitotic podocyte is exposed to high levels of distending forces due to glomerular blood pressure and not being bound on its apical side. The podocyte is exposed to high levels of toxic stress as well and must maintain its complicated architecture, while regulating the location and number of slit diaphragms in order to maintain the glomerular filtration barrier. It is also responsible for maintaining the GBM and producing growth factors that influence glomerular and systemic endothelial cell health. The data herein provide evidence that the glomerular podocyte should be a major therapeutic target in age-related CKD. Finding therapies that help podocytes maintain or restore autophagic flux, such as ARBs, antioxidants, or factors that renew lysosomal degradation, may be key in preventing or regulating NF-κB inflammatory signaling and kidney failure that can occur with age.

4.0 SUMMARY AND FUTURE DIRECTIONS

The main goal of this thesis was to introduce a new tool to study kidney aging, and to use this tool to address the hypothesis that accumulated unrepaired DNA damage in podocytes causes age-related kidney disease. I systematically compared the structural, functional, and cellular changes that occur in an accelerated manner in the *Ercc1* deficient mouse kidney to those of naturally aged mice, drawing extremely strong parallels that validate it as tool to study kidney aging in an accelerated manner. This work also provides evidence that endogenous DNA damage and plays an important role in causing age-related kidney disease, perhaps by activating the DNA damage response and NF-κB in the glomerular microenvironment. In addition to this model providing a more efficient way of studying aging without confounding factors seen in humans, it also allowed us to study the effects of accelerated aging in specific cell types. I demonstrated the *Ercc1* knockout in podocytes was able to cause the same changes in kidney function in a similar progression of cellular changes, including tubule injury, endothelial cell activation, macrophage infiltration, and fibrosis. A proximal tubule-specific knock-out resulted in some ultrastructural changes within the tubules, but no noticeable change in function or cellular changes, as well as no impact on lifespan currently (1 year). A significantly decreased lifespan resulted from podocyte-specific *Ercc1* knock-out, providing evidence that renal failure due to podocyte damage may be a cause of morbidity in *Ercc1* deficient mice. Finally, I demonstrated a correlation between the onset of chronic NF-κB activation and autophagy impairment in the podocytes of the progeroid mice. My *in vitro* experiments, for the first time, demonstrate that there is a relationship between IKK/ NF-κB and autophagy in podocytes, and that this warrants further study to uncover the mechanism

of podocyte injury with aging and to develop and new, targeted therapies to address these pathologies.

I aimed to both quantitatively and qualitatively determine the time-course and progression of pathological changes that occurred in the *Ercc1*$^{-/\Delta}$ kidney, compared to changes detected in 2-3 yr old, naturally aged WT mice. Importantly, analyses of the glomerular transcriptional profiles demonstrated strong similarities in gene expression changes between the *Ercc1*$^{-/\Delta}$ kidney and old WT, compared to young WT(131). I determined that podocyte injury and elevated ACR occurs before subsequent tubule injury, as detected by KIM-1 protein expression and ultrastructural studies. I strengthened my hypothesis that tubule injury was secondary to podocyte injury by demonstrating tubule injury in the podocyte-specific knock-out, indicated by Kim-1 staining and EM studies. Although EM studies also showed some build-up of lysosomal structures and irregularities in the tubules of the proximal tubule specific knock-out, these did not result in the increased ICAM expression on the tubules seen in the *Ercc1*$^{-/\Delta}$ or *Ercc1*-pod-KO, nor did they result in KIM-1 expression or changes in kidney function, etc. Therefore, *Ercc1* deficiency in the proximal tubule is not sufficient to cause any evidence of CKD, and is likely not the primary cause of the aging pathologies seen in the *Ercc1*$^{-/\Delta}$ kidney. However, it will be important to further characterize the proximal tubule specific knock-out. It is also important to determine whether proximal tubule cells in this knock-out animal are turning over in response to injury. *Ercc1* deficiency in proximal tubules could make the kidneys more susceptible to kidney damage with systemic disease or acute kidney injury (such as cisplatin or ischemia-reperfusion induced), and this would be an interesting and relevant hypothesis to explore.

I observed an early increase in ICAM in both the podocyte-specific knock-out and in the Ercc1$^{-/}$ mouse, indicating that podocyte injury likely causes vascular changes early in the disease

process. It would be interesting to determine the extent of endothelial cell damage that results, as well as the extent and progression of vascular dysfunction and rarefaction. An endothelial cell specific knock-out of *Ercc1* will serve as a valuable tool to determine whether vascular aging can cause glomerular injury. Durik et al found evidence of age-related vascular dysfunction in the *Ercc1*$^{-/\Delta}$ mouse model by 8 weeks, including arterial stiffness, accelerated vasodilator dysfunction, and a slight yet significant rise in blood pressure compared to WT littermates(177). Could an endothelial cell specific knock-out recapitulate these changes? Or, perhaps a podocyte-specific knock-out could cause age-related vascular dysfunction. These experiments, currently in development, could provide extremely valuable knowledge as to whether renal aging can cause systemic disease, as well as disease in other organ systems.

IKK increase and chronic NF-κB activation in the podocytes of *Ercc1* deficient mice also parallels that seen in naturally aged mice. There is evidence that NF-κB activation with aging, causes some of the age-related pathologies in multiple tissues, and inhibition can delay some age-related conditions(168, 178). Additionally, NF-κB activation can cause ICAM gene expression, as well as many other genes seen in kidney aging(32). The data in this thesis show that NF-κB activation occurs after initial detection of albuminuria and podocyte injury. While NF-κB inhibition may prevent some of the subsequent inflammatory changes seen with aging, it may not reverse podocyte injury or loss. This would be an interesting area to explore with the kidney relevant *Ercc1* deficient mouse models. Timing and titration of NF-κB inhibition would likely be important. It may be necessary to address the cause of podocyte stress and injury that results in this dis-regulated, chronic NF-κB activation, in order to prevent a decrease in kidney function with age.

One of the first changes detected in podocytes by immunofluorescence was IKK increase and LC3 increase in the *Ercc1*$^{-/\Delta}$ mouse and the podocyte specific knock out. At this same time, at approximately 1 month, ACR becomes slightly elevated and ultrastructural irregularities were detected in podocytes by EM. IKK induction also occurs early in the podocyte specific knock-out, as well, indicating this is due to inherent podocyte damage. The *in vitro* data presented here indicate that perhaps autophagy induction is caused by IKK activation. This data warrants further exploration, such as quantification of LC3 and other autophagy proteins with IKK manipulation. Additionally, does increased IKK activity induce autophagy protein expression, such as Beclin or Ulk-1? Is this NF-κB activation dependent or is it an independent function of IKK as others have found(153, 154)? Experiments could be performed with p65 knockdown or deletion in podocytes to explore independent effects of IKK on autophagy proteins.

By 8 wks in the *Ercc1*$^{-/\Delta}$ kidney, although LC3 protein levels remain increased, p62 protein has also begun to accumulate, indicating the degradation of autophagic substrates is defective. This autophagic flux impairment is also detected in the podocyte specific knock-out indicating that this impairment is due to inherent podocyte damage; however, further investigation is needed to determine time of onset. At this same time in the *Ercc1*$^{-/\Delta}$ kidney, chronic NF-κB activation begins specifically in the podocyte. Smooth muscle actin-positive cell populations increase, and macrophage infiltration follows by 12 wks. Is the onset of chronic NF-κB activation and autophagy impairment related? As discussed, there is evidence that all IKK subunits are degraded by autophagy, and autophagic impairment can cause increased levels of IKK(155). Also, defective autophagy in the hypothalamus, as an example, can lead to IKK/ NF-κB -dependent changes in metabolism that result in obesity in a mouse model(159). In order to address these possibilities in podocytes, one could impair autophagy in the differentiated mouse podocyte cell line using

chloroquine or 3-MA, or by utilizing genetic knock-down of an autophagy protein, and determining whether IKK/ NF-κB activation occurs. Relevant to this aging model, it would be interesting to create a stable knock-down of *Ercc1* to explore whether it eventually leads to chronic NF-κB activation and autophagy impairment, in order to tease out mechanistic details of the cross-talk between the two pathways with long-term *Ercc1* deficiency.

In order to more effectively bridge the gap between the *in vitro* and *in vivo* experiments presented in this thesis, I would suggest extending the glomerular isolation and autophagy experimental protocol I developed for the experiment presented in Figure 24 of Appendix C. Ideally, one could isolate glomeruli from a 1 month old eGFP- NF-κB; $Ercc1^{-/\Delta}$ mouse kidney (before chronic NF-κB activation begins) and a 3 month eGFP- NF-κB; $Ercc1^{-/\Delta}$ mouse kidney (when chronic NF-κB activation is at its peak in the glomerulus) to do autophagic flux assays. Autophagic flux should be in tact at 1 month, but become impaired in 3 month, eGFP+ podocytes. It may also be useful here to explore autophagic flux using high-speed confocal imaging, in young and old, isolated glomeruli from transgenic RFP-LC3 mouse kidneys. Additionally, one could inhibit autophagy in the 1 month old $Ercc1^{-/\Delta}$ isolated glomeruli as well as in young WT glomeruli to see if IKK protein increases or NF-κB activation results. Finally, in autophagy-deficient mice, is there accelerated chronic NF-κB activation as I have shown here with aging?

In this thesis, I have presented a new, efficient way of studying the kidney aging process, without other confounding factors. Using this model, I have shown that damage accumulation in the glomerular podocyte, but not the proximal tubule, is sufficient to cause aging nephropathy. Ideally, this model can be used to identify new therapies or suggest prophylactic measures to maintain glomerular health in the face of the inevitability of aging. This could be achieved by NF-κB inhibition, but I hypothesize that the cause of podocyte injury that results in dis-regulation of

NF-κB and autophagy impairment must be addressed. It would be interesting to treat the mice with an angiotensin receptor blocker (ARB) to look for prevention and reversal of disease. In fact, the ARB, losartan, has been shown to inhibit NF-κB -induced inflammatory responses in naturally-aged rat kidneys, whereby decreasing oxidative damage(50, 179). ARBs are also used to treat patients with albuminuria, and there is evidence that they can prevent or lessen podocyte injury in diabetic nephropathy animal models. In fact, Angiotensin receptor 1 (ATR1) deficient mice live longer, and have lower levels of oxidative stress in many tissues(95). Angiotensin II induces autophagy in podocytes, which can be inhibited with antioxidants. In addition to being localized on the cell membrane, ATR1 is active on the mitochondrial membrane, and there is evidence that AT1 blockade can actually protect mitochondria from damage in experimental diabetes models(180). The podocyte specific knock-out of *Ercc1* presented here would be a very valuable tool with which to study the effectiveness and mechanism of action of ARBs in preventing/reversing age-related podocyte injury.

Finally, in patients where aging nephropathy has progressed to the point of profound autophagic flux impairment in the podocyte, it may be necessary to pursue therapies that can renew the degradative capacity of the cell, in combination with those that reduce oxidative stress. For example, there is evidence that activation of the lysosome/autophagy biogenesis transcription factor, TFEB, can have beneficial effects in Parkinson's disease models(181). There are compounds, such as cobalt protoporphyrin (CoPPIX), which activate TFEB and have been shown to inhibit NF-κB activation and restore autophagy and lysosome function in cardiac tissue in sepsis models(84). These therapies may be beneficial in treating aging nephropathy that has already progressed, in order to restore remaining podocyte health and restore kidney function.

In this thesis, I tested the hypothesis that DNA damage can drive kidney aging in the *Ercc1*$^{-/\Delta}$ and I demonstrated that this model serves as a new tool to study the mechanism and progression of aging nephropathy. I used the podocyte and proximal tubule specific *Ercc1* knock-out mice to determine that podocyte injury during aging is responsible for causing the observed pathological changes and kidney function decline, which can eventually cause death. Finally, I demonstrated that autophagy impairment and chronic NF-κB activation in the aging podocyte may be related and provide possible targets for therapeutic discoveries.

4.1 ACKNOWLEDGEMENTS

I’d like to thank Ryan Romanovsky and Jonathan Franks, as well as the rest of the EM lab at the Center for Biologic Imaging for help with EM sample processing and quantification of measurements. Thank you to Lauren Goldshen who contributed to imaging samples on the Nikon 90i microscope, as well as for performing some cryostat sectioning and immune-labeling. Thank you to the Niedernhofer lab at Scripps in Florida, especially Amanda Beck, Sara McGowan, Tania Rozgaja, and Diana Navarro, for continuing animal work, sending tissue and urine samples, performing GFR experiments, and for histological analyses. Thank you to the Center for Biologic Imaging for imaging and analysis training and support. Finally, thank you to the Pittsburgh Center for Kidney Research Pilot Program (P30DK079307), the NIDDK Renal Training Grant (5T32DK061296-09), the Angiopathy Training Grant (5T32HL094295), and the NIA (PO1AG043376) for supporting me during this work.

APPENDIX A

ABBREVIATION	DEFINITION
ACR	Albumin creatinine ratio
ALP	Alkaline phosphatase
AMPK	5’ adenosine monophosphate-activated kinase
Ang II	Angiotensin II
ARB	Angiotensin receptor blocker
ATG	Autophagy-related protein
ATR1	Angiotensin II receptor type 1
Bcl-2	B cell lymphoma 2
BrdU	Bromodeoxyuridine
BUN	Blood urea nitrogen
CD31	Cluster of differentiation 31
CD45	Cluster of differentiation 45
CD68	Cluster of differentiation 68
CHIP	Chromatin immune-precipitation
CKD	Chronic kidney disease
COFS	Cerebro-oculo facioskeletal

CoPPIX	Cobalt protoporphyrin
CPD	Cyclopyrimidine dimer
cPu	Cyclopurine
CR	Calorie restriction
CS	Cockayne syndrome
DAPI	4',6-diamidino-2-phenylindole
DSB	Double strand breaks
eGFR	Estimated glomerular filtration rate
Ercc1	Excision repair cross-complementary group 1
ESRD	End stage renal disease
FGF23	Fibroblast growth factor 23
FITC	Fluorescein isothiocynate
g-GT	Gamma-glutamyl transferase
GBM	Glomerular basement membrane
GFP	Green fluorescent protein
GFR	Glomerular filtration rate
GH	Growth hormone
gH2AX	Gamma histone family 2A, member X
H&E	Haematoxylin and eosin
HRP	Horseradish peroxidase
ICAM	Intracellular adhesion molecule
ICL	Interstrand crosslinks
IFN-γ	Interferon gamma
IGF-1	Insulin-like growth factor 1

IHC	Immunohistochemistry
IKK	Inhibitor of kappa B kinase
KIM-1	Kidney injury molecule 1
LAMP-2	Lysosomal-associated membrane protein 2
LC3	Light chain-3
LPS	lipopolysaccharide
mTOR	Mammalian target of rapamycin
NER	Nucleotide excision repair
NF-κB	Nuclear factor light-chain-enhancer of activated B cells
p62	Also called sequestosome-1
PAS	Periodic acid-Schiff
PBS	Phosphate buffered saline
PECAM	Platelet endothelial cell adhesion molecule
PT	Proximal tubule
RA	Renin-angiotensin
ROS	Reactive oxygen species
SA-β–gal	SA-β–galactosidase
SASP	Senescence-associated secretory phenotype
SIRT1	Sirtuin 1
SMA	Smooth muscle actin
TASCC	Tor-associated spatial coupling compartment
TBM	Tubular basement membrane
TFEB	Transcription factor EB
TRPV-5	Transient receptor potential vallinoid-5

TSC1	Tuberous sclerosis 1
TUNEL	Terminal deoxynucleotidyl dUTP nick ending labeling
ULK-1	Unc-51-like kinase 1
VEGF	Vascular endothelial growth factor
WGA	Wheat germ agglutinin
WT	Wild-type
XP	Xeroderma pigmentosum
XPF	Xeroderma pigmentosum group F
3-MA	3-methyladenine

Table 4. List of abbreviations

APPENDIX B

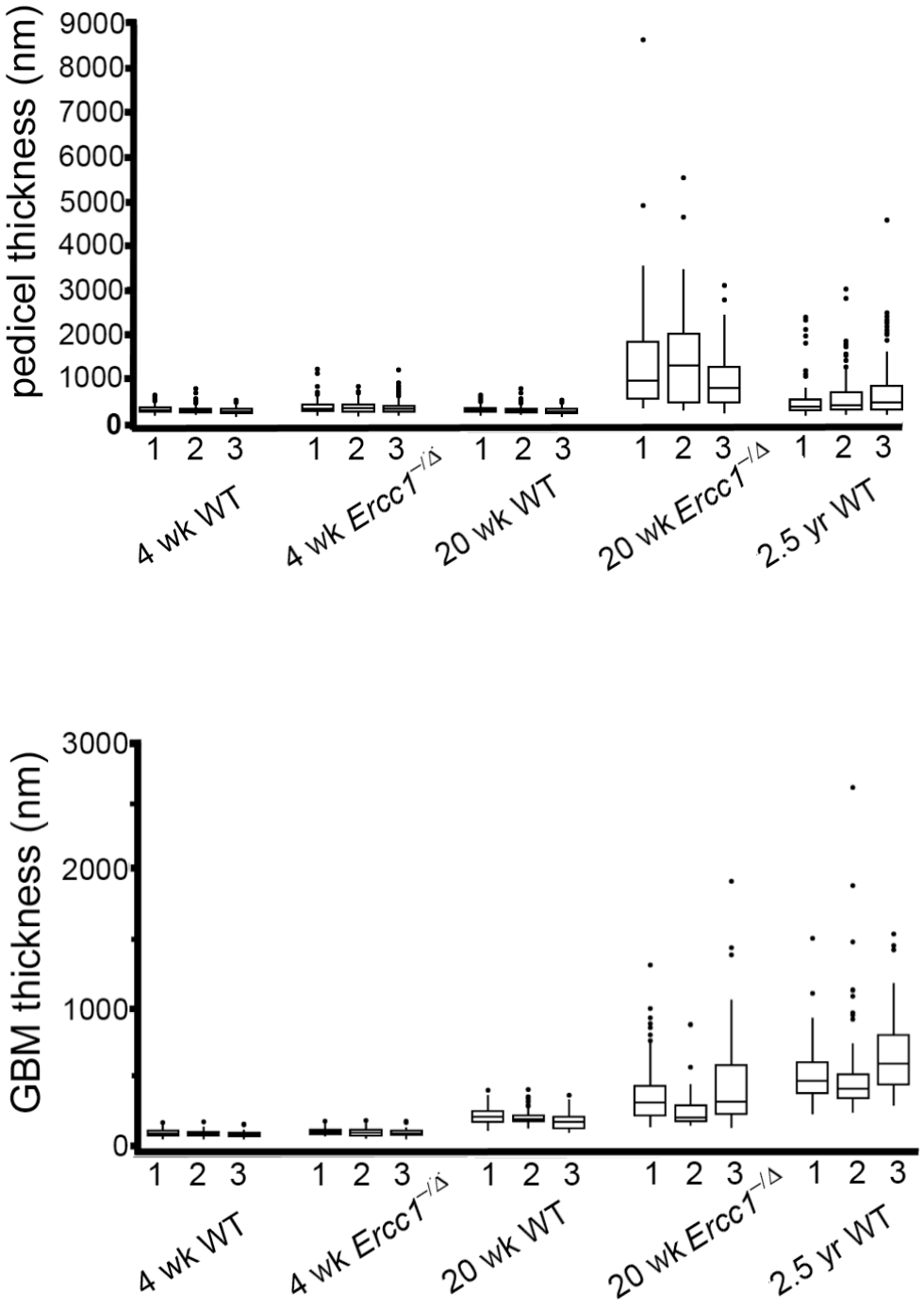

Figure 25. Quantification of Podocyte Pedicel and GBM Thickening with Age

Foot process *(pedicel)* thickness was measured in TEM images as the width of the pedicel abutting the basement membrane. Only images were used in which a complete cross section of the glomerulus was captured. The data represent 3 mice per age and genotype, a minimum of 4 glomeruli and ≥50 pedicels measured per mouse. Each box represents an individual mouse, where the top is the first quartile, the bottom is the third quartile and the band in the middle equals the median. The whiskers represent the most extreme point no more than 1.5 interquartile range. The plots illustrate increasing thickness *as well as variability with age.* GBM thickness was measured in TEM images as the distance between the foot process attachment and the endothelial cell fenestrate. The data represent 3 mice per age and genotype, a minimum of 4 glomeruli and ≥40 measurements per mouse.

APPENDIX C

SUPPLEMENTARY TABLE 1:

Gene Symbol	Gene description	Entrez Gene ID	Affymetrix Transcripts Cluster Id	Fold change (Ercc1 14 wks/ WT 14 wks)	p-value (Ercc1 14 wks vs. WT 14 wks)	Fold change (WT 96 wks/ WT 14 wks)	p-value (WT 96 wks vs. WT 14 wks)
Aldh1a1	aldehyde dehydrogenase family 1, subfamily A1	11668///	10461979	6.02	8.52E-07	2.34	3.37E-05
S100g	S100 calcium binding protein G	12309///	10607705	4.84	1.41E-02	2.98	4.72E-02
Gp49a	glycoprotein 49 A	14727///	10363070	3.87	3.96E-03	4.06	2.35E-03
Calb1	calbindin 1	12307///	10503416	3.53	4.31E-02	3.26	4.09E-02
Mt2	metallothionein 2	17750///	10574023	2.89	1.07E-02	1.76	4.10E-03
Cdkn1a	cyclin-dependent kinase inhibitor 1A (P21)	12575///	10443463	2.76	7.29E-04	1.50	1.70E-02
Epha6	Eph receptor A6	13840///	10440216	2.70	2.51E-06	2.17	2.06E-05
Prss23	protease, serine, 23	76453///	10554814	2.61	2.55E-05	1.98	2.10E-05
Cxcl13	chemokine (C-X-C motif) ligand 13	55985///	10523359	2.61	1.29E-03	4.42	6.30E-06
Ctss	cathepsin S	13040///	10494271	2.32	7.92E-04	3.36	2.86E-04
			10433431	2.28	1.61E-05	2.38	1.09E-05
Lilrb4	leukocyte immunoglobulin-	14728///	10363082	2.26	1.71E-02	3.15	1.30E-03

	like receptor, subfamily B, member 4						
Pigr	polymeric immunoglobulin receptor	18703///	10349580	2.25	3.68E-02	2.67	4.79E-03
Ctsc	cathepsin C	13032///	10554789	2.14	3.47E-03	2.64	3.93E-03
Gpr65	G-protein coupled receptor 65	14744///	10397645	2.12	8.26E-03	3.73	1.60E-03
Prss23	protease, serine, 23	76453///	10565456	2.12	4.72E-05	1.72	3.35E-04
			10598081	2.11	2.06E-02	2.12	1.70E-03
Fyb	FYN binding protein	23880///	10422760	2.11	8.10E-03	3.30	1.23E-03
Lyz2	lysozyme 2	17105///	10372648	2.08	3.64E-02	3.88	8.69E-04
Ptgfr	prostaglandin F receptor	19220///	10502805	2.03	2.58E-02	1.59	3.29E-02
Clu	clusterin	12759///	10416057	2.02	3.90E-02	2.16	1.73E-02
Fam26e	family with sequence similarity 26, member E	103511///	10368638	1.99	5.42E-05	1.69	2.07E-05
			10598079	1.99	3.86E-02	2.07	1.51E-03
H2-Aa	histocompatibility 2, class II antigen A, alpha	14960///	10450154	1.97	5.14E-03	4.11	9.48E-05
Cybb	cytochrome b-245, beta polypeptide	13058///	10603551	1.95	6.96E-03	2.69	1.20E-03
Gdpd2	glycerophosphodiester phosphodiesterase domain containing 2	71584///	10601044	1.95	4.59E-04	2.04	2.62E-03
			10433428	1.93	6.69E-05	2.06	4.94E-05
Adm	adrenomedullin	11535///	10556297	1.91	3.83E-04	1.54	4.81E-03
			10598077	1.90	1.37E-02	1.86	2.21E-03

Cd68	CD68 antigen	12514///	10387536	1.88	1.52E-03	2.61	1.17E-03
C3ar1	complement component 3a receptor 1	12267///	10547657	1.87	2.94E-03	2.26	1.19E-02
Mpeg1	macrophage expressed gene 1	17476///	10461721	1.86	7.52E-03	2.54	1.67E-03
Hpgds	hematopoietic prostaglandin D synthase	54486///	10545101	1.86	8.47E-05	1.92	2.04E-03
			10598071	1.86	1.92E-02	2.26	9.10E-04
			10598023	1.85	5.84E-03	1.68	1.73E-03
			10598075	1.82	3.21E-02	2.12	1.29E-03
Cyp1b1|1700038P13Rik	cytochrome P450, family 1, subfamily b, polypeptide 1 | RIKEN cDNA 1700038P13 gene	13078///73265///	10453057	1.78	1.92E-04	1.72	4.68E-06
Ms4a6c	membrane-spanning 4-domains, subfamily A, member 6C	73656///	10461614	1.75	1.47E-02	1.95	7.39E-03
Cd74	CD74 antigen (invariant polypeptide of major histocompatibility complex, class II antigen-associated)	16149///	10456005	1.74	2.94E-03	3.07	3.27E-04
			10598053	1.72	1.33E-02	1.72	3.63E-03
Trim30d	tripartite motif-containing 30D	209387///	10566366	1.71	1.49E-03	1.97	1.30E-04

Plbd1	phospholipase B domain containing 1	66857///	10548817	1.68	4.42E-03	2.15	3.08E-04
Ly86	lymphocyte antigen 86	17084///	10404606	1.67	5.26E-04	2.26	2.44E-03
H2-Ab1	histocompatibility 2, class II antigen A, beta 1	14961///	10444291	1.65	1.85E-02	3.04	3.69E-04
Spink8	serine peptidase inhibitor, Kazal type 8	78709///	10589407	1.64	2.78E-02	1.65	4.23E-03
Cd209a	CD209a antigen	170786///	10576784	1.64	8.35E-03	1.76	1.21E-03
Ccr2	chemokine (C-C motif) receptor 2	12772///	10590631	1.63	5.35E-03	1.76	2.32E-03
			10598041	1.62	1.70E-02	1.84	1.06E-03
Tyrobp	TYRO protein tyrosine kinase binding protein	22177///	10551883	1.61	5.37E-03	2.76	1.19E-03
C1qc	complement component 1, q subcomponent, C chain	12262///	10517513	1.61	3.15E-03	3.19	1.82E-03
Dcn	decorin	13179///	10365974	1.60	8.26E-03	1.76	1.39E-02
Msr1	macrophage scavenger receptor 1	20288///	10578264	1.58	6.92E-03	1.82	4.66E-03
Luzp2	leucine zipper protein 2	233271///	10553537	1.58	8.96E-03	4.07	2.09E-06
Pilra	paired immunoglobin-like type 2 receptor alpha	231805///	10534927	1.57	1.78E-02	2.04	2.49E-03
			10598032	1.55	4.08E-02	1.71	2.10E-03

			10598064	1.55	3.03E-02	1.58	4.66E-03
Ptprc	protein tyrosine phosphatase, receptor type, C	19264///	10358224	1.55	9.63E-03	2.16	6.53E-03
Stap1	signal transducing adaptor family member 1	56792///	10522788	1.54	1.32E-02	1.66	1.50E-02
Mmp12	matrix metallopeptidase 12	17381///	10583056	1.54	3.42E-02	2.40	4.09E-03
Lcp1	lymphocyte cytosolic protein 1	18826///	10416437	1.54	1.77E-02	2.07	5.18E-03
Stk17b	serine/threonine kinase 17b (apoptosis-inducing)	98267///	10354588	1.53	2.05E-03	1.54	3.16E-03
Clec4a3	C-type lectin domain family 4, member a3	73149///	10541564	1.51	2.66E-02	2.10	8.39E-03

Table 5. Gene information from transcriptional analysis of Ercc1$^{-/\Delta}$ and WT kidneys(131)

APPENDIX D

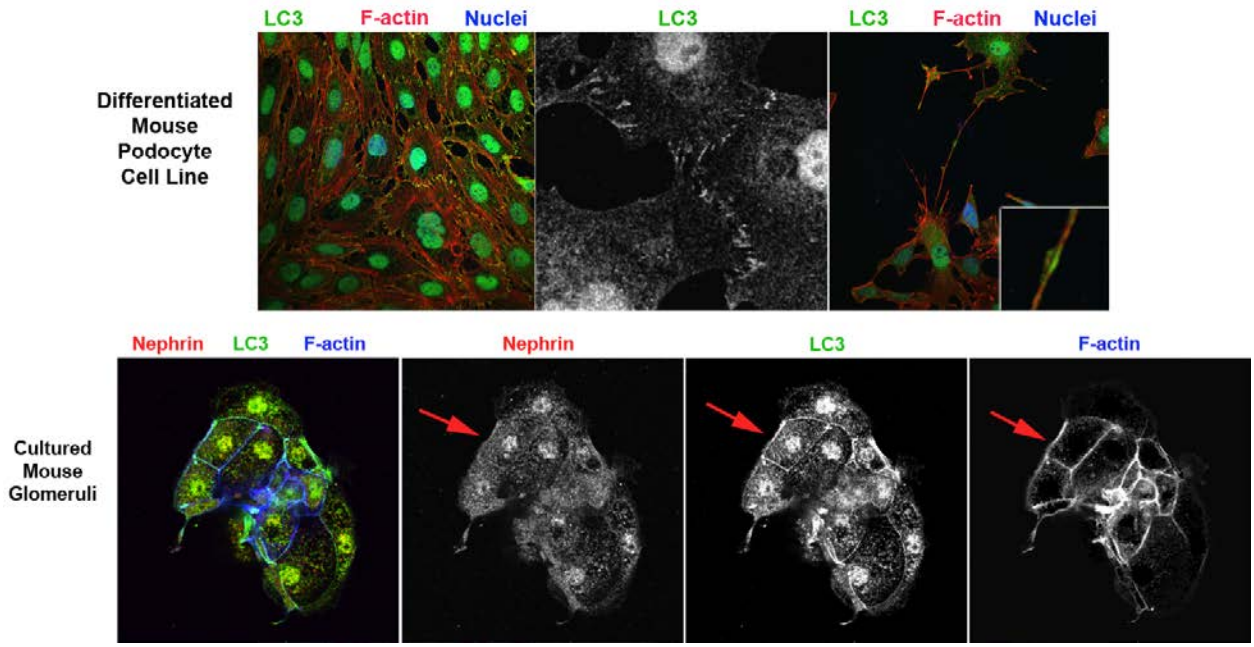

Figure 26. LC3 puncta at cell-cell junctions in podocytes.

First row: LC3 present at cell-cell junctions, independent of cell density in differentiated mouse podocyte cell line. Second row: LC3-present at cell-cell junctions, co-localizing with nephrin and F-actin in podocytes from freshly isolated mouse glomeruli (8 wk old mice).

APPENDIX E

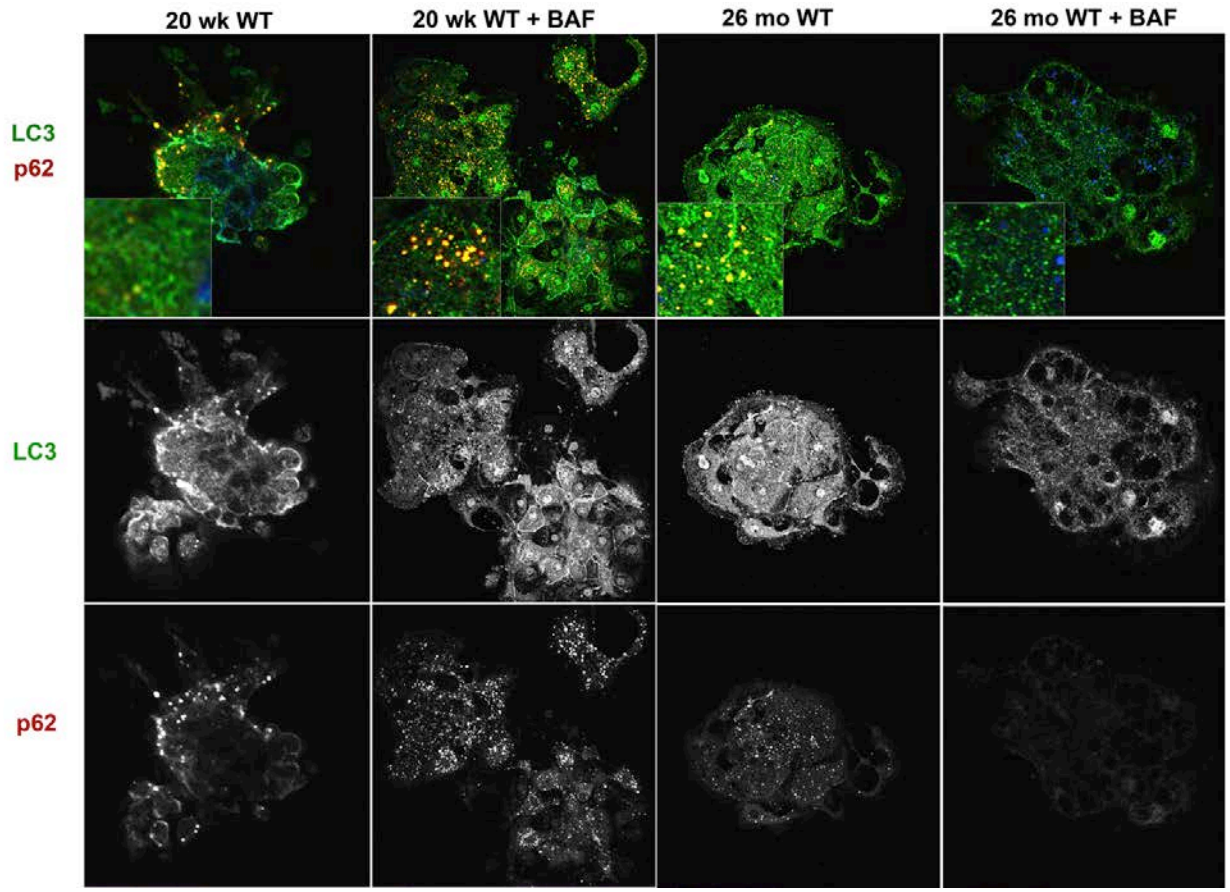

Figure 27. Accumulation of LC3+p62+ puncta, decreased autophagy in isolated glomeruli from old WT mice

Glomeruli were isolated from 5 month WT and 2.5 yr WT mice and cultured overnight on collage IV with or without 5nM balifomycin. 5 month WT glomeruli displayed high levels of LC3, both diffusely and in puncta and p62 localized diffusely and in few puncta. LC3+p62+ puncta accumulated with balifomycin, indicating active autophagy. Glomeruli from old WT mice displayed an accumulation of the LC3+p62+ puncta and no additional accumulation with bafilomycin, indicating impaired autophagy.

BIBLIOGRAPHY

1. USRDS. Atlas of CKD and ESRD 2013.
2. Foley RN, Collins AJ. The USRDS: what you need to know about what it can and can't tell us about ESRD. Clinical journal of the American Society of Nephrology : CJASN. 2013;8(5):845-51.
3. Nations U. World Population Prospects Report, 2005-2010. 2010.
4. (NKUDIC) NNKaUDIC. The Kidneys and How They Work 2014. Available from: http://kidney.niddk.nih.gov/kudiseases/pubs/yourkidneys/index.aspx - kidneys.
5. Hartleben B, Wanner N, Huber TB. Autophagy in Glomerular Health and Disease. Seminars in nephrology. 2014;34(1):42-52.
6. Wanner N, Hartleben B, Herbach N, Goedel M, Stickel N, Zeiser R, et al. Unraveling the role of podocyte turnover in glomerular aging and injury. Journal of the American Society of Nephrology : JASN. 2014;25(4):707-16.
7. Kriz W. Podocyte is the major culprit accounting for the progression of chronic renal disease. Microscopy research and technique. 2002;57(4):189-95.
8. Kestila M, Lenkkeri U, Mannikko M, Lamerdin J, McCready P, Putaala H, et al. Positionally cloned gene for a novel glomerular protein--nephrin--is mutated in congenital nephrotic syndrome. Molecular cell. 1998;1(4):575-82.
9. Kim YH, Goyal M, Kurnit D, Wharram B, Wiggins J, Holzman L, et al. Podocyte depletion and glomerulosclerosis have a direct relationship in the PAN-treated rat. Kidney international. 2001;60(3):957-68.
10. Wharram BL, Goyal M, Wiggins JE, Sanden SK, Hussain S, Filipiak WE, et al. Podocyte depletion causes glomerulosclerosis: diphtheria toxin-induced podocyte depletion in rats expressing human diphtheria toxin receptor transgene. Journal of the American Society of Nephrology : JASN. 2005;16(10):2941-52.
11. Shankland SJ, Smeets B, Pippin JW, Moeller MJ. The emergence of the glomerular parietal epithelial cell. Nature reviews Nephrology. 2014;10(3):158-73.
12. Guo JK, Marlier A, Shi H, Shan A, Ardito TA, Du ZP, et al. Increased tubular proliferation as an adaptive response to glomerular albuminuria. Journal of the American Society of Nephrology : JASN. 2012;23(3):429-37.
13. Barisoni L. Podocyte biology in segmental sclerosis and progressive glomerular injury. Advances in chronic kidney disease. 2012;19(2):76-83.
14. Xiong J, Xia M, Xu M, Zhang Y, Abais JM, Li G, et al. Autophagy maturation associated with CD38-mediated regulation of lysosome function in mouse glomerular podocytes. Journal of cellular and molecular medicine. 2013;17(12):1598-607.
15. Fang L, Zhou Y, Cao H, Wen P, Jiang L, He W, et al. Autophagy attenuates diabetic glomerular damage through protection of hyperglycemia-induced podocyte injury. PloS one. 2013;8(4):e60546.

16. Narita M, Young AR, Arakawa S, Samarajiwa SA, Nakashima T, Yoshida S, et al. Spatial coupling of mTOR and autophagy augments secretory phenotypes. Science. 2011;332(6032):966-70.
17. Klionsky DJ, Abdalla FC, Abeliovich H, Abraham RT, Acevedo-Arozena A, Adeli K, et al. Guidelines for the use and interpretation of assays for monitoring autophagy. Autophagy. 2012;8(4):445-544.
18. Yang Z, Klionsky DJ. Eaten alive: a history of macroautophagy. Nature cell biology. 2010;12(9):814-22.
19. Yen WL, Klionsky DJ. How to live long and prosper: autophagy, mitochondria, and aging. Physiology. 2008;23:248-62.
20. Cina DP, Onay T, Paltoo A, Li C, Maezawa Y, De Arteaga J, et al. MTOR regulates autophagic flux in the glomerulus. Autophagy. 2012;8(4):696-8.
21. Cina DP, Onay T, Paltoo A, Li C, Maezawa Y, De Arteaga J, et al. Inhibition of MTOR disrupts autophagic flux in podocytes. Journal of the American Society of Nephrology : JASN. 2012;23(3):412-20.
22. Inoki K. mTOR signaling in autophagy regulation in the kidney. Seminars in nephrology. 2014;34(1):2-8.
23. Fukuda A, Chowdhury MA, Venkatareddy MP, Wang SQ, Nishizono R, Suzuki T, et al. Growth-dependent podocyte failure causes glomerulosclerosis. Journal of the American Society of Nephrology : JASN. 2012;23(8):1351-63.
24. Inoki K, Mori H, Wang J, Suzuki T, Hong S, Yoshida S, et al. mTORC1 activation in podocytes is a critical step in the development of diabetic nephropathy in mice. The Journal of clinical investigation. 2011;121(6):2181-96.
25. Godel M, Hartleben B, Herbach N, Liu S, Zschiedrich S, Lu S, et al. Role of mTOR in podocyte function and diabetic nephropathy in humans and mice. The Journal of clinical investigation. 2011;121(6):2197-209.
26. Vollenbroker B, George B, Wolfgart M, Saleem MA, Pavenstadt H, Weide T. mTOR regulates expression of slit diaphragm proteins and cytoskeleton structure in podocytes. American journal of physiology Renal physiology. 2009;296(2):F418-26.
27. Hartleben B, Godel M, Meyer-Schwesinger C, Liu S, Ulrich T, Kobler S, et al. Autophagy influences glomerular disease susceptibility and maintains podocyte homeostasis in aging mice. The Journal of clinical investigation. 2010;120(4):1084-96.
28. Nitta K, Okada K, Yanai M, Takahashi S. Aging and chronic kidney disease. Kidney & blood pressure research. 2013;38(1):109-20.
29. Rodriguez-Puyol D. The aging kidney. Kidney international. 1998;54(6):2247-65.
30. Pannarale G, Carbone R, Del Mastro G, Gallo C, Gattullo V, Natalicchio L, et al. The aging kidney: structural changes. J Nephrol.23 Suppl 15:S37-40.
31. Weinstein JR, Anderson S. The aging kidney: physiological changes. Advances in chronic kidney disease. 2010;17(4):302-7.
32. Wiggins JE. Aging in the glomerulus. The journals of gerontology Series A, Biological sciences and medical sciences. 2012;67(12):1358-64.
33. Kaplan C, Pasternack B, Shah H, Gallo G. Age-related incidence of sclerotic glomeruli in human kidneys. The American journal of pathology. 1975;80(2):227-34.
34. Rule AD, Semret MH, Amer H, Cornell LD, Taler SJ, Lieske JC, et al. Association of kidney function and metabolic risk factors with density of glomeruli on renal biopsy samples from living donors. Mayo Clinic proceedings Mayo Clinic. 2011;86(4):282-90.

35. Poggio ED, Rule AD, Tanchanco R, Arrigain S, Butler RS, Srinivas T, et al. Demographic and clinical characteristics associated with glomerular filtration rates in living kidney donors. Kidney international. 2009;75(10):1079-87.
36. Epstein M, Hollenberg NK. Age as a determinant of renal sodium conservation in normal man. The Journal of laboratory and clinical medicine. 1976;87(3):411-7.
37. Zhou XJ, Rakheja D, Yu X, Saxena R, Vaziri ND, Silva FG. The aging kidney. Kidney international. 2008;74(6):710-20.
38. Perazella MA, Mahnensmith RL. Hyperkalemia in the elderly: drugs exacerbate impaired potassium homeostasis. Journal of general internal medicine. 1997;12(10):646-56.
39. ElDesoky ES. Pharmacokinetic-pharmacodynamic crisis in the elderly. American journal of therapeutics. 2007;14(5):488-98.
40. Haley DP, Bulger RE. The aging male rat: structure and function of the kidney. The American journal of anatomy. 1983;167(1):1-13.
41. Lindeman RD, Goldman R. Anatomic and physiologic age changes in the kidney. Experimental gerontology. 1986;21(4-5):379-406.
42. Bolignano D, Mattace-Raso F, Sijbrands EJ, Zoccali C. The aging kidney revisited: a systematic review. Ageing research reviews. 2014;14:65-80.
43. Baert L, Steg A. Is the diverticulum of the distal and collecting tubules a preliminary stage of the simple cyst in the adult? The Journal of urology. 1977;118(5):707-10.
44. Takazakura E, Sawabu N, Handa A, Takada A, Shinoda A, Takeuchi J. Intrarenal vascular changes with age and disease. Kidney international. 1972;2(4):224-30.
45. Wiggins JE, Patel SR, Shedden KA, Goyal M, Wharram BL, Martini S, et al. NFkappaB promotes inflammation, coagulation, and fibrosis in the aging glomerulus. Journal of the American Society of Nephrology : JASN. 2010;21(4):587-97.
46. Johnson FB, Sinclair DA, Guarente L. Molecular biology of aging. Cell. 1999;96(2):291-302.
47. Melk A, Ramassar V, Helms LM, Moore R, Rayner D, Solez K, et al. Telomere shortening in kidneys with age. Journal of the American Society of Nephrology : JASN. 2000;11(3):444-53.
48. Sanchez-Nino MD, Poveda J, Sanz AB, Mezzano S, Carrasco S, Fernandez-Fernandez B, et al. Fn14 in podocytes and proteinuric kidney disease. Biochimica et biophysica acta. 2013;1832(12):2232-43.
49. Choudhury D, Levi M. Kidney aging--inevitable or preventable? Nature reviews Nephrology. 2011;7(12):706-17.
50. Kim JM, Heo HS, Choi YJ, Ye BH, Mi Ha Y, Seo AY, et al. Inhibition of NF-kappaB-induced inflammatory responses by angiotensin II antagonists in aged rat kidney. Experimental gerontology. 2011;46(7):542-8.
51. McCay CM, Crowell MF, Maynard LA. The effect of retarded growth upon the length of life span and upon the ultimate body size. 1935. Nutrition. 1989;5(3):155-71; discussion 72.
52. Colman RJ, Anderson RM, Johnson SC, Kastman EK, Kosmatka KJ, Beasley TM, et al. Caloric restriction delays disease onset and mortality in rhesus monkeys. Science. 2009;325(5937):201-4.
53. Cruzen C, Colman RJ. Effects of caloric restriction on cardiovascular aging in non-human primates and humans. Clinics in geriatric medicine. 2009;25(4):733-43, ix-x.

54. Rezzi S, Martin FP, Shanmuganayagam D, Colman RJ, Nicholson JK, Weindruch R. Metabolic shifts due to long-term caloric restriction revealed in nonhuman primates. Experimental gerontology. 2009;44(5):356-62.
55. Wiggins JE, Goyal M, Sanden SK, Wharram BL, Shedden KA, Misek DE, et al. Podocyte hypertrophy, "adaptation," and "decompensation" associated with glomerular enlargement and glomerulosclerosis in the aging rat: prevention by calorie restriction. Journal of the American Society of Nephrology : JASN. 2005;16(10):2953-66.
56. Cui J, Shi S, Sun X, Cai G, Cui S, Hong Q, et al. Mitochondrial autophagy involving renal injury and aging is modulated by caloric intake in aged rat kidneys. PloS one. 2013;8(7):e69720.
57. Jiang T, Liebman SE, Lucia MS, Phillips CL, Levi M. Calorie restriction modulates renal expression of sterol regulatory element binding proteins, lipid accumulation, and age-related renal disease. Journal of the American Society of Nephrology : JASN. 2005;16(8):2385-94.
58. Ning YC, Cai GY, Zhuo L, Gao JJ, Dong D, Cui S, et al. Short-term calorie restriction protects against renal senescence of aged rats by increasing autophagic activity and reducing oxidative damage. Mechanisms of ageing and development. 2013;134(11-12):570-9.
59. Holzenberger M, Dupont J, Ducos B, Leneuve P, Geloen A, Even PC, et al. IGF-1 receptor regulates lifespan and resistance to oxidative stress in mice. Nature. 2003;421(6919):182-7.
60. Bluher M, Kahn BB, Kahn CR. Extended longevity in mice lacking the insulin receptor in adipose tissue. Science. 2003;299(5606):572-4.
61. Bartke A. Long-lived Klotho mice: new insights into the roles of IGF-1 and insulin in aging. Trends in endocrinology and metabolism: TEM. 2006;17(2):33-5.
62. Zha Y, Le VT, Higami Y, Shimokawa I, Taguchi T, Razzaque MS. Life-long suppression of growth hormone-insulin-like growth factor I activity in genetically altered rats could prevent age-related renal damage. Endocrinology. 2006;147(12):5690-8.
63. Zha Y, Taguchi T, Nazneen A, Shimokawa I, Higami Y, Razzaque MS. Genetic suppression of GH-IGF-1 activity, combined with lifelong caloric restriction, prevents age-related renal damage and prolongs the life span in rats. American journal of nephrology. 2008;28(5):755-64.
64. Chen NY, Chen WY, Bellush L, Yang CW, Striker LJ, Striker GE, et al. Effects of streptozotocin treatment in growth hormone (GH) and GH antagonist transgenic mice. Endocrinology. 1995;136(2):660-7.
65. Shimokawa I, Higami Y, Utsuyama M, Tuchiya T, Komatsu T, Chiba T, et al. Life span extension by reduction in growth hormone-insulin-like growth factor-1 axis in a transgenic rat model. The American journal of pathology. 2002;160(6):2259-65.
66. Zuo Z, Lei H, Wang X, Wang Y, Sonntag W, Sun Z. Aging-related kidney damage is associated with a decrease in klotho expression and an increase in superoxide production. Age. 2011;33(3):261-74.
67. Kuro-o M, Matsumura Y, Aizawa H, Kawaguchi H, Suga T, Utsugi T, et al. Mutation of the mouse klotho gene leads to a syndrome resembling ageing. Nature. 1997;390(6655):45-51.
68. Kurosu H, Yamamoto M, Clark JD, Pastor JV, Nandi A, Gurnani P, et al. Suppression of aging in mice by the hormone Klotho. Science. 2005;309(5742):1829-33.

69. Mitobe M, Yoshida T, Sugiura H, Shirota S, Tsuchiya K, Nihei H. Oxidative stress decreases klotho expression in a mouse kidney cell line. Nephron Experimental nephrology. 2005;101(2):e67-74.
70. Torres PU, Prie D, Molina-Bletry V, Beck L, Silve C, Friedlander G. Klotho: an antiaging protein involved in mineral and vitamin D metabolism. Kidney international. 2007;71(8):730-7.
71. Cohen HY, Miller C, Bitterman KJ, Wall NR, Hekking B, Kessler B, et al. Calorie restriction promotes mammalian cell survival by inducing the SIRT1 deacetylase. Science. 2004;305(5682):390-2.
72. Kitada M, Kume S, Takeda-Watanabe A, Kanasaki K, Koya D. Sirtuins and renal diseases: relationship with aging and diabetic nephropathy. Clinical science. 2013;124(3):153-64.
73. Kume S, Uzu T, Horiike K, Chin-Kanasaki M, Isshiki K, Araki S, et al. Calorie restriction enhances cell adaptation to hypoxia through Sirt1-dependent mitochondrial autophagy in mouse aged kidney. The Journal of clinical investigation. 2010;120(4):1043-55.
74. Kitada M, Takeda A, Nagai T, Ito H, Kanasaki K, Koya D. Dietary restriction ameliorates diabetic nephropathy through anti-inflammatory effects and regulation of the autophagy via restoration of Sirt1 in diabetic Wistar fatty (fa/fa) rats: a model of type 2 diabetes. Experimental diabetes research. 2011;2011:908185.
75. Yoshizaki T, Schenk S, Imamura T, Babendure JL, Sonoda N, Bae EJ, et al. SIRT1 inhibits inflammatory pathways in macrophages and modulates insulin sensitivity. American journal of physiology Endocrinology and metabolism. 2010;298(3):E419-28.
76. He W, Wang Y, Zhang MZ, You L, Davis LS, Fan H, et al. Sirt1 activation protects the mouse renal medulla from oxidative injury. The Journal of clinical investigation. 2010;120(4):1056-68.
77. Saldanha JF, Leal Vde O, Stenvinkel P, Carraro-Eduardo JC, Mafra D. Resveratrol: why is it a promising therapy for chronic kidney disease patients? Oxidative medicine and cellular longevity. 2013;2013:963217.
78. Yadav A, Vallabu S, Arora S, Tandon P, Slahan D, Teichberg S, et al. ANG II promotes autophagy in podocytes. American journal of physiology Cell physiology. 2010;299(2):C488-96.
79. Ma T, Zhu J, Chen X, Zha D, Singhal PC, Ding G. High glucose induces autophagy in podocytes. Experimental cell research. 2013;319(6):779-89.
80. Huber TB, Edelstein CL, Hartleben B, Inoki K, Jiang M, Koya D, et al. Emerging role of autophagy in kidney function, diseases and aging. Autophagy. 2012;8(7):1009-31.
81. Weide T, Huber TB. Implications of autophagy for glomerular aging and disease. Cell and tissue research. 2011;343(3):467-73.
82. Rajawat YS, Hilioti Z, Bossis I. Aging: central role for autophagy and the lysosomal degradative system. Ageing research reviews. 2009;8(3):199-213.
83. Saftig P, Eskelinen EL. Live longer with LAMP-2. Nature medicine. 2008;14(9):909-10.
84. Unuma K, Aki T, Funakoshi T, Yoshida K, Uemura K. Cobalt protoporphyrin accelerates TFEB activation and lysosome reformation during LPS-induced septic insults in the rat heart. PloS one. 2013;8(2):e56526.

85. Lim JH, Kim EN, Kim MY, Chung S, Shin SJ, Kim HW, et al. Age-associated molecular changes in the kidney in aged mice. Oxidative medicine and cellular longevity. 2012;2012:171383.
86. Abrass CK, Adcox MJ, Raugi GJ. Aging-associated changes in renal extracellular matrix. The American journal of pathology. 1995;146(3):742-52.
87. Zhuo L, Cai G, Liu F, Fu B, Liu W, Hong Q, et al. Expression and mechanism of mammalian target of rapamycin in age-related renal cell senescence and organ aging. Mechanisms of ageing and development. 2009;130(10):700-8.
88. Nath KA. Tubulointerstitial changes as a major determinant in the progression of renal damage. American journal of kidney diseases : the official journal of the National Kidney Foundation. 1992;20(1):1-17.
89. Rule AD, Amer H, Cornell LD, Taler SJ, Cosio FG, Kremers WK, et al. The association between age and nephrosclerosis on renal biopsy among healthy adults. Annals of internal medicine. 2010;152(9):561-7.
90. Dmitrieva NI, Burg MB. Increased insensible water loss contributes to aging related dehydration. PloS one. 2011;6(5):e20691.
91. Zhou XJ, Saxena R, Liu Z, Vaziri ND, Silva FG. Renal senescence in 2008: progress and challenges. International urology and nephrology. 2008;40(3):823-39.
92. Wiggins JE, Goyal M, Wharram BL, Wiggins RC. Antioxidant ceruloplasmin is expressed by glomerular parietal epithelial cells and secreted into urine in association with glomerular aging and high-calorie diet. Journal of the American Society of Nephrology : JASN. 2006;17(5):1382-7.
93. Sarioglu S, Celik A, Ersen A, Ucer I, Saglam F, Camsari T, et al. Vascular endothelial growth factor expression and vascularity in renal allograft biopsies. Transplantation proceedings. 2008;40(1):178-80.
94. Friedlander J, Janulis M, Tembe V, Ro HK, Wong MS, Favus MJ. Loss of parathyroid hormone-stimulated 1,25-dihydroxyvitamin D3 production in aging does not involve protein kinase A or C pathways. Journal of bone and mineral research : the official journal of the American Society for Bone and Mineral Research. 1994;9(3):339-45.
95. Mattson MP, Maudsley S. Live longer sans the AT1A receptor. Cell metabolism. 2009;9(5):403-5.
96. Belmin J, Levy BI, Michel JB. Changes in the renin-angiotensin-aldosterone axis in later life. Drugs & aging. 1994;5(5):391-400.
97. Goyal VK. Changes with age in the human kidney. Experimental gerontology. 1982;17(5):321-31.
98. Wiggins J. Podocytes and glomerular function with aging. Seminars in nephrology. 2009;29(6):587-93.
99. Fu RG, Wu JJ, Xue RL, Zhang T, Wang L, Wu XL, et al. Premature senescence and cellular phenotype transformation of mesangial cells induced by TGF-B1. Renal failure. 2013;35(8):1142-5.
100. Niedernhofer LJ, Odijk H, Budzowska M, van Drunen E, Maas A, Theil AF, et al. The structure-specific endonuclease Ercc1-Xpf is required to resolve DNA interstrand cross-link-induced double-strand breaks. Molecular and cellular biology. 2004;24(13):5776-87.
101. Gregg SQ, Robinson AR, Niedernhofer LJ. Physiological consequences of defects in ERCC1-XPF DNA repair endonuclease. DNA repair. 2011;10(7):781-91.

102. Niedernhofer LJ, Garinis GA, Raams A, Lalai AS, Robinson AR, Appeldoorn E, et al. A new progeroid syndrome reveals that genotoxic stress suppresses the somatotroph axis. Nature. 2006;444(7122):1038-43.
103. Bhagwat N, Olsen AL, Wang AT, Hanada K, Stuckert P, Kanaar R, et al. XPF-ERCC1 participates in the Fanconi anemia pathway of cross-link repair. Molecular and cellular biology. 2009;29(24):6427-37.
104. Kashiyama K, Nakazawa Y, Pilz DT, Guo C, Shimada M, Sasaki K, et al. Malfunction of nuclease ERCC1-XPF results in diverse clinical manifestations and causes Cockayne syndrome, xeroderma pigmentosum, and Fanconi anemia. American journal of human genetics. 2013;92(5):807-19.
105. Zhou W, Otto EA, Cluckey A, Airik R, Hurd TW, Chaki M, et al. FAN1 mutations cause karyomegalic interstitial nephritis, linking chronic kidney failure to defective DNA damage repair. Nature genetics. 2012;44(8):910-5.
106. Sijbers AM, de Laat WL, Ariza RR, Biggerstaff M, Wei YF, Moggs JG, et al. Xeroderma pigmentosum group F caused by a defect in a structure-specific DNA repair endonuclease. Cell. 1996;86(5):811-22.
107. Kraemer KH, Levy DD, Parris CN, Gozukara EM, Moriwaki S, Adelberg S, et al. Xeroderma pigmentosum and related disorders: examining the linkage between defective DNA repair and cancer. The Journal of investigative dermatology. 1994;103(5 Suppl):96S-101S.
108. Jaspers NG, Raams A, Silengo MC, Wijgers N, Niedernhofer LJ, Robinson AR, et al. First reported patient with human ERCC1 deficiency has cerebro-oculo-facio-skeletal syndrome with a mild defect in nucleotide excision repair and severe developmental failure. American journal of human genetics. 2007;80(3):457-66.
109. McWhir J, Selfridge J, Harrison DJ, Squires S, Melton DW. Mice with DNA repair gene (ERCC-1) deficiency have elevated levels of p53, liver nuclear abnormalities and die before weaning. Nature genetics. 1993;5(3):217-24.
110. Weeda G, Donker I, de Wit J, Morreau H, Janssens R, Vissers CJ, et al. Disruption of mouse ERCC1 results in a novel repair syndrome with growth failure, nuclear abnormalities and senescence. Current biology : CB. 1997;7(6):427-39.
111. Tian M, Shinkura R, Shinkura N, Alt FW. Growth retardation, early death, and DNA repair defects in mice deficient for the nucleotide excision repair enzyme XPF. Molecular and cellular biology. 2004;24(3):1200-5.
112. Selfridge J, Hsia KT, Redhead NJ, Melton DW. Correction of liver dysfunction in DNA repair-deficient mice with an ERCC1 transgene. Nucleic acids research. 2001;29(22):4541-50.
113. Gregg SQ, Gutierrez V, Robinson AR, Woodell T, Nakao A, Ross MA, et al. A mouse model of accelerated liver aging caused by a defect in DNA repair. Hepatology. 2012;55(2):609-21.
114. Wang J, Clauson CL, Robbins PD, Niedernhofer LJ, Wang Y. The oxidative DNA lesions 8,5'-cyclopurines accumulate with aging in a tissue-specific manner. Aging cell. 2012;11(4):714-6.
115. Jung T, Bader N, Grune T. Lipofuscin: formation, distribution, and metabolic consequences. Annals of the New York Academy of Sciences. 2007;1119:97-111.

116. Kumar P, Kale RK, Baquer NZ. Estradiol modulates membrane-linked ATPases, antioxidant enzymes, membrane fluidity, lipid peroxidation, and lipofuscin in aged rat liver. Journal of aging research. 2011;2011:580245.
117. Farahmand SK, Samini F, Samini M, Samarghandian S. Safranal ameliorates antioxidant enzymes and suppresses lipid peroxidation and nitric oxide formation in aged male rat liver. Biogerontology. 2013;14(1):63-71.
118. Stevens LA, Viswanathan G, Weiner DE. Chronic kidney disease and end-stage renal disease in the elderly population: current prevalence, future projections, and clinical significance. Advances in chronic kidney disease. 2010;17(4):293-301.
119. Levey AS, Coresh J, Balk E, Kausz AT, Levin A, Steffes MW, et al. National Kidney Foundation practice guidelines for chronic kidney disease: evaluation, classification, and stratification. Annals of internal medicine. 2003;139(2):137-47.
120. John R, Webb M, Young A, Stevens PE. Unreferred chronic kidney disease: a longitudinal study. American journal of kidney diseases : the official journal of the National Kidney Foundation. 2004;43(5):825-35.
121. Heron M, Hoyert DL, Murphy SL, Xu J, Kochanek KD, Tejada-Vera B. Deaths: final data for 2006. Natl Vital Stat Rep. 2009;57(14):1-134.
122. Lysaght MJ. Maintenance dialysis population dynamics: current trends and long-term implications. Journal of the American Society of Nephrology : JASN. 2002;13 Suppl 1:S37-40.
123. Tan JC, Workeneh B, Busque S, Blouch K, Derby G, Myers BD. Glomerular function, structure, and number in renal allografts from older deceased donors. Journal of the American Society of Nephrology : JASN. 2009;20(1):181-8.
124. Melk A, Schmidt BM, Takeuchi O, Sawitzki B, Rayner DC, Halloran PF. Expression of p16INK4a and other cell cycle regulator and senescence associated genes in aging human kidney. Kidney international. 2004;65(2):510-20.
125. Hasty P, Campisi J, Hoeijmakers J, van Steeg H, Vijg J. Aging and genome maintenance: lessons from the mouse? Science. 2003;299(5611):1355-9.
126. Ahmad A, Robinson AR, Duensing A, van Drunen E, Beverloo HB, Weisberg DB, et al. ERCC1-XPF endonuclease facilitates DNA double-strand break repair. Molecular and cellular biology. 2008;28(16):5082-92.
127. Sijbers AM, van der Spek PJ, Odijk H, van den Berg J, van Duin M, Westerveld A, et al. Mutational analysis of the human nucleotide excision repair gene ERCC1. Nucleic acids research. 1996;24(17):3370-80.
128. Prasher JM, Lalai AS, Heijmans-Antonissen C, Ploemacher RE, Hoeijmakers JH, Touw IP, et al. Reduced hematopoietic reserves in DNA interstrand crosslink repair-deficient Ercc1-/- mice. The EMBO journal. 2005;24(4):861-71.
129. de Waard MC, van der Pluijm I, Zuiderveen Borgesius N, Comley LH, Haasdijk ED, Rijksen Y, et al. Age-related motor neuron degeneration in DNA repair-deficient Ercc1 mice. Acta Neuropathol.120(4):461-75.
130. Dolle ME, Kuiper RV, Roodbergen M, Robinson J, de Vlugt S, Wijnhoven SW, et al. Broad segmental progeroid changes in short-lived Ercc1(-/Delta7) mice. Pathobiology of aging & age related diseases. 2011;1.
131. Schermer B, Bartels V, Frommolt P, Habermann B, Braun F, Schultze JL, et al. Transcriptional profiling reveals progeroid Ercc1(-/Delta) mice as a model system for glomerular aging. BMC genomics. 2013;14:559.

132. Rieg T. A High-throughput Method for Measurement of Glomerular Filtration Rate in Conscious Mice. Journal of visualized experiments : JoVE. 2013(75).
133. Debacq-Chainiaux F, Erusalimsky JD, Campisi J, Toussaint O. Protocols to detect senescence-associated beta-galactosidase (SA-betagal) activity, a biomarker of senescent cells in culture and in vivo. Nature protocols. 2009;4(12):1798-806.
134. Spoor M, Nagtegaal AP, Ridwan Y, Borgesius NZ, van Alphen B, van der Pluijm I, et al. Accelerated loss of hearing and vision in the DNA-repair deficient Ercc1(delta/-) mouse. Mechanisms of ageing and development. 2012;133(2-3):59-67.
135. Jaruga P, Dizdaroglu M. 8,5'-Cyclopurine-2'-deoxynucleosides in DNA: mechanisms of formation, measurement, repair and biological effects. DNA repair. 2008;7(9):1413-25.
136. Lyman JL. Blood urea nitrogen and creatinine. Emerg Med Clin North Am. 1986;4(2):223-33.
137. Clampitt RB, Hart RJ. The tissue activities of some diagnostic enzymes in ten mammalian species. Journal of comparative pathology. 1978;88(4):607-21.
138. The Clinical Chemistry of Laboratory Animals. 2nd ed. Ann Arbor, MI: Taylor and Francis; 1999.
139. Rahn KH, Heidenreich S, Bruckner D. How to assess glomerular function and damage in humans. J Hypertens. 1999;17(3):309-17.
140. Tsaih SW, Pezzolesi MG, Yuan R, Warram JH, Krolewski AS, Korstanje R. Genetic analysis of albuminuria in aging mice and concordance with loci for human diabetic nephropathy found in a genome-wide association scan. Kidney international.77(3):201-10.
141. Qi Z, Breyer MD. Measurement of glomerular filtration rate in conscious mice. Methods in molecular biology. 2009;466:61-72.
142. Shankland SJ. The podocyte's response to injury: role in proteinuria and glomerulosclerosis. Kidney international. 2006;69(12):2131-47.
143. Ortmann J, Amann K, Brandes RP, Kretzler M, Munter K, Parekh N, et al. Role of podocytes for reversal of glomerulosclerosis and proteinuria in the aging kidney after endothelin inhibition. Hypertension. 2004;44(6):974-81.
144. Price PM, Safirstein RL, Megyesi J. The cell cycle and acute kidney injury. Kidney international. 2009;76(6):604-13.
145. Rodier F, Munoz DP, Teachenor R, Chu V, Le O, Bhaumik D, et al. DNA-SCARS: distinct nuclear structures that sustain damage-induced senescence growth arrest and inflammatory cytokine secretion. Journal of cell science. 2011;124(Pt 1):68-81.
146. Baker DJ, Wijshake T, Tchkonia T, LeBrasseur NK, Childs BG, van de Sluis B, et al. Clearance of p16Ink4a-positive senescent cells delays ageing-associated disorders. Nature. 2011;479(7372):232-6.
147. Sedelnikova OA, Horikawa I, Zimonjic DB, Popescu NC, Bonner WM, Barrett JC. Senescing human cells and ageing mice accumulate DNA lesions with unrepairable double-strand breaks. Nature cell biology. 2004;6(2):168-70.
148. Naesens M. Replicative senescence in kidney aging, renal disease, and renal transplantation. Discov Med. 2011;11(56):65-75.
149. Wang D, Luo X, Zhong Y, Yang W, Xu M, Liu Y, et al. Pu-erh black tea extract supplementation attenuates the oxidative DNA damage and oxidative stress in Sprague-Dawley rats with renal dysfunction induced by subchronic 3-methyl-2-quinoxalin benzenevinylketo-1,4-dioxide exposure. Food Chem Toxicol. 2012;50(2):147-54.

150. Abe Y, Sakairi T, Kajiyama H, Shrivastav S, Beeson C, Kopp JB. Bioenergetic characterization of mouse podocytes. American journal of physiology Cell physiology. 2010;299(2):C464-76.
151. Wanner N, Hartleben B, Herbach N, Goedel M, Stickel N, Zeiser R, et al. Unraveling the Role of Podocyte Turnover in Glomerular Aging and Injury. Journal of the American Society of Nephrology : JASN. 2014.
152. Wiggins J. Why do our kidneys get old? Nephron Experimental nephrology. 2011;119 Suppl 1:e1-5.
153. Comb WC, Cogswell P, Sitcheran R, Baldwin AS. IKK-dependent, NF-kappaB-independent control of autophagic gene expression. Oncogene. 2011;30(14):1727-32.
154. Criollo A, Senovilla L, Authier H, Maiuri MC, Morselli E, Vitale I, et al. The IKK complex contributes to the induction of autophagy. The EMBO journal. 2010;29(3):619-31.
155. Niida M, Tanaka M, Kamitani T. Downregulation of active IKK beta by Ro52-mediated autophagy. Molecular immunology. 2010;47(14):2378-87.
156. Qing G, Yan P, Qu Z, Liu H, Xiao G. Hsp90 regulates processing of NF-kappa B2 p100 involving protection of NF-kappa B-inducing kinase (NIK) from autophagy-mediated degradation. Cell research. 2007;17(6):520-30.
157. Salminen A, Hyttinen JM, Kauppinen A, Kaarniranta K. Context-Dependent Regulation of Autophagy by IKK-NF-kappaB Signaling: Impact on the Aging Process. International journal of cell biology. 2012;2012:849541.
158. Salminen A, Kaarniranta K, Kauppinen A. Inflammaging: disturbed interplay between autophagy and inflammasomes. Aging. 2012;4(3):166-75.
159. Meng Q, Cai D. Defective hypothalamic autophagy directs the central pathogenesis of obesity via the IkappaB kinase beta (IKKbeta)/NF-kappaB pathway. The Journal of biological chemistry. 2011;286(37):32324-32.
160. Moeller MJ, Sanden SK, Soofi A, Wiggins RC, Holzman LB. Podocyte-specific expression of cre recombinase in transgenic mice. Genesis. 2003;35(1):39-42.
161. Iwano M, Plieth D, Danoff TM, Xue C, Okada H, Neilson EG. Evidence that fibroblasts derive from epithelium during tissue fibrosis. The Journal of clinical investigation. 2002;110(3):341-50.
162. Magness ST, Jijon H, Van Houten Fisher N, Sharpless NE, Brenner DA, Jobin C. In vivo pattern of lipopolysaccharide and anti-CD3-induced NF-kappa B activation using a novel gene-targeted enhanced GFP reporter gene mouse. Journal of immunology. 2004;173(3):1561-70.
163. Schumacher VA, Schlotzer-Schrehardt U, Karumanchi SA, Shi X, Zaia J, Jeruschke S, et al. WT1-dependent sulfatase expression maintains the normal glomerular filtration barrier. Journal of the American Society of Nephrology : JASN. 2011;22(7):1286-96.
164. Shankland SJ, Pippin JW, Reiser J, Mundel P. Podocytes in culture: past, present, and future. Kidney international. 2007;72(1):26-36.
165. Takemoto M, Asker N, Gerhardt H, Lundkvist A, Johansson BR, Saito Y, et al. A new method for large scale isolation of kidney glomeruli from mice. The American journal of pathology. 2002;161(3):799-805.
166. Adler AS, Sinha S, Kawahara TL, Zhang JY, Segal E, Chang HY. Motif module map reveals enforcement of aging by continual NF-kappaB activity. Genes & development. 2007;21(24):3244-57.

167. Korhonen P, Helenius M, Salminen A. Age-related changes in the regulation of transcription factor NF-kappa B in rat brain. Neuroscience letters. 1997;225(1):61-4.
168. Tilstra JS, Robinson AR, Wang J, Gregg SQ, Clauson CL, Reay DP, et al. NF-kappaB inhibition delays DNA damage-induced senescence and aging in mice. The Journal of clinical investigation. 2012;122(7):2601-12.
169. Lee DF, Kuo HP, Chen CT, Hsu JM, Chou CK, Wei Y, et al. IKK beta suppression of TSC1 links inflammation and tumor angiogenesis via the mTOR pathway. Cell. 2007;130(3):440-55.
170. Sandoval RM, Wagner MC, Patel M, Campos-Bilderback SB, Rhodes GJ, Wang E, et al. Multiple factors influence glomerular albumin permeability in rats. Journal of the American Society of Nephrology : JASN. 2012;23(3):447-57.
171. Satirapoj B, Nast CC, Adler SG. Novel insights into the relationship between glomerular pathology and progressive kidney disease. Advances in chronic kidney disease. 2012;19(2):93-100.
172. Lim AI, Tang SC, Lai KN, Leung JC. Kidney injury molecule-1: more than just an injury marker of tubular epithelial cells? Journal of cellular physiology. 2013;228(5):917-24.
173. Bechtel W, Helmstadter M, Balica J, Hartleben B, Kiefer B, Hrnjic F, et al. Vps34 deficiency reveals the importance of endocytosis for podocyte homeostasis. Journal of the American Society of Nephrology : JASN. 2013;24(5):727-43.
174. Helenius M, Hanninen M, Lehtinen SK, Salminen A. Changes associated with aging and replicative senescence in the regulation of transcription factor nuclear factor-kappa B. The Biochemical journal. 1996;318 (Pt 2):603-8.
175. Brink TC, Regenbrecht C, Demetrius L, Lehrach H, Adjaye J. Activation of the immune response is a key feature of aging in mice. Biogerontology. 2009;10(6):721-34.
176. Liebau MC, Braun F, Hopker K, Weitbrecht C, Bartels V, Muller RU, et al. Dysregulated autophagy contributes to podocyte damage in Fabry's disease. PloS one. 2013;8(5):e63506.
177. Durik M, Kavousi M, van der Pluijm I, Isaacs A, Cheng C, Verdonk K, et al. Nucleotide excision DNA repair is associated with age-related vascular dysfunction. Circulation. 2012;126(4):468-78.
178. Osorio FG, Lopez-Otin C, Freije JM. NF-kB in premature aging. Aging. 2012;4(11):726-7.
179. Kim JM, Heo HS, Ha YM, Ye BH, Lee EK, Choi YJ, et al. Mechanism of Ang II involvement in activation of NF-kappaB through phosphorylation of p65 during aging. Age. 2012;34(1):11-25.
180. de Cavanagh EM, Ferder L, Toblli JE, Piotrkowski B, Stella I, Fraga CG, et al. Renal mitochondrial impairment is attenuated by AT1 blockade in experimental Type I diabetes. American journal of physiology Heart and circulatory physiology. 2008;294(1):H456-65.
181. Ebrahimi-Fakhari D, Wahlster L. Restoring impaired protein metabolism in Parkinson's disease--TFEB-mediated autophagy as a novel therapeutic target. Movement disorders : official journal of the Movement Disorder Society. 2013;28(10):1346.